

# POLITECNICO DI TORINO

Master's Degree in Biomedical Engineering



Master's Degree Thesis

## Analysis of the pupillary response in Amyotrophic Lateral Sclerosis patients

Supervisors

Prof. Luca MESIN

Candidate

Sara Jlassi

July 2022



## Abstract

Amyotrophic Lateral Sclerosis (ALS) is an extremely disabling pathology that leads to complete paralysis in a short time. In particular, the patient could reach a condition known as "Locked-In Syndrome" (LIS), in which all voluntary movements are prevented (or "Complete Locked-In Syndrome", if also ocular movements are compromised). In this state, communication with the outside world is impossible and support strategies are required.

The disease affects only upper and lower motor neurons, whereas other neurological functions remain unchanged.

The pupillary activity is under the control of the Autonomic Nervous System (ANS), whose functions do not appear to be affected as the disease progresses. The pupil size varies in response to external stimuli, such as an ambient light change, or to a variation in mental load. Moreover, pupillary diameter oscillations are present even in the absence of stimuli, which represent the so-called "Pupillary Hippius". The purpose of this study is to understand if the pupillary activity is not altered by the ALS progression, to exploit it as a mean of communication with the outside.

To achieve this goal, the pupillographic signals of 33 ALS patients and 10 healthy subjects have been analysed, by separately studying the first part of the time series, that represents the Hippius, and the second one, which shows the pupil response to light stimuli (that is the "Pupillary Light Reflex"). In both cases, a series of indices has been extracted from the signal in the time domain and from its power spectral density (PSD), allowing to create a data set of variables and divided into classes according to the severity of the disease (dictated by the ALSFRS-R score).

Multiple tests were carried out: initially, only the data set of ALS patients was considered, which was divided into three classes (severely, moderately and poorly invalidated subjects); then, the recordings of healthy people were included and some tests on both two (healthy and pathological subjects) and three (ALS patients with severe disease or moderate symptoms and healthy subjects) classes subdivision have been carried out.

For any index, the frequency distributions of each class have been compared, through the Kruskal-Wallis and the Wilcoxon tests, in order to assess if the groups belonged to the same population. Moreover, a binary tree classifier has been exploited to predict the class of each subject.

From this analysis, it resulted that some indices show significant difference among the classes: variance, skewness and kurtosis of the Hippius frequency distribution and other features like the PSD mean frequency (MNF) and the PLR amplitude have been taken into account to discriminate the groups.

Furthermore, it has been found that, given a good combination of features as input,

the two classes subdivision of data set is the best one, with a classification accuracy of 93.75%.

However, the high data variability and the limited size of the data set do not allow to affirm that there are evident variations in pupillary activity and, consequently, the hypothesis that the ANS activity is not altered by the progression of the disease cannot be rejected. Therefore, the communication through pupil size variations could be an effective strategy for LIS people.





# Table of Contents

<b>List of Tables</b>	IV
<b>List of Figures</b>	V
<b>Acronyms</b>	XI
<b>1 Introduction</b>	1
<b>2 Background</b>	3
2.1 Amyotrophic lateral sclerosis . . . . .	3
2.1.1 Clinical features and onset . . . . .	3
2.1.2 Epidemiology . . . . .	5
2.1.3 Diagnosis . . . . .	6
2.1.4 Clinical care . . . . .	7
2.1.5 Locked-In Syndrome and communication systems . . . . .	8
2.2 Autonomic Nervous System: anatomy and physiology . . . . .	10
2.2.1 Anatomy of the sympathetic nervous system . . . . .	11
2.2.2 Anatomy of the parasympathetic system . . . . .	13
2.3 The visual system . . . . .	14
2.3.1 Eye anatomy . . . . .	14
2.3.2 Autonomic control of the pupil . . . . .	15
<b>3 Methods and materials</b>	21
3.1 Data set . . . . .	21
3.1.1 Longitudinal Study Group . . . . .	21
3.1.2 Transversal Study Group . . . . .	22
3.2 Experimental setup . . . . .	22
3.3 Signal processing . . . . .	24
3.3.1 First part: Pupillary Hippus . . . . .	24
3.3.2 Second part: Pupillary Light Reflex . . . . .	31
3.3.3 Extraction of other indices and database compilation . . . . .	36

3.4	Data analysis . . . . .	41
3.4.1	Trend over time of power percentages in the LF and HF bands	41
3.4.2	Pupillary indices as a function of the ALSFRS score . . . . .	43
3.4.3	Stage of the disease classification . . . . .	46
3.4.4	Classification results . . . . .	49
<b>4</b>	<b>Pupillary acquisitions on healthy subjects</b>	<b>52</b>
4.1	Pupillometry system . . . . .	52
4.1.1	Pupil Capture . . . . .	52
4.1.2	Pupil Player . . . . .	55
4.2	Data set . . . . .	57
4.3	Experimental setup . . . . .	57
4.4	Signal processing . . . . .	58
4.4.1	First part: Pupillary Hippus . . . . .	58
4.4.2	Second part: Pupillary Light Reflex . . . . .	61
4.5	Data analysis . . . . .	63
4.5.1	Two classes partition . . . . .	63
4.5.2	Three classes partition . . . . .	69
<b>5</b>	<b>Discussion of results and conclusions</b>	<b>76</b>
	<b>Bibliography</b>	<b>81</b>

# List of Tables

3.1	Summary table of VLF, LF and HF frequency band selection methods.	31
3.2	Summary table of the indices extracted from the pupillographic recordings. . . . .	40
3.3	Classification performance results. . . . .	51
4.1	p-values resulting from the Wilcoxon rank sum test. . . . .	66
4.2	Classification performance results - 2 classes . . . . .	69
4.3	p-values resulting from the Kruskal-Wallis test. . . . .	72
4.4	p-values resulting from Wilcoxon test for each pair of classes. . . . .	74
4.5	Classification performance results - 3 classes . . . . .	75
5.1	Summary table of classification performance results of the three tests.	78
5.2	Summary table of the best features combinations provided to the binary tree classifier. . . . .	79

# List of Figures

2.1	The primary motor system showing connections among upper motor neurons, lower motor neurons, and the muscle effector organ. . . . .	4
2.2	The prevalence rate in Italy. Source: <i>EURALS Consortium - European amyotrophic lateral sclerosis consortium</i> [14]. . . . .	6
2.3	Autonomic Nervous System anatomy. . . . .	11
2.4	Preganglionic and postganglionic sympathetic connections via the three anatomical arrangement. . . . .	12
2.5	Preganglionic and postganglionic neurons connection in the Parasympathetic Nervous System. . . . .	13
2.6	Eye anatomy . . . . .	14
2.7	Summary diagram of current understanding of the afferent, central, and efferent pathways controlling pupil diameter. The iris musculature innervated by autonomic efferents from both the parasympathetic and sympathetic components of the autonomic nervous system. . . . .	16
2.8	Pupilloconstriction elicited by a 10 s light stimulus of 493 nm wavelength light at 14.0 log quanta $cm^{-2}$ per second irradiance (blue trace), and 613 nm wavelength light at 14.1 log quanta $cm^{-2}$ per second irradiance (red trace). Note that a 473 nm stimulus, drives a larger pupillary response than the 613 nm stimulus (red trace). The pupilloconstriction induced by the 473 nm light is maintained following stimulus offset. . . . .	18
2.9	Pupillary light reflex pathway: from light stimulation of the retina to the midbrain. Afferent pathway (red and blue lines): Left light stimulus goes from the left retina to the optic chiasm to the optic tract, ending at the ipsilateral pretectal nucleus. The pretectal nucleus supplies both left and right Edinger-Westphal nuclei. Yellow lines show impulse from both nuclei reaching both ciliary ganglia and resulting in bilateral miosis. . . . .	19
2.10	Schematic diagram of accommodation. . . . .	20

3.1	The Eye Tribe Tracker of IMotions®, the device used for the pupillographic signal acquisition. . . . .	24
3.2	Representation of the average pupillary diameter of the original signal (in blue) and of the cleaned signal (in red) in the first 60 seconds of the acquisition. This signal was recorded during the 3 <sup>rd</sup> visit (7 June 2018) of Subject 10 (Longitudinal Group). . . . .	25
3.3	The result of Chebyshev filter and Tukey's window application. The first and the last 5 seconds of the recording have been cut off. This signal was recorded during the 3 <sup>rd</sup> visit (7 June 2018) of Subject 10 (Longitudinal Group). . . . .	26
3.4	Subdivision of the Power Spectral Density (PSD) related to the pupillographic signal of Subject 10, recorded during his 3 <sup>rd</sup> visit on 7 Jun 2018 (Longitudinal). The spectrum is divided in three ranges of frequency, that are VLF (8 - 50 mHz), LF (50 - 150 mHz) and HF (150 - 450 mHz). The PSD has been estimated via Welch's method. . . . .	27
3.5	Power Spectral Density (PSD) related to Subject 14 (Longitudinal) recording, during his 1 <sup>st</sup> visit on 23 January 2018. The spectrum has been divided into the VLF, LF and HF ranges through two alternative methods of intervals selection: extended fixed ranges (3.5a) and automatic peaks and intervals research (3.5b). In the latter case, the integration of PSD in the LF and HF is more precise and it leads to a more accurate estimation of the $P_{LF}/P_{HF}$ index. . . . .	30
3.6	Comparison between the original signal (upper subplot), obtained from the second part of the pupillary recording and the processed signal (lower subplot). The resulting signal appears free of abnormal peaks and PLRs are clearly visible. The signal belongs to Subject 02 - 2 <sup>nd</sup> visit on 18 April 2018 (Longitudinal Group). . . . .	32
3.7	Example of the manual selection of a PLR. In the figure, the descending (3.7a) and the ascending (3.7b) tracts of a PLR have been selected and the respective time intervals have been collected. The signal belongs to Subject 02 - 2 <sup>nd</sup> visit on 18 April 2018 (Longitudinal Group). . . . .	33
3.8	Interpolation of the three descending traits (Dis 1, Dis 2 and Dis 3) and of the ascending ones (Asc 1, Asc 2 and Asc 3) through the two exponential model 3.2, in linear scale (Figure <b>3.8a</b> ) and semi-logarithmic scale (Figure <b>3.8b</b> ). The blue points in Figure 3.8a represents the original signal and the red functions are the interpolating exponentials. These PLRs have been extracted from the recording session of Subject 1001 - 1 <sup>st</sup> Visit on 16 February 2018 (LIS). . . . .	34

3.9	Interpolation of the PLRs constriction (Dis 1, Dis 2 and Dis 3) and dilatation (Asc 1, Asc 2 and Asc 3) traits, through the exponential models described by the Equations 3.3 and 3.4, respectively. The recording session refers to Subject 1001 - 1 <sup>st</sup> Visit on 16 February 2018 (LIS). . . . .	35
3.10	Representation of the mean frequency (MNF) evaluated on the hippus PSD of Subject 1012 - 1 <sup>st</sup> Visit (20 June 2018) (Transversal Group). . . . .	37
3.11	Descending response time (3.11a) and ascending response time (3.11b) evaluation for a single PLR extracted from the recording of Subject 02 - 5 <sup>th</sup> Visit (22 January 2019) (Longitudinal Group). . . .	38
3.12	Example of questionnaires filled by two hypothetical ALS patients. Each questionnaire is composed by 12 items about subject's physical functions, ranging from 4 (normal) to 0 (no ability). Even if the ALSFRS-R score is the same, each patient experiences drastically different symptoms. For instance, both Steven and Mary have the same ALSFRS-R score; however, while Steven experiences symptoms in his head, throat, and upper body, Mary experiences symptoms in her legs and respiratory system. . . . .	40
3.13	Representation of the trend over time of power percentages in the LF and HF bands ( $P_{LF}$ and $P_{HF}$ ), related to subjects 18 (Figure 3.13a) and 26 (Figure 3.13b) of Longitudinal Group. . . . .	42
3.14	Box plots related to angular coefficients $m$ of the fitting straight lines in the LF and HF frequency bands. . . . .	43
3.15	Pupillary Hippus - Time domain indices as function of ALSFRS-R score . . . . .	44
3.16	Pupillary Hippus - Frequency domain indices as function of ALSFRS-R score . . . . .	45
3.17	PLR - Time domain indices as function of ALSFRS-R score . . . .	45
3.18	Data set partition through LOOCV. . . . .	47
3.19	Training of the classifier through all possible combinations of the 13 indices. As an example, the case $k = 5$ items is represented. . . . .	49
3.20	Binary decision tree rules of classification, exploiting the amplitude of pupil diameter and the kurtosis as input for the classification. . .	50
3.21	Confusion matrix related to the binary decision tree predictions. For each class, the number of correct classifications is reported on the diagonal of the matrix (blue boxes), whereas wrong classifications are inserted in the orange boxes. . . . .	51
4.1	Pupil Core® headset. . . . .	53
4.2	Pupil Capture World window. . . . .	53

4.3	Eye cameras enabling from <i>General Settings</i> menu. . . . .	54
4.4	Pupil Capture windows that shows eye recordings and pupil detection. . . . .	55
4.5	Pupil Player home screen. . . . .	55
4.6	Player window. . . . .	56
4.7	Representation of the pupillary diameter as a function of time, in the second minute of the recording. In each plot the original signal, the results of the median filter and Tukey's window application, and the signal obtained after high-pass filtering are reported. This signal has been taken from Subject 006 of Healthy Subjects Group. . . . .	59
4.8	Pupillograms comparison, referring to right pupil (in blue), left pupil (in red) and to the average signal (in yellow) over time. . . . .	61
4.9	Constriction and dilatation intervals selection for PLRs' indices evaluation. The signal has been taken from Subject 006 of Healthy Subjects Group. . . . .	62
4.10	Pupillary hippus - time domain indices distribution, represented by box-plots. . . . .	64
4.11	Pupillary hippus - frequency domain indices distribution, represented by box-plots. . . . .	64
4.12	PLR - time domain indices distribution, represented by box-plots. . . . .	65
4.13	Boxplots showing the significantly different frequency distributions of variance, skewness, kurtosis and $P_{LF}/P_{HF}$ related to Class 0 and Class 1. The levels of significance are also reported: * $p < 0.05$ and ** $p < 0.01$ . . . . .	67
4.14	Decision tree rules for Class 0 and Class 1 prediction. . . . .	68
4.15	Confusion matrix showing the results of the binary tree classification for Class 0 and Class 1 with <i>variance</i> , <i>kurtosis</i> , $P_{LF}/P_{HF} - \tau_{dis}$ and <i>PLR range</i> as input variables. . . . .	68
4.16	Pupillary hippus - Time domain indices distribution, represented by box-plots. . . . .	70
4.17	Pupillary hippus - frequency domain indices distribution, represented by box-plots. . . . .	71
4.18	PLR - time domain indices distribution, represented by box-plots. . . . .	71
4.19	Boxplots showing the significantly different frequency distributions of variance, skewness, kurtosis, MNF, response time - constriction and response time - dilatation, related to Class 0, Class 1 and Class 2. The levels of significance are also reported: * $p < 0.05$ and ** $p < 0.01$ . . . . .	73
4.20	Decision tree rules for Class 0, Class 1 and Class 2 prediction. . . . .	74
4.21	Confusion matrix showing the results of the binary tree classification for Class 0, Class 1 and Class 2. . . . .	75



5.1	Pupillary Hippus - time domain indices as a function of the ALSFRS-R score. . . . .	77
5.2	Pupillary Hippus - frequency domain indices as a function of the ALSFRS-R score. . . . .	77
5.3	PLR - time domain indices as a function of the ALSFRS-R score. .	78



# Acronyms

**AAC**

Augmentative and Alternative Communication

**ALS**

Amyotrophic Lateral Sclerosis

**ALSFRS-R**

Amyotrophic Lateral Sclerosis Functional Rating Scale-Revised

**ANS**

Autonomic Nervous System

**BCI**

Brain Computer Interface

**CBF**

Cerebral Blood Flow

**CNS**

Central Nervous System

**CLIS**

Complete Locked-In Syndrome

**EEG**

Electroencefalography

**EMG**

Electromyography

**HRV**

Heart Rate Variability

**LF**

Low Frequencies

**LIS**

Locked-In Syndrome

**LMN**

Lower Motor Neurons

**LOOCV**

Leave-One-Out Cross Validation

**MRI**

Magnetic Resonance Imaging

**NCV**

Nerve conduction velocity

**PAR**

Pupillary Accommodation Reflex

**PLR**

Pupillary Light Reflex

**PSD**

Power Spectral Density

**PNS**

Parasympathetic Nervous System

**SNS**

Sympathetic Nervous System

**UMN**

Upper Motor Neurons

**VLF**

Very Low Frequencies

# Chapter 1

## Introduction

Amyotrophic Lateral Sclerosis (ALS), commonly known as Lou Gehrig's disease, is a progressive neurodegenerative disease. ALS is characterized by a progressive degeneration of motor nerve cells in the brain (upper motor neurons) and spinal cord (lower motor neurons) and when the motor neurons can no longer send impulses to the muscles, they begin to atrophy, causing increased weakness.

People affected by this pathology undergo complete paralysis in a short time, involving also autonomous breathing, swallowing and communication. In particular, in the later stages of the disease, the patient enters a condition known as "Locked-In Syndrome" (LIS): the individual becomes a "prisoner" of his own body, since the ability to move and speak is compromised. For this reason, support devices are needed to allow the individual to express himself, although in a limited way, exploiting the residual functionalities of the oculomotor apparatus (i.e. gaze direction, eye blinking...).

However, this type of devices loses effectiveness when even the ocular musculature is paralysed and the ALS patient enters a worse state, that is "Complete Locked-In Syndrome" (CLIS). In this context, it is necessary to think about new communication strategies to allow CLIS subjects to maintain a little contact with the outside. New studies[1] are oriented to the use of Brain Computer Interfaces (BCI) which exploit the EEG signal, taken by means of electrodes, to allow the patient to communicate. However, this method still requires the development of a stable communication protocol and a long and difficult training for the subject.

It has been shown that ALS affects only the locomotor system, without involving the activity of the Autonomic Nervous System (ANS). The ANS regulates the involuntary functions of the organism, including cardiac activity, digestion, breathing... Even the pupil size is controlled by the antagonistic activity of the Parasympathetic Nervous System (PNS) and the Sympathetic Nervous System (SNS), whose action causes miosis and mydriasis, respectively.

Pupil diameter varies in order to regulate the amount of light reaching the retina

(Pupillary Light Reflex), to allow the focusing of the images on the retina (Pupillary Accommodation Reflex) and even as result of mental tasks. Low frequency pupillary oscillations (Pupillary Hippius) are also observed in steady condition, without any external stimulus, but their origin is still not well defined.

The purpose of this thesis is the study of spontaneous and induced pupillary oscillations, so as to be able to trace the activity of the ANS and check whether the progress of Amyotrophic Lateral Sclerosis has effects on the sympathetic and parasympathetic functions. Consequently, it can be inferred whether pupillary diameter variations could be exploited to allow LIS and CLIS subjects to communicate.

To this end, the pupillary activity of 33 ALS patients and 10 healthy subjects has been studied, by considering the Hippius and the PLR in two distinct phases. A series of indices have been extracted from each record, such as the ratio between the powers evaluated in the LF and HF frequency bands ( $P_{LF}/P_{HF}$ ), the statistical moments from the first to the fourth order, the response time to light and dark stimuli... by considering the trend over time of these features, interesting information about pupillary activity may be obtained.

Finally, the indices extracted from the two categories of subjects (healthy and pathological) have been analyzed and provided as input to a binary tree classifier, in order to assess if there is a real difference between the two classes and, eventually, to find a combination of features that can be useful for clinicians to determine the level of neural impairment of patients.

# Chapter 2

## Background

### 2.1 Amyotrophic lateral sclerosis

Amyotrophic lateral sclerosis (ALS) is a neurodegenerative disease characterized by the degeneration of the motor neurones in the primary motor cortex, corticospinal tracts, brainstem, and spinal cord, which leads to a progressive muscular paralysis[2].

The term "amyotrophic lateral sclerosis" was coined in 1869 by the French neurologist Jean-Martin Charcot: "amyotrophy" refers to the atrophy of the muscle fibres, which are denervated as their corresponding anterior horn cells degenerate, leading to weakness of affected muscles and visible fasciculations; "lateral sclerosis" describes the scarring or hardening of tissues in the lateral spinal cord[3].

#### 2.1.1 Clinical features and onset

The motor neurons are the cells of the nervous system which allow the contraction of voluntary muscles, making movement and other vital functions (such as swallowing, phonation, and respiration) possible. Both lower (LMN) and upper motor neurons (UMN) are involved (Figure 2.1): loss of lower motor neurons, which extend from the spinal cord to the muscles, leads to muscle weakness, wasting, cramps, and fasciculations, although sensory, sexual, sphincter, and (in most cases) cognitive functions are preserved. This tends to begin in the limbs and progresses to the eye and sphincter muscle neurons in the later stages[4].

When the motor neurons of the spinal cord and brain stem are affected by the disease, the ventral roots thin and the limb, tongue, and oropharynx muscles become amyotrophic. These lower motor neuron features contribute to mortality more so than the features caused by the loss of upper motor neurons in the brain, which include spasticity, clumsiness, brisk reflexes, and functional limitations[5]. Paralysis is progressive and leads to death due to respiratory failure within 2–3 years for bulbar onset cases and 3–5 years for limb onset ALS cases.

The disease can be classified into two categories, according to the localization of the motor neurons involved:

- **Spinal onset**, where spinal motor neurons are compromised. The degeneration of the corticospinal neurons causes the spinal cord's lateral tracts to scar. Inclusions, or aggregated proteins consisting of round or threadlike shrunk spinal motor neurons, deposit as ALS progresses[4]. These cytoplasmic proteins are commonly present in the motor neurons of sporadic and patients with familial ALS[4]. In this case early symptoms are related to muscle weakness and focal atrophy.
- **Bulbar onset**, in which lesions are related to the motor neurons of the brainstem: in this case, the disease begins with dysarthria and dysphagia for solids or liquids and facial weakness, poor palate elevation, difficulty chewing, impaired swallowing, tongue fasciculations, and atrophy are later symptoms [6]. About a third of patients experience this type of disease onset[4].

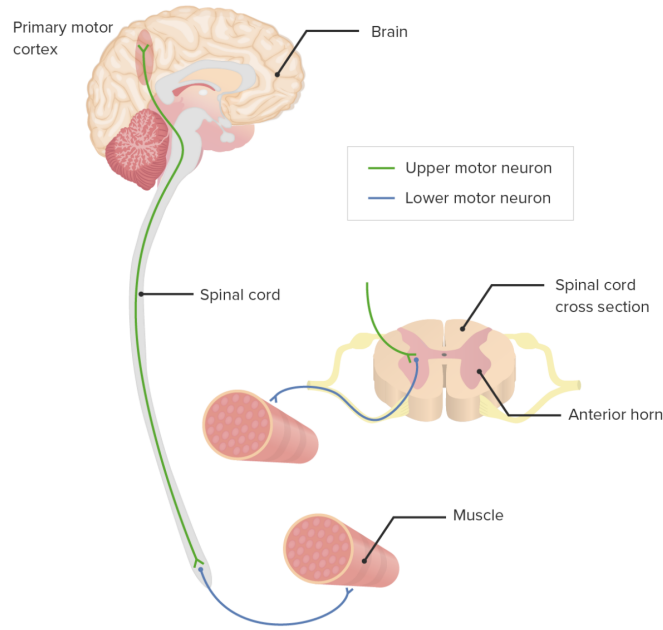


**Figure 2.1:** The primary motor system showing connections among upper motor neurons, lower motor neurons, and the muscle effector organ.

However, these distinctions, useful for defining the appearance of the disease, do not always appear so clear in the evolution of the same, as the two forms can overlap.

Another classification, based on the genesis of the disease, distinguishes ALS in two forms:



- **Sporadic ALS** (90 - 95% of cases): it is not related to a familial transmission. In most cases, no genetic causes have been identified. Sporadic ALS usually occurs in patients in their mid-to-late fifties.
- **Familial ALS** (5 - 10% of cases): 20% of them is related to a mutation of the SOD1 gene, about 2-5% has mutations in the TARDBP gene (TDP-43) and about 25% of them have nucleotide expansion of the C9ORF72 gene[7]. Familial ALS occurs in patients in their late teens or early adulthood.

There is usually a progressive loss of the ability to move, which can lead over time to complete immobility. However, even in the most advanced stages, the disease affects only the motor system, while the other neurological functions (such as sphincter and sensory functions) remain unchanged. It has been shown that deficits of the Autonomic Nervous System are common (75% of patients) but mild in most patients (85%), and they were moderate involvement in a minority (15%)[8].

Also Ocular Motor Neurons (OMNs), including the oculomotor, trochlear and abducens nuclei, which regulate eye movement, persist throughout the disease[9], because the anatomy and the innervation patterns of the oculomotor system are different from those of motor neurons. Consequently, eye-tracking devices are used to enable paralysed ALS patients (who can no longer speak) to communicate. However, in many patients with sporadic ALS, abnormalities in eye movements occur, such as an increasing latency in the antisaccade task, a decrease in the speed of smooth pursuits, and an increase in the amplitude of saccadic intrusions. These abnormalities may be due to complications in the frontal lobe[10]. As the disease progresses, and especially in tracheostomized patients for a long time, oculomotor dysfunction may appear which could lead to a complete paralysis of the eye and to a complete external ophthalmoplegia[11][12].

### 2.1.2 Epidemiology

Amyotrophic Lateral Sclerosis is more common in men than in women by a factor of 1.5, and the rate of disease progression may be more rapid in patients with an older age at onset, a bulbar site of onset, cognitive impairment, and certain genotypes. The average age of onset of the disease is about 60 years in sporadic ALS, unlike in familial cases with an earlier onset[13].

The **incidence rate**, i.e the number of new cases diagnosed in a year, is 1-3 in 100,000 inhabitants. The **prevalence rate**, that is the number of patients living with ALS, is about 5-7 cases per 100,000 inhabitants/year, especially thanks to improvements in the diagnosis of the disease. In Italy, there are more than 6,000 patients with ALS and about 2,000 are expected each year[14](Figure 2.2). What differs most for every person is how fast and in what order symptoms and progression occur. And, while the average survival time is three years, about 20%



**Figure 2.2:** The prevalence rate in Italy. Source: *EURALS Consortium - European amyotrophic lateral sclerosis consortium*[14].

of people with ALS live five years, 10% survive 10 years and 5% live 20 years or longer[15].

### 2.1.3 Diagnosis

ALS is a difficult disease to diagnose since there is no one test or procedure to ultimately establish the diagnosis of ALS. It's only through a clinical examination and series of diagnostic tests, often ruling out other diseases that mimic ALS, that a diagnosis can be established. The initial symptoms are variable among patients depending on the degree of upper and lower motor neuron involvement and which regions of the body are affected. They are also common in other neurodegenerative diseases, so the diagnosis may be uncertain initially and the development of additional features is necessary. Common diagnostic techniques include[15]:

- electrodiagnostic tests, including electromyography (EMG) and nerve conduction velocity (NCV);
- blood and urine studies, including high resolution serum protein electrophoresis, thyroid and parathyroid hormone levels and 24-hour urine collection for heavy

- metals;
- spinal tap;
- X-rays and magnetic resonance imaging (MRI);
- myelogram of cervical spine;
- muscle and/or nerve biopsy;
- through neurological examination.

### 2.1.4 Clinical care

Although the research is focused on understanding the pathophysiology of ALS, there is currently no effective cure. For this reason, treatment aims to improve the patient's quality of life, to preserve their autonomy and to prolong their life expectancy.

Until recently, the only approved drug is *riluzole*: it is a benzothiazole derivative that blocks glutamatergic neurotransmission in the Central Nervous System (CNS), which is thought to exert neuroprotective effects[16]. The drug is generally well-tolerated, but its effectiveness is limited to delaying the use of mechanical ventilation. Given the severity of the illness and lack of effective disease modifying agents, most patients with ALS consider trying complementary and alternative therapies.[17] Some of the most commonly considered ones include special diets, nutritional supplements, cannabis, acupuncture, chelation and energy healing[17].

In May 2017, FDA approved a new intranervous drug, the *edaravone*, but in Europe ALS investigators recommend additional studies before an European approval. A six-month clinical trial conducted in Japan on 139 ALS patients[18], reported remarkable results, showing a slowing in the decline of the ALS Functional Rating Scale-Revised (ALSFRRS-R) score by 33%. The ALS quality-of-life measures also tracked accordingly showing a significantly slower decline as well respiratory measures but without statistical significance[5].

Moreover, in recent years, stem cell therapies are being evaluated as a new frontier for the treatment of ALS and other neurodegenerative diseases, aiming to protect surviving motor neurons (they are not able to replace dead motor neurons). Mesenchymal stromal cells (MSCs), which are isolated from fat or bone marrow biopsies, expanded in vitro, and then injected into the thecal space via lumbar puncture or directly intraspinally, are primarily being used as an autologous stem cell-therapy for ALS due to their ability to secrete neurotrophic factors and modulate the immune system. The study, which is in the early stages of the trial, shows that this type of stem cells appears safe and the results warrant further exploration of efficacy in phase II trials[19].

Another clinical study, involving fetal human neural stem cells, reports interesting results. Stem cells are directly injected into the anterior horns of the spinal cord of the ALS patients and no increase of disease progression was observed for up to 18 months after surgery[20]. This strategy represents a safe cell therapy approach that will allow for the treatment of a great number of later-phase ALS patient, although concomitant immunosuppression treatment is needed to prevent transplant rejection.

Ventilatory failure is the leading cause of death. Pulmonary functions, pulse oxymetry and reported symptoms are constantly monitored in order to assess the progressive respiratory weakness. Assisted ventilation allows to prolong the patient's life. This in a non-invasive procedure and in case of failure, invasive ventilation methods (e.g. tracheostomy) are required.

During the disease, swallowing difficulties can arise, which can lead to poor nutrition and a loss of weight in the patient. If swallowing worsens further, not allowing the patient to feed and hydrate sufficiently, enteral nutrition through endoscopic percutaneous gastrostomy become necessary.

### **2.1.5 Locked-In Syndrome and communication systems**

Because of the progressive deterioration of motor neurons, which leads to complete paralysis of voluntary muscles, approximately 80 to 96% of people with ALS become unable to communicate through natural speech. As disease progresses and dysarthria becomes severe, profound weakness resulting in reduced movement of the speech musculature and severely reduced phonation become increasingly common. Patients at advanced state of the disease, who are subject to tracheotomy and mechanical ventilation, degenerate into a locked-in state. Individuals affected by Locked-In Syndrome (LIS) are deprived of any voluntary muscle function except for blinking and limited eye movements; in Complete Locked-In Syndrome (CLIS) also eyelid and eye movements are lost[21]. In this way, any form of communication through movements is gradually compromised and a supporting strategy is required and tools, environmental, partner adaptations, and behavioral changes are introduced.

People with ALS often request oral exercises to improve strength and mobility for speech and swallowing; however, recent studies[22] report that speech treatment strategies should be discouraged, because of the pathophysiology and the degenerative nature of ALS[23]. The patient should be immediately associated with support devices, which have a growing technological level as the subject's communication skills worsen. In this way, patients can preserve their energy for priority speaking tasks and reduce fatigue.

These communication supports are referred to as Augmentative and Alternative Communication (AAC) strategies and includes a great variety of strategies,

techniques, and devices, ranging from simple yes/no eye blinks to sophisticated computer-based systems and speech-generating devices. According to the technological level of the devices, AAC can be classified as follows:

- **No-tech AAC:** it refers to any form of communication through human body, such as vocalizations, tongue clicks, eye movements and blinks, and gestures. No other support devices are required.
- **Low-tech AAC:** simple equipment like pen, paper, communication boards... and other non-computer based devices. There are many strategies of communication. For example, the subject with the impairment can choose one option among those proposed by the interlocutor.
- **High-tech AAC:** it regards electronic systems that allow the user to type or select a message that is spoken aloud. They are called speech-generating devices (SGDs) and each one differs from the others in technology, symbols to represent language on the machine, the way the user produces messages and output method or type of speech generated.

SGDs can be adapted for access by individuals with a variety of physical abilities. As long as eye activity is preserved, eye movements or even pupillary contraction/dilatation can be considered to generate output. The latter one is a possible alternative only if there is certainty that the sympathetic and parasympathetic activity of the ANS is unaffected by the illness. In recent years, Brain-computer interface (BCI) systems are being evaluated to allow individuals in the late stages of ALS, who enter LIS or CLIS, to control an SGD using only their brain activity.

### **Pupil response as a communication system**

Typical BCI either use invasive methods or EEG in combination with machine learning techniques to measure neural activity. Moreover, such techniques require surgical procedure, maintenance (for example, electrode cleaning), and a training with the individual. An alternative way is represented by communication through pupil responses.

Pupil dilation is known to accompany emotionally arousing events, but also a variety of mental functions, including decision-making. Therefore, pupil diameter variations can be exploited as a means of communication: Stoll J. et al.[24] found that mental arithmetic could be a tool for patients to control and maximize their pupil dilation to signal their responses. Participants were asked to perform a series of mental tasks and to answer question with a clear yes/no choice. Both healthy and LIS subjects were involved in this study and the results showed a correlation between pupil size variations and the mental effort: up to 90% decoding performance was reached.

Pupil size controlled through mental effort reflects neuro-physiological activity that is easy and inexpensive to measure in daily life, requiring only a bedside camera. Furthermore, in cases of complete locked-in syndrome, approaches that require some residual volitional movements, such as sniffing or blinking, are by definition unsuitable. In contrast, pupillary system may be exploited in CLIS patients without training.

## 2.2 Autonomic Nervous System: anatomy and physiology

The Autonomic Nervous System (ANS) is that part of the nervous system which regulates the visceral functions of the organism and controls smooth muscles, heart, and glandular functions[25]. Assisted in many cases by the endocrine system, it has a modulating function on cardiac output and blood pressure, gastrointestinal activity, glandular secretions and many other visceral functions; however, it is much faster than the endocrine system, being able to respond promptly, even in the interval of a few seconds, to any changes in the internal environment, ensuring a rapid restoration of the conditions of stability.

The autonomic nervous system is so defined because its activity is carried out in an *unconscious* way. For example, it is not possible to decide independently to increase own heart rate; this is achieved through unconscious nervous mechanisms, when it is necessary. For this reason, the autonomic nervous system is also defined as an *involuntary nervous system*.

Based on anatomical, neurochemical and functional differences, it is possible to distinguish the autonomic nervous system in two branches: the **parasympathetic nervous system** (PNS) and the **sympathetic nervous system** (SNS). Both innervate most of the organs and they assume a configuration known as *double innervation*. The two systems perform opposite functions and so are their effects. However, this antagonism does not create conflicts, because when vegetative nervous system is required, the two autonomous divisions are activated in a complementary way, with one of them more activated than the other one. For example, the parasympathetic system is at the peak of its activity during rest conditions, when it stimulates the digestive organs and inhibits the cardiovascular system; this state is called *rest and digest condition*. On the contrary, the sympathetic system is more active during periods of excitement or intense physical activity, when it coordinates a set of physiological changes known as *fight-or-flight* response[26], which prepares the body to face threatening situations. During the fight-or-flight response, the heart frequency and contraction force increases, blood flow is diverted from the gastrointestinal organs to the skeletal muscles and heart, and energy stores are mobilized. Organs are innervated by both systems, except for the sweat glands, the

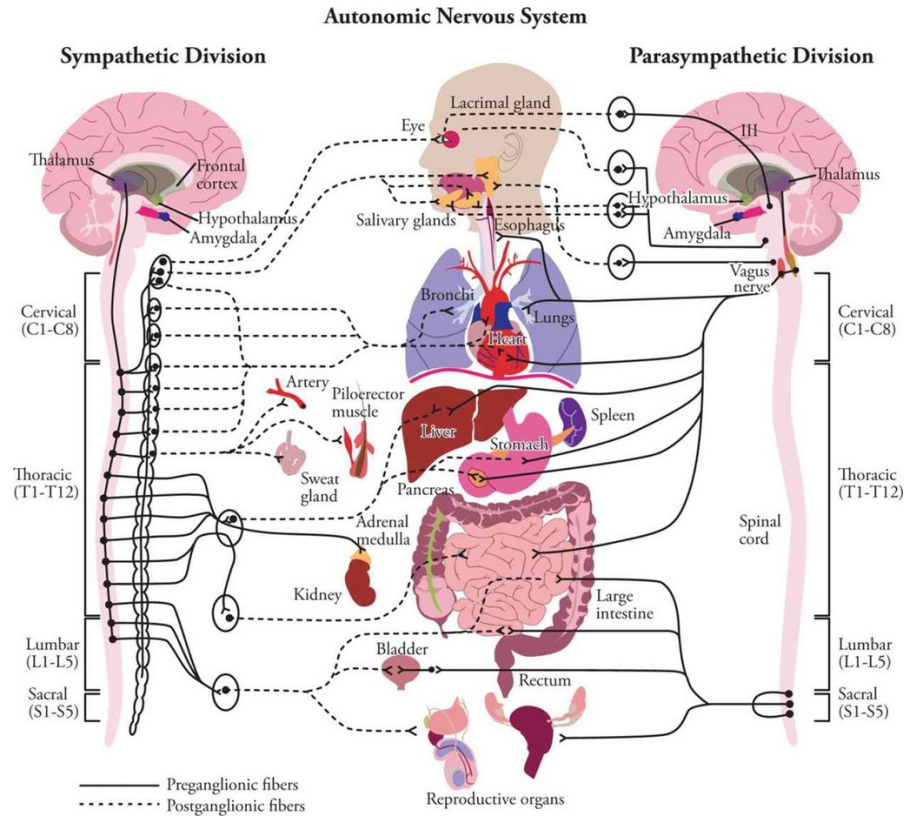


**Figure 2.3:** Autonomic Nervous System anatomy.

arrector pili muscles, and most blood vessels, which receive uniquely sympathetic influences.

The main function of the autonomic nervous system is to regulate the activity of the effector organs in order to maintain homeostasis through a mechanism of "fast and loose" that allows a great control over the effector organs. For example, both parasympathetic and sympathetic nervous system control heart rate frequency; when an increased heart rate is required, the frequency action potentials of sympathetic neurons increases, while that of parasympathetic neurons decreases.

### 2.2.1 Anatomy of the sympathetic nervous system

The sympathetic nervous system is also known as the *thoracolumbar* autonomic nervous system. The preganglionic neurons of the sympathetic nervous system, in fact, emerge from the thoracic and lumbar tracts of the spinal cord and originate in a region of gray matter called lateral horn or intermediolateral column.

Preganglionic and postganglionic neurons are anatomically connected in three ways

(Figure 2.4):

- In the first and most common type of anatomical arrangement, preganglionic neurons have short axons that originate in the lateral horn of the spinal cord, from which they emerge through the ventral root. Then, the ventral and dorsal roots join to form the spinal nerve, through a branch called *white rami communicantes* (preganglionic neurons are myelinated) and penetrates into one or more sympathetic ganglia located just outside the spinal cord. Most postganglionic axons return to the spinal nerve via a branch called *gray ramus communicans* (postganglionic neurons have unmyelinated axons) and reach the effector organ. The sympathetic ganglia are connected to each other, forming the *sympathetic chain* or *sympathetic trunk* that runs in parallel to the vertebral column, on both sides of it. In this way, the activation of the sympathetic nervous system simultaneously produces diffuse effects on many target organs.
- The second possible organization of sympathetic fibers involves the direct innervation of the target organs by the preganglionic neurons, but do not form synapses with postganglionic neurons, such as the adrenal medulla of the adrenal gland.

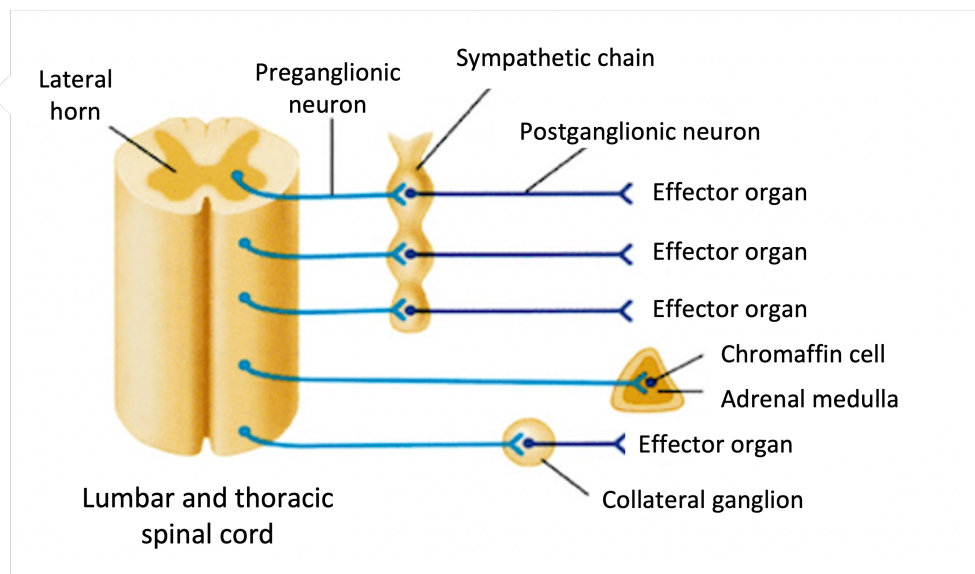


**Figure 2.4:** Preganglionic and postganglionic sympathetic connections via the three anatomical arrangement.

- Finally, the third possible organization of sympathetic neurons consists in the formation of synapses between preganglionic and postganglionic fibers in



structures called *collateral ganglia*, located between the central nervous system and the effector organs. Inside the collateral ganglion, the preganglionic neuron forms synapses with many postganglionic neurons, which innervate multiple target organs. Since the collateral ganglia are not connected to each other, the sympathetic nervous system can reach well-defined target organs and thus exert less widespread effects. They innervate organs of the abdominal and pelvic region. These include the celiac ganglia, superior mesenteric ganglia, and inferior mesenteric ganglia.

### 2.2.2 Anatomy of the parasympathetic system

Parasympathetic preganglionic neurons originate in the brain stem or sacral spinal cord. In this case, the axons are relatively long and end in ganglia located near the effector organs, forming synapses with short postganglionic neurons. In this case, the axons are long and end in ganglia located near the effector organs, forming synapses with short postganglionic neurons. At the cranial level, the axons of originate from cranial nerve nuclei located in the brainstem and send the own axons in the cranial nerves.

An important cranial nerve is the *vagus nerve* which originates in the *medulla oblongata* and innervates many organs including lungs, stomach and heart. Other cranial nerves consisting of parasympathetic preganglionic axons are the **oculomotor nerve**, which innervates the smooth muscle of the eye in order to control the pupillary diameter and curvature of the crystalline lens, the facial nerve, and the glossopharyngeal nerve. Unlike the sympathetic preganglionic neurons, the fibers that originate in the spinal cord do not run into the spinal nerves, but travel along it with other preganglionic parasympathetic neurons to form the pelvic nerves.

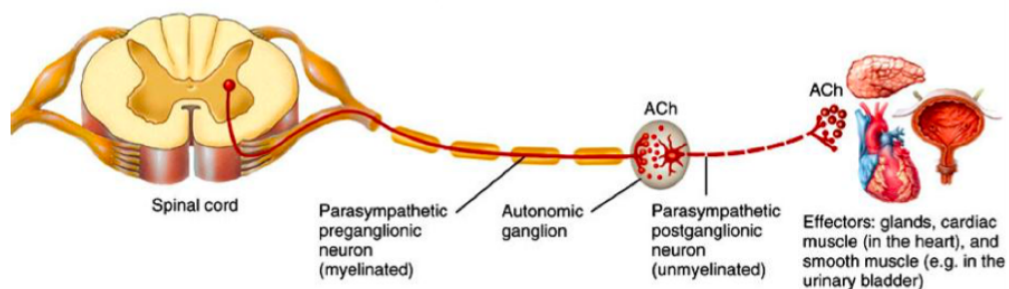


**Figure 2.5:** Preganglionic and postganglionic neurons connection in the Parasympathetic Nervous System.

## 2.3 The visual system

### 2.3.1 Eye anatomy

The eye can be divided into three concentric layers. The most external one consists of the *sclera* and the *cornea*. The **sclera**, a consistent connective tissue, form the "white" part of the eye. In the anterior part, the **cornea** originates from the sclera, a transparent structure that allows light to penetrate in the eye.

The middle layer of the eye consists of the *choroid*, the *ciliary body* and the *iris*. The **choroid** is a layer of highly pigmented tissue placed below the sclera, it also contains blood vessels that nourish the deep layer of the eye, where photoreceptors are placed. The **ciliary body** contains the ciliary muscles, that are attached to the *crystalline lens*, through thin tendons of connective tissue called *zonular fibers*. The **lens** focuses the light on the *retina*, where visual information is transduced. The ciliary muscles, which contract and relax, change the shape of the lens, allowing light focusing. The **iris**, which is formed by two layers of pigmented smooth muscle cells, is located in front of the lens and determines the color of the eyes. The **pupil** is a hole at the center of the iris, which allows light to penetrate into the back of the eye. The iris regulates the diameter of the pupil, thus varying the amount of light reaching the back of the eye.

The most inner layer of the eye is represented by the retina, which is formed by nerve tissue containing the photoreceptors, cells sensitive to light waves. There are two types of photoreceptors, *cones* and *rods*, which perceive the intense and the suffused light, respectively. Thus the retina is a *phototransductor*, which transforms

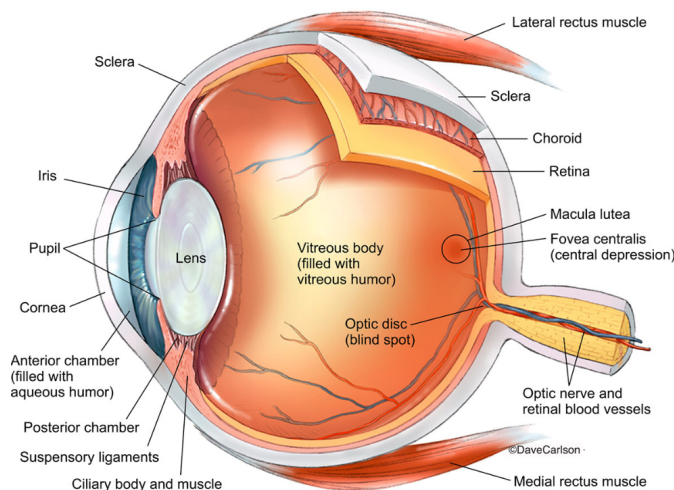


Figure 2.6: Eye anatomy

light energy into electricity. In the outer part of the retina and attached to the choroid there is the *retinal pigment epithelium*, with an high concentration of melanin, which prevents light reflexion through the retina; this phenomenon would lead to an image distortion.

There are two important retinal areas: the central point of the retina, the **fovea**, where the light from the centre of the visual field is directed and the **optic disk**, that is beginning of the optic nerve and the entry point for the major blood vessels that supply the retina. Because of the lack of photoreceptors, this region is a **blind point** and here the light can not be perceived.

The lens and the ciliary body split eye in two fluid-filled chambers: the **anterior segment**, in front of the lens and the ciliary body and the **posterior segment**, behind them. The anterior segment contains the **aqueous humor**, which provides nutrients to the cornea and the lens while the posterior segment contains the **vitreous humor** that maintains the spherical structure of the eye.

### 2.3.2 Autonomic control of the pupil

The Autonomic Nervous System plays a crucial role in the maintenance of body's homeostasis. In this context, pupillary changes (mediated by the parasympathetic and sympathetic nervous system), may provide a window into the complex psychophysiological regulatory network mechanisms and a means of assessing whether the ANS is impaired by neurodegenerative diseases such as ALS.

The pupil is the optical element which control the amount of light that reaches the retina, according to its contraction/dilatation level. Furthermore, pupil diameter changes size in response to emotional and cognitive stimuli (i.e. task-evoked stimulation) which is increasingly used to identify potential abnormalities in emotional/cognitive processes and thus in ANS, since it predominantly controls pupillary responses[27].

The normal human pupil can change diameter from 8 mm to 1.5 mm, it depends on iris size and it is controlled by two concentric smooth muscles:

- the **sphincter pupillae**, which is located in the inner layer of the iris, consists of circular musculature and it is controlled by the parasympathetic nervous system; its contraction causes a reduction in the pupil diameter (**miosis**);
- the **dilator pupillae** is a layer of radial muscle fibers in the external part of the iris; it is under the control of the sympathetic nervous system and its contraction produces pupil dilatation (**mydriasis**).

These muscles are innervated by postganglionic neurons originating from the ciliary and superior cervical ganglia, which in turn receive preganglionic inputs from the Edinger-Westhal preganglionic cells (EWpg) and intermediolateral cell (IML)

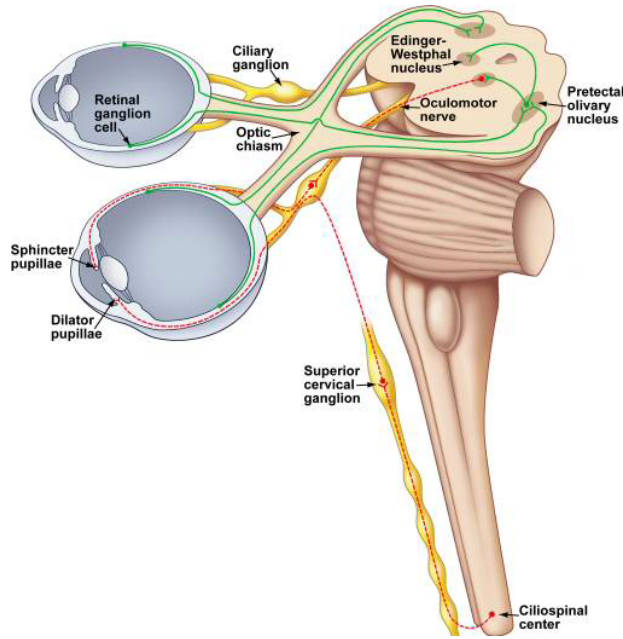


**Figure 2.7:** Summary diagram of current understanding of the afferent, central, and efferent pathways controlling pupil diameter. The iris musculature innervated by autonomic efferents from both the parasympathetic and sympathetic components of the autonomic nervous system.

respectively[28]. Neurons in the EWpg and IML are controlled by central nervous system inputs that are influenced by a variety of factors such as retinal irradiance, viewing distance, alertness and cognitive load.

In Figure 2.7 a diagram of afferent, central, and efferent pathways controlling pupil diameter is reported. The *pretectal olivary nucleus* receives input from the temporal retina of the ipsilateral eye and the nasal retina of the contralateral eye.

The pretectal olivary nucleus projects bilaterally to the *Edinger-Westphal nucleus*, which contains **parasympathetic**, preganglionic, pupilloconstriction neurons. Their axons travel in the third cranial nerve to synapse upon postganglionic pupilloconstriction neurons in the *ciliary ganglion*. The axons of these postganglionic neurons leave the ciliary ganglion and enter the eye via the short *ciliary nerves* and travel through the choroid to innervate the sphincter muscle of the iris.

The **sympathetic** preganglionic pupillodilation neurons are found at the C8-T1 segmental levels of the spinal cord. The axons of these neurons project from the spinal cord via the dorsal roots, enter the sympathetic trunk and then project rostrally to the superior cervical ganglion where they synapse with the postganglionic neurons. These neurons project from the superior cervical ganglion through the neck and carotid plexus and into the orbit of the eye. These fibers enter the eye

either by passing through the ciliary ganglion and entering in the short ciliary nerves, by bypassing the ciliary ganglion and entering via the long ciliary nerves, or through the optic canal. Upon entering the eyes, these axons travel through the choroid and innervate the dilator muscle of the iris[28].

The sphincter pupillae is an annular band of smooth muscle (100–170  $\mu\text{m}$  thick; 0.7–1.0 mm wide) encircling the pupil. The smooth muscle cells of the sphincter are clustered in small bundles and connected by gap junctions which ensure synchronized contraction of the sphincter muscle. The sphincter receives muscarinic, cholinergic innervation from the short ciliary nerves. The dilator pupillae is composed of radially oriented smooth muscle fibers that are myoepithelial in origin. Individual fibers are approximately 50  $\mu\text{m}$  long and 5–7  $\mu\text{m}$  wide. In the pupillary zone, dilator muscle processes fuse with the sphincter pupillae, while peripherally, their processes attach to the ciliary body. The dilator receives adrenergic innervation from the long ciliary nerve.

### Pupillary Light Reflex

The Pupillary Light Reflex (PLR) is the constriction of the pupil that is elicited by an increase in illumination of the retina. The reflex allows the eye to adjust the amount of light reaching the retina and protects the photoreceptors from bright lights. Both sphincter pupillae and dilator pupillae act to control the amount of light entering the eye. The action of the two muscles is antagonistic, since they are controlled by the parasympathetic and sympathetic branch, respectively:

- when the amount of light reaching the retina increases, the iris sphincter contracts in order to reduce pupil size (**miosis**) and at the same time the dilator relaxes;
- on the contrary, when light is removed, pupils dilate (**mydriasis**) thanks to iris dilator contraction and sphincter relaxation.

The direct PLR, present in almost all vertebrates, is the constriction of the pupil in the same eye as it is stimulated with light. The reflex is *consensual*: if one eye only is stimulated, both pupils constrict. The **direct response** is the change in pupil size in the eye to which the light is directed whereas the **consensual response** is the change in pupil size in the opposite eye.

The PLR has typically been divided into two separate pathways based on the clinical manifestations of the defects in this reflex (Figure 2.9). The *afferent pathway* is composed of both the retinal cells that project to the pretectum as well as their recipient neurons, which project bilaterally to the EW nucleus. The *efferent pathway* is composed of the preganglionic pupilloconstriction fibers of the EW nucleus and their postganglionic recipient neurons in the ciliary ganglion, which project to the sphincter muscle of the iris.

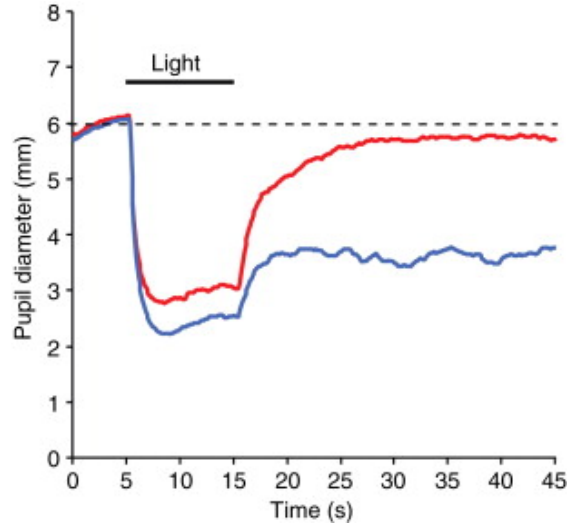


**Figure 2.8:** Pupilloconstriction elicited by a 10 s light stimulus of 493 nm wavelength light at  $14.0 \log \text{ quanta } \text{cm}^{-2}$  per second irradiance (blue trace), and 613 nm wavelength light at  $14.1 \log \text{ quanta } \text{cm}^{-2}$  per second irradiance (red trace). Note that a 473 nm stimulus, drives a larger pupillary response than the 613 nm stimulus (red trace). The pupilloconstriction induced by the 473 nm light is maintained following stimulus offset.

### Pupillary Hippus

Even in the absence of light or cognitive stimuli, the pupil is in constant motion. Such pupillary unrest is known as **hippus**[29], which consists of low frequency spontaneous pupillary oscillations: hippus frequency ranges from 0.04 to 2 Hz (with a peak frequency near 0.3 Hz in most studies) and the magnitude of the pupil size variations ranges from not detectable (usually with naked eye observation) to over 0.5 mm. Pupillary hippus is usually considered benign, although exaggerated hippus has been associated with disorders like epileptic seizures[30] and increased mortality[31]. Hippus is spasmodic, cyclic, bilaterally in phase and oscillation amplitude varies with many neural factors, including arousal and cortical excitability[32].

The mechanism behind the pupillary hippus is not well known yet: there are some hypothesis that pupil diameter is influenced by the relative input of the sympathetic nervous system and parasympathetic nervous system and hippus is likely due to feedback or noise from their continuous neurological antagonism.

However, Turnbull et al.[29] found that hippus is mainly influenced by the level of PNS input, after perturbing the balance between PNS and SNS activity to produce mydriasis; it challenges the assumption that it originates from the relative

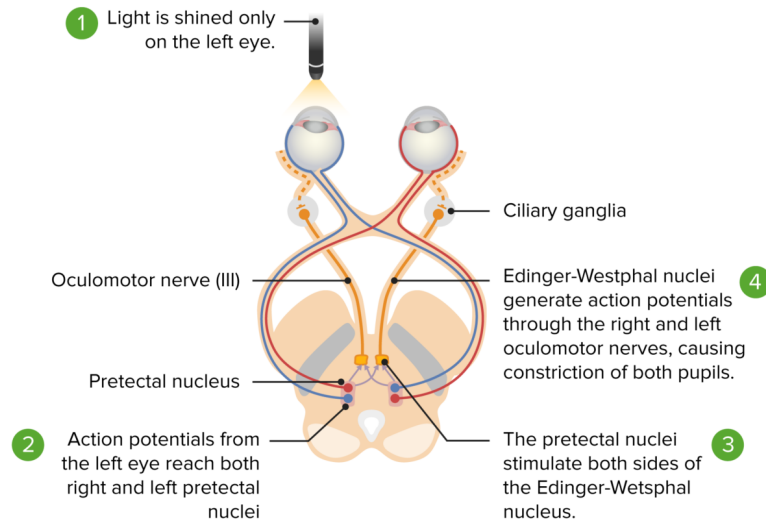


**Figure 2.9:** Pupillary light reflex pathway: from light stimulation of the retina to the midbrain. Afferent pathway (red and blue lines): Left light stimulus goes from the left retina to the optic chiasm to the optic tract, ending at the ipsilateral pretectal nucleus. The pretectal nucleus supplies both left and right Edinger-Westphal nuclei. Yellow lines show impulse from both nuclei reaching both ciliary ganglia and resulting in bilateral miosis.

PNS-to-SNS input or that it is related to the absolute level of SNS activity. Hippus movements are bilaterally consensual and this suggests that they originate in the central nervous system rather than in the eye. Moreover, it has been shown that pupillary hippus is correlated with respiratory, cardiac activity and neural plasticity. The latter is found by testing binocular rivalry before and after monocular deprivation (MD)[33], which transiently shifts ocular dominance in favor of the deprived eye. Increased amplitude hippus is recorded and this suggests that, by observing amplitude variations of pupillary oscillations, it is possible to find a direct correlation with visual cortical excitability changes.

## Pupillary Accommodation Reflex

The Pupillary Accommodation Reflex (PAR) is the property of varying the refractive power of the crystalline lens. The *refraction* describes the deflection of light rays to change their angle as they pass onto the retina, which is necessary for the formation of a focused image. The cornea contributes the majority of the refractive power of the eye, the remaining percentage being attributed by the lens. The shape of the lens is due to two opposing forces:

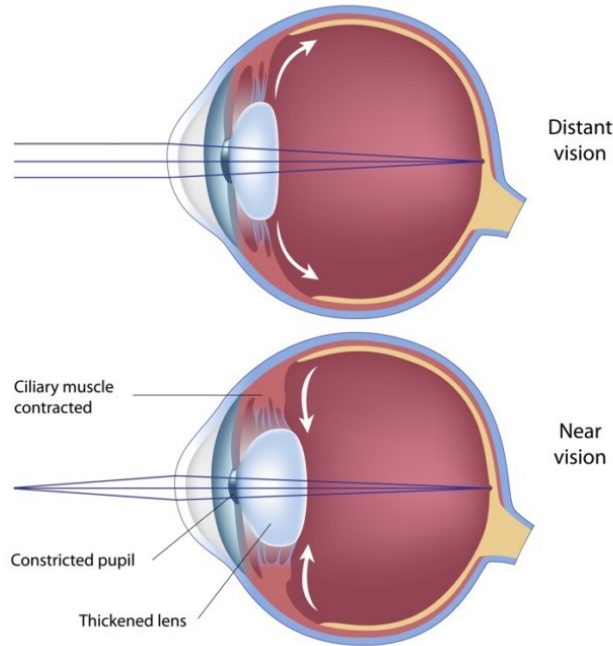


**Figure 2.10:** Schematic diagram of accommodation.

- The internal elasticity of the lens, which tends to keep the lens rounded up. A more curved lens refracts light to a greater degree, as a result of the circular muscle fibres contraction.
- The force exerted by radially arranged zonule fibers, which flatten the lens when stretched. The zonule fibers are attached to the ciliary muscle.

The variation of the lens is equal on all meridians and it occurs *consensually* in both eyes. Thus, accommodation allows to focus on the retina images that form on anterior or posterior planes. When focusing on a distant object, the lens is flat and thin, and therefore has less refractive power. To achieve this, the force exerted by the radially arranged zonule fibres exceeds the intrinsic elasticity of the lens. The tension in the zonule fibres is caused by the relaxation of the ciliary muscle. For nearby objects, the lens becomes thicker and rounder, increasing its refractive power. Accordingly, the intrinsic elasticity of the lens prevails, while the zonule fibres relax as a consequence of the ciliary muscle contraction.

The accommodation reflex is an adjustment of the eye for near vision and it is part of a complex mechanism which include two more phenomena: *miosis*, which allow to increase the depth of focus, and *convergence of the eyes*[34], that is due to the contraction of both medial rectus muscles. All these movements are controlled by the fibres of the oculomotor nerve.



## Chapter 3

# Methods and materials

### 3.1 Data set

In order to assess the possible effects of the pathology on the Autonomic Nervous System through the study of pupillary behaviour, 33 ALS patients were recruited and subjected to the acquisition of their own pupillographic signal. The subjects chosen for this study were selected in collaboration with the Amyotrophic Lateral Sclerosis Expert Center (CRESLA, Turin) and the “Mons. Luigi Novarese” Recovery and Functional Re-education Center (CRRF “Mons. Luigi Novarese”, Mocrivello), with the understanding and written consent of the subjects, following the tenets of the Declaration of Helsinki, under the approval of the Ethics Committee of University of Turin.

The data set is divided into two subgroups, according to the temporal modalities of signals acquisition: **Longitudinal Study Group** and **Transversal Study Group**.

#### 3.1.1 Longitudinal Study Group

The Longitudinal group is composed of 20 subjects (15 male and 5 female subjects, with a median age of 66 years and a standard deviation of 11 years) and they were selected with the objective of monitoring pupillary characteristics over time, beginning from the initial diagnosis of ALS or other motor neuron diseases and continuing throughout the progression of the disease. A professional orthoptic evaluations prior to each of the tests was carried out, to characterize ocular function. The patients recruitment and testing began on October 3, 2017 and continued up until February 8, 2019.

In order to this, the subjects were selected after their initial diagnosis, after which the first tests were performed. Subsequent tests were performed during their following control visits to the Molinette Hospital of Turin, separated by a time

period of around three months, depending on the subject's availability. If the subjects missed any of the programmed tests (due to any number of complications, varying from personal to health issues) another one would be programmed for the next temporal window, that coincided with the subjects' control visits to the hospital.

### 3.1.2 Transversal Study Group

The second study group was selected with the objective of monitoring pupillary characteristics at the later stages of ALS, specifically the LIS stage. Additionally, if subjects other than those diagnosed with ALS, but still suffering from LIS condition were available, they would also be taken into consideration for participation in the current study.

15 cognitively unimpaired subjects (8 male and 7 female subjects, with a median age of 57 years and a standard deviation of 6 years) were selected, again following professional orthoptic evaluations prior to each of the tests, to characterize ocular function. The pupillographic signals have been recorded only once, during the control visit to the Molinette Hospital.

Moreover, a subset of 5 subjects (2 male and 3 female) belonging to the Transversal Study Group was selected to participate in a second test session with the objective of evaluating the effectiveness of the PAR as an input method for binary communications systems.

## 3.2 Experimental setup

The acquisition of the pupillographic signal is also divided into two phases:

1. **Hippus recording:** in the first part of signal acquisition, the patients were presented with a dark canopy made from thick black cloth, that completely covered the surrounding environment, and the test elements that were located inside it. This allowed to insert subjects in a standardized dark environment without being dependent of the testing location or subject position. As a result, the recordings represent only the spontaneous pupillary oscillations of both eyes (i.e. the hippus);
2. **PLR recording:** the last part of the acquisition consists in the recording of light stimuli response of the pupil. The patients were subject to four cycles of bright and dark stimuli through a monitor placed inside the canopy, at 50 centimeters in front of the face of the subjects. This was achieved by alternating between complete black (dark stimulus) or white (bright stimulus) screens. The monitor used for this purpose was a 17 inch, 1280 x 1024 pixel,

75 Hz Belinea 1705 S1 LCD monitor. A small gray square (20 by 20 pixels) was also displayed at the center of the screen to allow subjects to focus on a single point.

During the test, the stimuli were managed and presented by a MATLAB® algorithm, as detailed by the following procedure: during the first 60 seconds the dark stimulus was presented, to allow for an initial adaptation to the dark environment and hippus recording, after which four cycles of bright and dark stimuli, lasting 4 and 30 seconds respectively, were presented, allowing the observation of four different PLR events.

The sensor involved in the pupillographic signal recording was the Eye Tribe Tracker [35] realized by IMotions® (Figure 3.1), a device which provides reliable pupillometry data. It allows controlling applications with user's sight on desktop and tablet computers. The sensor was located at an approximate distance of 40 centimeters from the patient's face, and was set to a sampling frequency of 30 Hz. The recordings and software were executed on an Asus P2530U Notebook with an Intel Core i7-6500 (4 CPUs) processor, 8 GB of RAM and a 64-bit Windows 10.

For each subject and for each visit there is a matrix consisting of a number of rows that depends on the duration of the recording, and 8 columns, each representing a different measurement:

1. Test time
2. Average Pupil Size
3. Right Pupil Size
4. Right Pupil X coordinates
5. Right Pupil Y coordinates
6. Left Pupil Size
7. Left Pupil X coordinates
8. Left Pupil Y coordinates



**Figure 3.1:** The Eye Tribe Tracker of IMotions®, the device used for the pupillo-graphic signal acquisition.

### 3.3 Signal processing

Once data acquisition has been completed, the study continued with the pupillo-graphic signals processing, in order to extract descriptive indices from both the first part (that represents the Pupillary Hippius) and the second part (which refers to the Pupillary Light Reflex) of the recordings. All the information about the signals has been extracted through a series of algorithms implemented in MATLAB®. Then, these features have been collected in a database, consisting of other clinical parameters of the same subjects, which will be described later.

#### 3.3.1 First part: Pupillary Hippius

##### Signal pre-processing

In order to obtain useful information about the spontaneous pupillary oscillations, the signal processing step started by considering the first and second column of the data matrix of each recording session, which correspond to the **Test Time** and to the **Average Pupil Size**, respectively.

The sampling frequency of the original signal is not constant. Therefore, as an initial step, a new time axes has been defined, choosing as sampling interval the smallest time difference between one sample and the next one of the Test Time array (which corresponds to approximately 33 ms). Accordingly, the Average Pupil

Size signal has been resampled at the new sampling frequency of 30 Hz, using a one-dimensional interpolation of the original signal.

The acquisition of the pupillographic signal could be difficult and for short time intervals the sensor did not detect the pupil diameter; in such cases, a value of zero was assigned to the pupillary diameter, causing a series of abnormal peaks on the original signal. A 21<sup>th</sup> - order median filter has been applied to reduce this effect. An example of the result is shown in Figure 3.2.

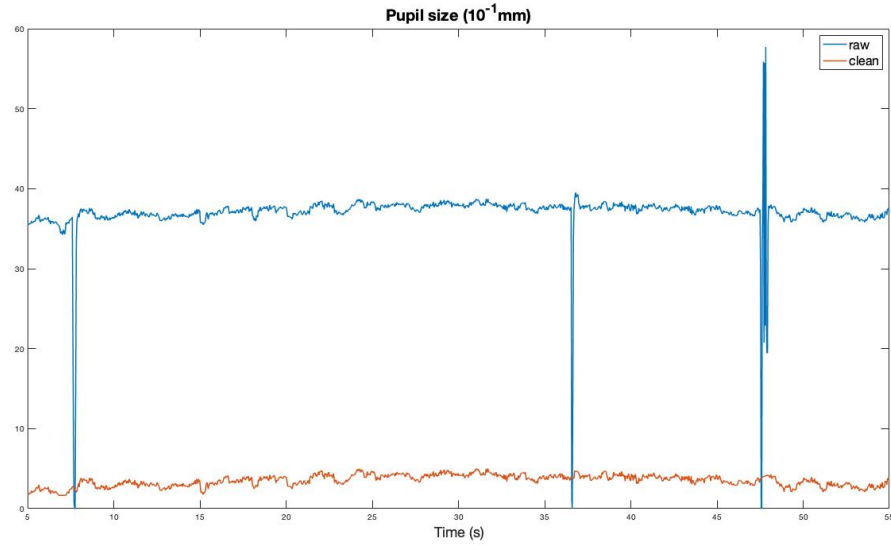


**Figure 3.2:** Representation of the average pupillary diameter of the original signal (in blue) and of the cleaned signal (in red) in the first 60 seconds of the acquisition. This signal was recorded during the 3<sup>rd</sup> visit (7 June 2018) of Subject 10 (Longitudinal Group).

The signal was then filtered with a third-order highpass Chebyshev II filter, with a stop band edge frequency of 0.05 Hz and a stop band ripple attenuation of 20 decibels. The effect of the filter is the attenuation of low frequency trends, so that the obtained array represents the amplitude of pupillary diameter oscillation.

Afterwards, the signal has been multiplied with a Tukey's window of the same length of the signal and with a cosine fraction of 0.1. In this way, the first and the last 3 seconds of the recordings have been cut off, since the high-pass filter introduces edge effects that distort the signal (Figure 3.3). Moreover, a zero-phase forward and reverse digital IIR filtering was applied in order to compensate for any phase distortions or delays introduced by the filter.

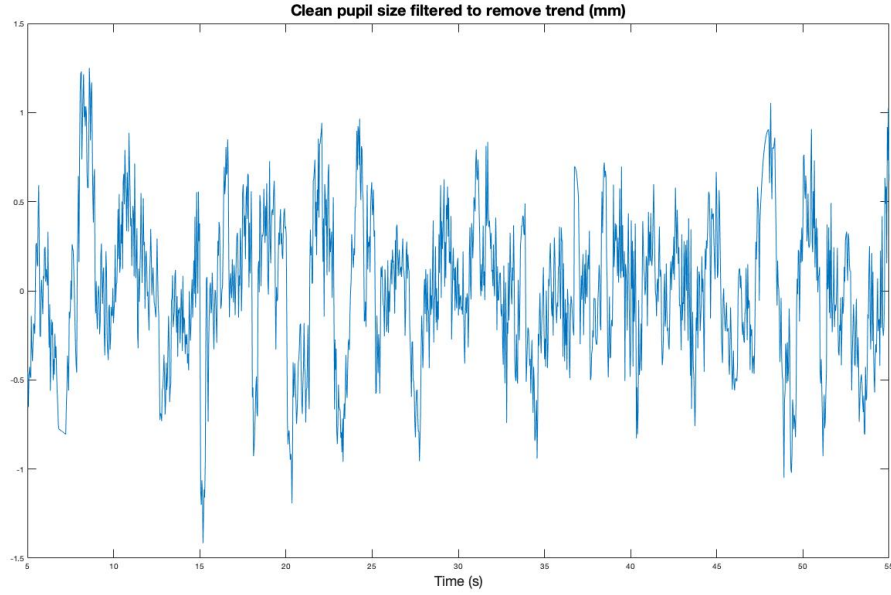


**Figure 3.3:** The result of Chebyshev filter and Tukey’s window application. The first and the last 5 seconds of the recording have been cut off. This signal was recorded during the 3<sup>rd</sup> visit (7 June 2018) of Subject 10 (Longitudinal Group).

### Power Spectral Density (PSD)

For the study of the Autonomic Nervous System activity and its influence on pupils’ behaviour, it is useful to switch to the frequency domain. The **Power Spectral Density** (PSD) of the signal obtained in the previous stage has been calculated, with the aim of evaluating the activation of sympathetic and parasympathetic branches. It is a very common practice in the study of the different autonomic functions, such as Heart Rate Variability (HRV) and Cerebral Blood Flow (CBF) autoregulation. Several studies quantify the balance between the SNS and the PNS’ action, through a relation between their respective power spectral densities (PSD). In this context, similar considerations can be made, based on the study of the hippus’ PSD.

Two methods of PSD estimation has been compared, with the aim of choosing the technique that could better preserve the information content of the signal: the **Welch’s method**, which is a non-parametric spectral estimation method, and the **Burg’s method**, which is instead a parametric estimator.

The Welch’s method is one of the main methods of spectral analysis because it offers good performance in terms of consistency and resolution; non-parametric methods are the first choice in spectral estimation. However, when the PSD of low

frequency signals is required (as in this case), parametric techniques are exploited, such as the Burg's method.

By comparing the spectra resulting from the application of both methods, **the Welch's estimator has been chosen** for subsequent analysis, because the resulting PSD showed a larger number of peaks (and consequently more information) than Burg's method output, which was a flatter spectrum with less precise power values.

The ANS activity can be observed in a frequency range between 0 and some hundreds of mHz. In particular, in literature[36], the spectrum related to the PSD can be divided in 3 subgroups (Figure 3.4):

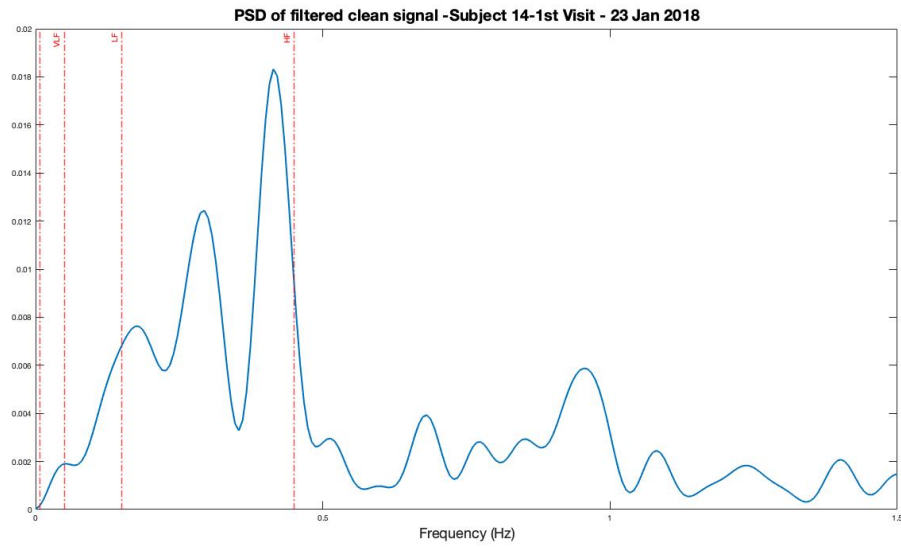


**Figure 3.4:** Subdivision of the Power Spectral Density (PSD) related to the pupillographic signal of Subject 10, recorded during his 3<sup>rd</sup> visit on 7 Jun 2018 (Longitudinal). The spectrum is divided in three ranges of frequency, that are VLF (8 - 50 mHz), LF (50 - 150 mHz) and HF (150 - 450 mHz). The PSD has been estimated via Welch's method.

- Very Low Frequencies (**VLF**) [8 - 50 mHz]: the origin of the autonomic activity in this range is mostly unknown and debated; it could represent the long-term autoregulation mediated by changes in the state of the subject;
- Low Frequencies (**LF**) [50 - 150 mHz]: the PSD in this range is associated to a mixture of **sympathetic** and **parasympathetic** activity;
- High Frequencies (**HF**) [150 - 450 mHz]: it is mostly associated to the **parasympathetic** activity and, consequently, to pupil constriction.

After the division of the spectrum, an integration operation for each interval has been carried out and as a result, a measure of the power in the ranges VLF, LF and HF was obtained. An interesting index consists in the ratio between powers in the LF and HF intervals ( $P_{LF}$  and  $P_{HF}$ , respectively) because it gives an idea about the complementary activation of the sympathetic and parasympathetic branches:

- $P_{LF}/P_{HF} < 1 \implies$  greater activation of the SNS compared to PNS activity;
- $P_{LF}/P_{HF} > 1 \implies$  greater activation of the parasympathetic branch.

Moreover, the SNS and PNS activity can be represented by the follow weighted ratio[37]:

$$\frac{P_{LF}}{P_{HF}} = \frac{0.5 \cdot PNS + 0.25 \cdot SNS}{0.9 \cdot PNS + 0.1 \cdot SNS} \quad (3.1)$$

### Alternative methods of LF and HF ranges selection

However, the subdivision of the PSD into the three frequency ranges suggested by the literature is often inaccurate: a whole spectral peak is expected for each interval, whereas, in many cases, power peaks are not selected entirely and they are wrongly divided before a valley is reached, as shown in Figure 3.4.

Two methods of intervals selection have been implemented to overcome this problem. The power peaks, indeed, seems to be shifted to higher frequencies, thus the first alternative strategy consists in considering extended fixed ranges to try to not cut the peaks in wrong points. The new extended ranges have been chosen arbitrarily and defined as follows:

- **VLF**: 8 - 50 mHz (unchanged);
- **LF**: 50 - 350 mHz;
- **HF**: 350 - 750 mHz.



By expanding the frequency range, the selection of the PSD parts improves than that provided by the previous method, since it better suites to the spectrum obtained from the pupillary hippus.

Anyway, this kind of subdivision is still imprecise, because it selects the PSD ranges without taking into account the actual position and the width of the peaks, that are different among the patients and for each recording. A better estimation of the ratio  $P_{LF}/P_{HF}$  could be obtained with an automatic method of range selection implementation.

Indeed, the second way to define intervals consisted in an automatic algorithm which takes in input the PSD and it detects the peaks with a certain prominence and the nearest valleys into the extended ranges, obtained through the previous method. The algorithm performs the following operations:

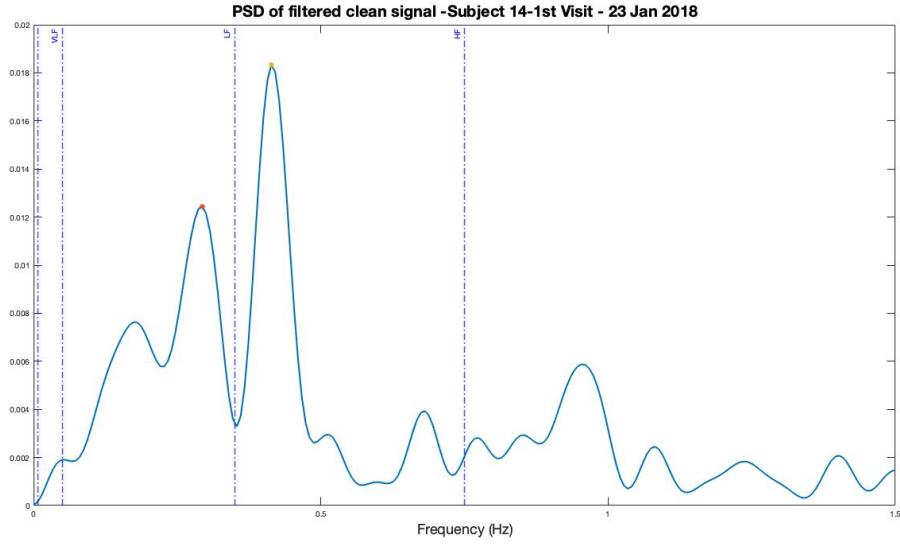
1. PSD calculation with Welch's method, starting from the cleaned signal.
2. Research of the most prominent peak in the extended LF range (50 - 350 mHz). The peaks with a prominence less than the 20% of the PSD maximum value in that interval have been rejected. For each one, the (x,y) coordinates have been collected.
3. Selection of the maximum peak in the LF range and of nearest valleys, by inverting the signal (the valleys are now represented by peaks);
4. Research of the HF most prominent peak in a frequency range between the x coordinate of LF peak + 0.06 Hz and 0.5 Hz.
5. Selection of the maximum HF value, among those resulting from the previous step and selection of the nearest valleys by inverting the signal (as in step 3).

Thanks to this strategy, it was possible to select the intervals in a customized way for each patient: the peaks are entirely identified and a more accurate estimation of the  $P_{LF}/P_{HF}$  index could be obtained.

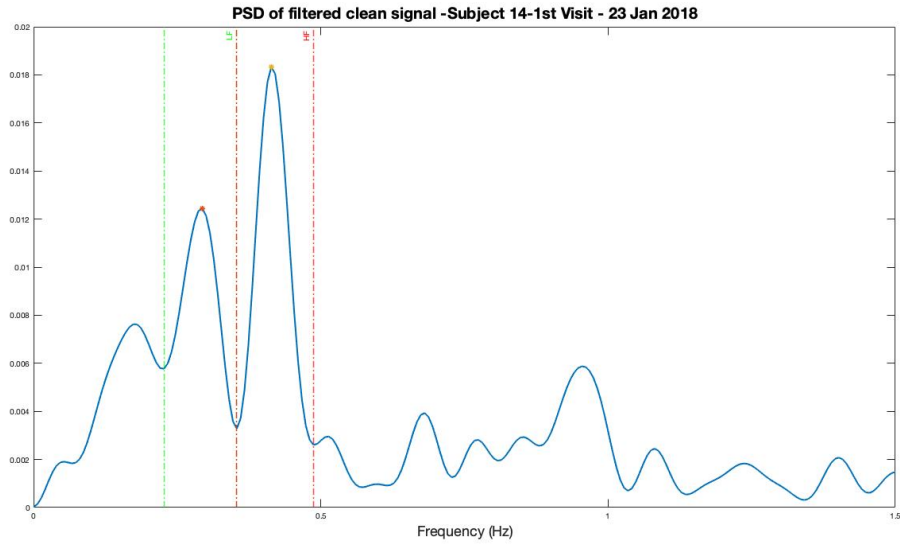
An example of PSD ranges selection, related to a pupillographic recording, is reported in Figure 3.5: in the first case, (Figure 3.5a), the ranges have been found following the established fixed extended intervals; the latter chart (Figure 3.5b) shows the selection of the PSD ranges through the automatic research of the intervals.

By comparing the two graphs, it is clear that a customized subdivision of PSD based on peaks position is more suitable in relation to the study.

Once the three methods of PSD subdivision have been implemented, the next step was its integration into the LF and HF frequency bands, by summing the power values which they include. Then, the resulting values have been combined to obtain the  $P_{LF}/P_{HF}$  index, for each recording session.



(a)



(b)

**Figure 3.5:** Power Spectral Density (PSD) related to Subject 14 (Longitudinal) recording, during his 1<sup>st</sup> visit on 23 January 2018. The spectrum has been divided into the VLF, LF and HF ranges through two alternative methods of intervals selection: extended fixed ranges (3.5a) and automatic peaks and intervals research (3.5b). In the latter case, the integration of PSD in the LF and HF is more precise and it leads to a more accurate estimation of the  $P_{LF}/P_{HF}$  index.

The methods for the frequency ranges selection are summarised in the Table 3.1.

Frequency bands selection			
METHOD	VLF (mHz)	LF (mHz)	HF (mHz)
Literature intervals	8 - 50	50 - 150	150 - 450
Expanded intervals	8 - 50	50 - 350	350 - 750
Adaptive intervals	8 - 50	customized	customized

**Table 3.1:** Summary table of VLF, LF and HF frequency band selection methods.

### 3.3.2 Second part: Pupillary Light Reflex

The next step of the analysis consisted in the study of the second part of the pupillographic acquisition, which shows the pupil's behaviour when it is stimulated with light pulses.

In response to flash stimuli, there is an increased parasympathetic activity, followed by the activation of the SNS. At pupillary level, this corresponds to a contraction, followed by a dilation.

In particular, for each PLR, an estimation of the pupillary constriction and dilatation rate was obtained, which is useful to understand if the ANS activity remains unchanged as the disease progresses. For this purpose, the PLRs have been interpolated through an exponential model, of which time constants have been studied. Moreover, the response time related to pupil's constriction and dilatation has been considered.

#### Selection of PLR traits and exponential interpolation

In order to study the pupillary dilation and constriction reflex, the second part of the time series has been selected, by eliminating the first 60 seconds of the recording which represent the hippus.

Even in this case, the signal has been re-interpolated following a new time axis, obtained through a constant sampling frequency of about 30 Hz. A 31<sup>th</sup> - order median filter has been applied to the signal, aiming to attenuate the abnormal peaks due to eye blinks or other artifacts during the recording; then, the mean value was removed and a Tukey's window was applied to the signal, with a cosine fraction of 0.1. In this case, no digital filter has been applied because the resulting signal was of good quality. The result of this signal pre-processing stage is reported in Figure 3.6.

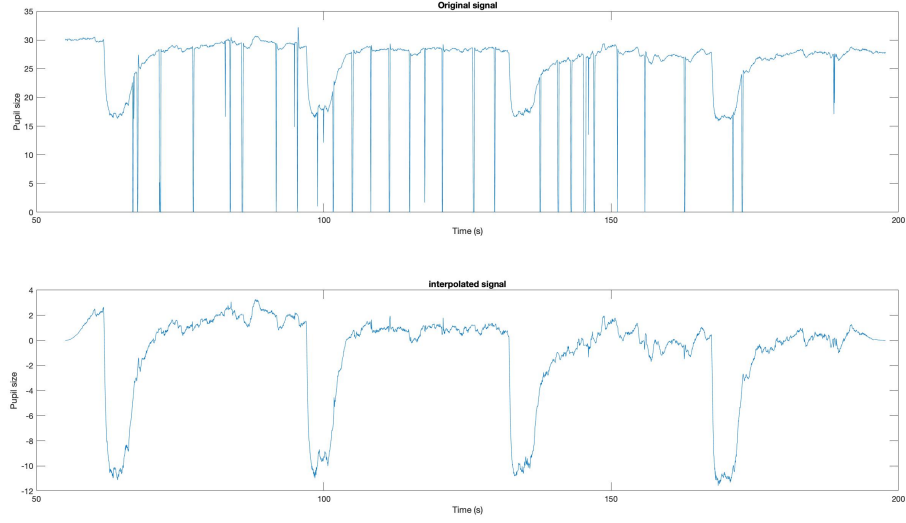


**Figure 3.6:** Comparison between the original signal (upper subplot), obtained from the second part of the pupillary recording and the processed signal (lower subplot). The resulting signal appears free of abnormal peaks and PLRs are clearly visible. The signal belongs to Subject 02 - 2<sup>nd</sup> visit on 18 April 2018 (Longitudinal Group).

Starting from the cleaned signal, three PLRs has been chosen, by manually selecting for each one the descending and the ascending tracts (Figure 3.7). The choice of not considering all four PLR is due to the fact that in some recordings, certain PLRs were not clearly visible whereas, in almost all cases, the extraction of three PLRs was always possible. As a results, three time ranges for the descending tracts and three time ranges for the ascending ones have been collected, in order to study separately the parasympathetic and sympathetic behavior of the pupil.

The signal represented in Figure 3.6, shows that the two PLRs stages have a behavior similar to an exponential model: the next step includes the exponential interpolation of each of the six tracts taken from the recording. This operation is obviously carried out for each recording session and for each patient.

The Curve Fitting Toolbox<sup>TM</sup> of MATLAB<sup>®</sup> was exploited to perform the exponential interpolation of the signals. As a preliminary operation, the descending and the ascending tracts have been interpolated through the sum of two exponential functions (Figure 3.8). The general model is:

$$val(x) = ae^{bx} + ce^{dx} \quad (3.2)$$

However, the aim of this part of the analysis is the extraction of the exponential

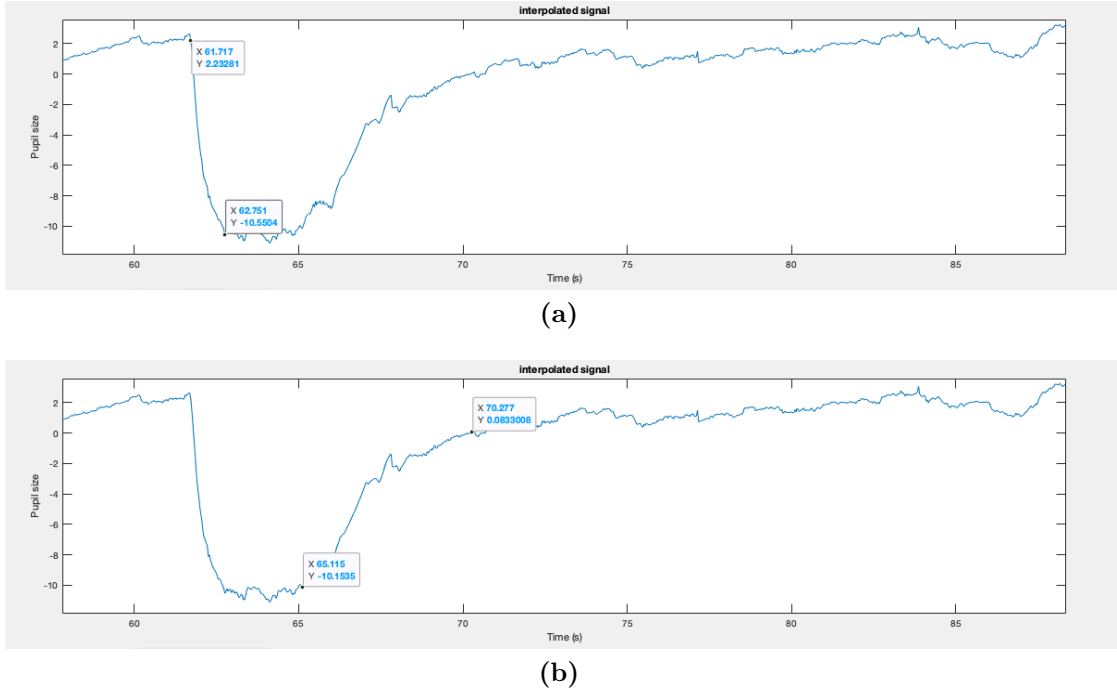
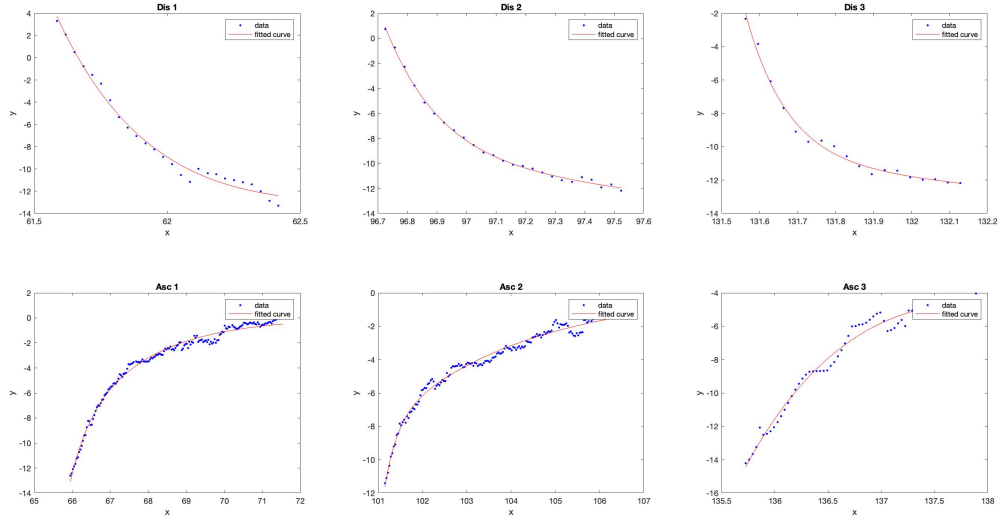


**Figure 3.7:** Example of the manual selection of a PLR. In the figure, the descending (3.7a) and the ascending (3.7b) tracts of a PLR have been selected and the respective time intervals have been collected. The signal belongs to Subject 02 - 2<sup>nd</sup> visit on 18 April 2018 (Longitudinal Group).

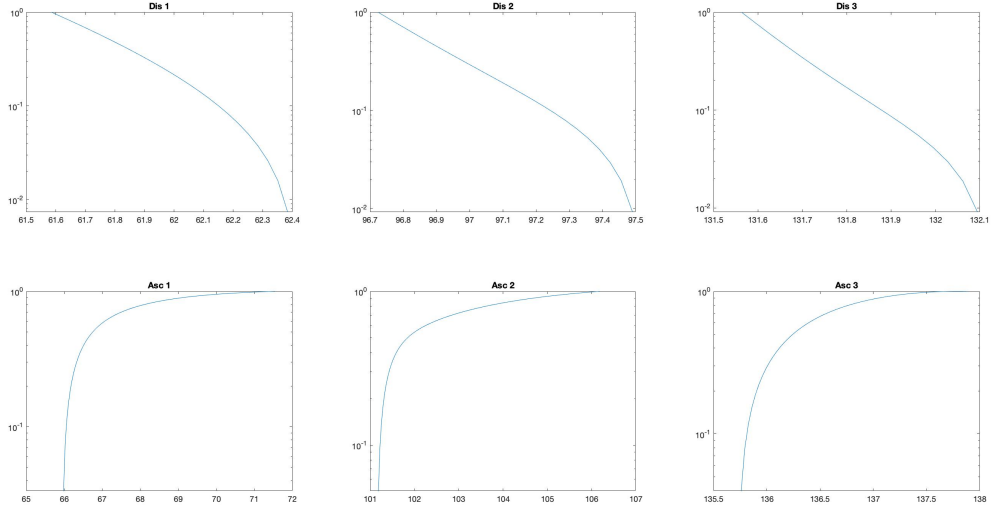
time constant and it is possible by separating the two exponential functions of the model described in Equation 3.2. Then, the same interpolating functions have been visualized in a semi-logarithmic scale in order to identify the time ranges in which only one exponential function is present, no more the sum of the two ones: the presence of a linear trend was evaluated and new intervals for the constriction and dilatation traits are defined, as shown in Figure 3.8b. This strategy works well for the descending traits: the first of the two exponential functions acts for approximately one second, that is the time interval to be considered. For the ascending traits, the intervals has been redefined by selecting the steepest part of the function.

Once the new ranges have been saved, the study continued using a simple exponential model for signal interpolation. For the constriction trait, the new model is defined by the following equation:

$$val(x) = ae^{bx} \quad (3.3)$$



(a)



(b)

**Figure 3.8:** Interpolation of the three descending traits (Dis 1, Dis 2 and Dis 3) and of the ascending ones (Asc 1, Asc 2 and Asc 3) through the two exponential model 3.2, in linear scale (Figure 3.8a) and semi-logarithmic scale (Figure 3.8b). The blue points in Figure 3.8a represents the original signal and the red functions are the interpolating exponentials. These PLRs have been extracted from the recording session of Subject 1001 - 1<sup>st</sup> Visit on 16 February 2018 (LIS).

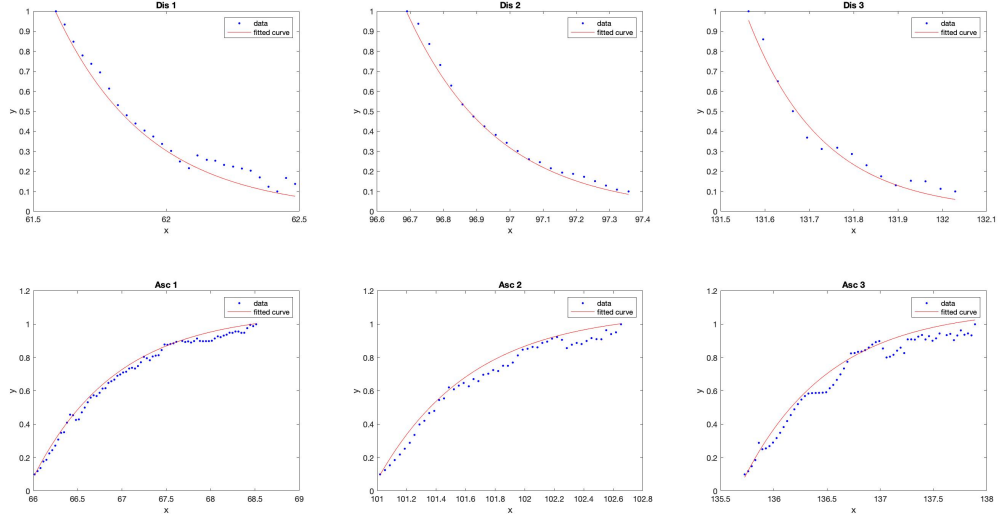


**Figure 3.9:** Interpolation of the PLRs constriction (Dis 1, Dis 2 and Dis 3) and dilatation (Asc 1, Asc 2 and Asc 3) traits, through the exponential models described by the Equations 3.3 and 3.4, respectively. The recording session refers to Subject 1001 - 1<sup>st</sup> Visit on 16 February 2018 (LIS).

while, for the dilatation behaviour the new model is:

$$val(x) = a - be^{-cx} \quad (3.4)$$

The results of the latter operation is reported in Figure 3.9. The MATLAB® function *fit* provides the coefficients of the interpolating functions. Among them, the most interesting one is the coefficient that multiplies the independent variable in the exponential equation: **b** for the decreasing exponential (Equation 3.3) and **-c** for the increasing one (Equation 3.4).

Considering the equation of the exponential decay

$$V(t) = V_0 e^{-t/\tau} \quad (3.5)$$

these coefficients represents the reciprocal value of the *time constant*  $\tau$ .

Physically, the time constant represents the elapsed time required for the system response to decay to the 36.8% of the initial value; in an increasing system, the time constant is the time for the system's step response to reach 63.2% of its final asymptotic value. In other words,  $\tau$  gives an idea of the speed of a system's response to an external stimulus, which is, in this case, the speed at which the pupil diameter decreases in the presence of a light stimulus and the rate of pupil

dilatation up to the rest value. In this context, a  $\tau$  value has been calculated for both the descending and ascending traits, which have been defined  $\tau_{dis}$  and  $\tau_{asc}$ , respectively.

### 3.3.3 Extraction of other indices and database compilation

The three previously calculated indices ( $P_{LF}/P_{HF}$ ,  $\tau_{dis}$  and  $\tau_{asc}$ ) are not the only values extracted from pupillographic recordings of the ALS patients. In order to have a better idea about the pupillary behaviour (and consequently about the autonomic control of the pupil), other interesting features have been considered. In this way, it may be possible to evaluate if there is a real difference in the ANS activity between healthy subjects and ALS patients.

The new indices have been extracted from both the hippus and the PLRs recordings. Moreover, the features related to the hippus have been also calculated in the time domain, and the remaining ones in the frequency domain (i.e the PSD of the hippus).

#### Pupillary Hippus - Time domain

From the part of the time series relating to the pupillary hippus, the following indices have been calculated in the time domain:

- average amplitude of pupillary diameter (before high-pass filtering);
- variance of the probability distribution of pupil size;
- skewness of the probability distribution of pupil size;
- kurtosis of the probability distribution of pupil size.

#### Pupillary Hippus - Frequency domain

Even considering the first 60 seconds of the records that reflects the hippus' oscillations, the features extracted from the PSD are:

- $P_{LF}/P_{HF}$ ;
  - 1<sup>st</sup> method;
  - 2<sup>nd</sup> method;
  - 3<sup>rd</sup> method;
- % of PSD included in the LF band ( $P_{LF}$ ), compared to the total power;
- % of PSD included in the HF band ( $P_{HF}$ ), compared to the total power;
- PSD mean frequency (MNF) (Figure 3.10).



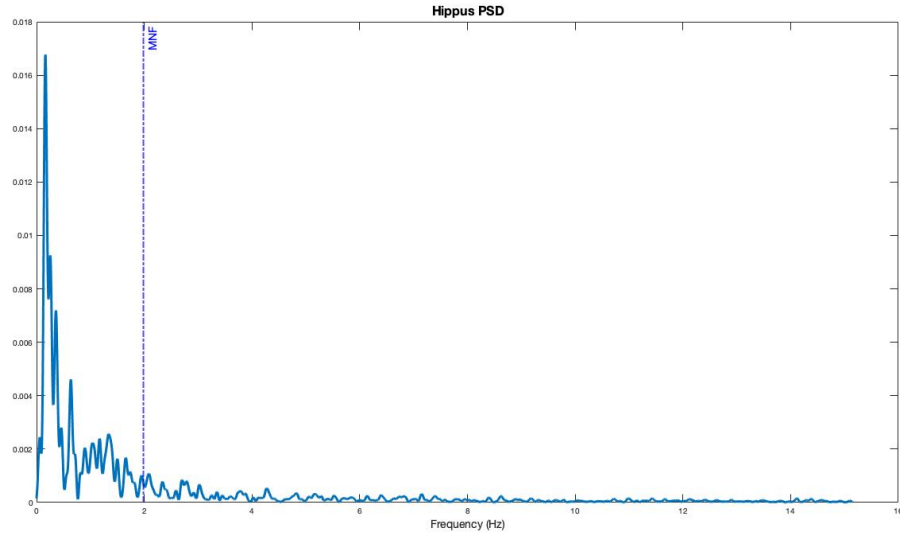


**Figure 3.10:** Representation of the mean frequency (MNF) evaluated on the hippus PSD of Subject 1012 - 1<sup>st</sup> Visit (20 June 2018) (Transversal Group).

### Pupillary Light Reflex - Time domain

The features of the second part of the recordings, which refers to the PLRs acquisition, have been calculated only in the time domain and they represent the mean value obtained from the three PLRs considered:

- time constant  $\tau_{dis}$  related to the interpolating exponential of the PLR descender trait (average value on three PLRs);
- time constant  $\tau_{asc}$  related to the interpolating exponential of the PLR riser trait (average value on three PLRs);
- response time of pupil constriction after the light pulse (average value on three PLRs) (Figure 3.11a);
- response time of pupil dilatation to reach the rest size (average value on three PLRs) (Figure 3.11b);
- PLR amplitude variation range (average value on three PLRs).

The response time after the light pulse, has been calculated in the descending trait of a PLR, considering the time interval required to reach the 66% of the minimum diameter amplitude, taking as reference the average diameter evaluated in the 0.5 seconds before the stimulus. In the pupil dilatation case, it represents the time

interval needed for the pupil to reach the 66% of amplitude between the maximum constriction value and the average diameter calculated in the 0.5 seconds before the stimulus (Figure 3.11).

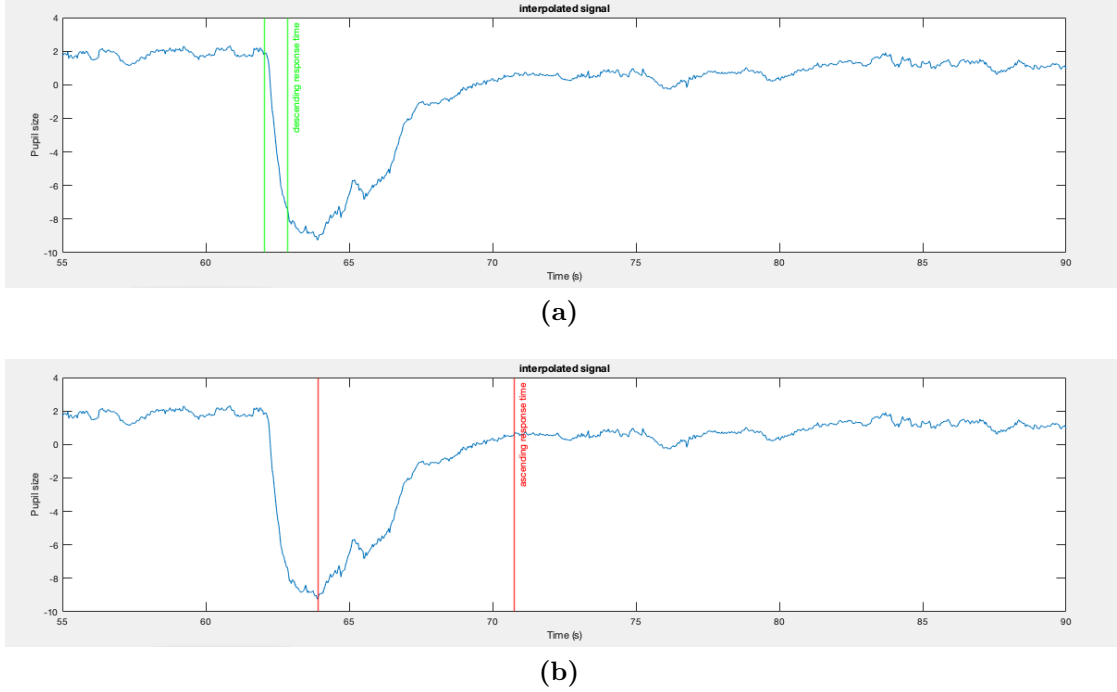


**Figure 3.11:** Descending response time (3.11a) and ascending response time (3.11b) evaluation for a single PLR extracted from the recording of Subject 02 - 5<sup>th</sup> Visit (22 January 2019) (Longitudinal Group).

### Pupillary Accommodation Reflex

In addition to hippus and PLR data, some information about the Pupillary Accommodation Reflex (PAR) was also extracted. A subset of 5 subjects (2 male and 3 female) belonging to the Transversal study group was selected to participate in a second test session with the objective of evaluating the effectiveness of the PAR as an input method for binary communications systems.

In order to perform the test, the subjects were presented with a solid round object with a 1 centimeter diameter, located at an approximate distance of 40 centimeters from the subject's face (referred to as the "near target"). A poster with a recognizable pattern was placed on the wall, located at an approximate distance of 3-5 meters, depending on the available distances of the testing environments, from the subject's face (referred to as the "far target"). Both the near and far targets

were approximately aligned with the subject's gaze. The subject's gaze would then be fixated upon the far target, and a MATLAB algorithm would indicate the subject via verbal commands to switch his/her gaze from the far target to the near target and vice versa, performing a PAR each time the switch occurred. The verbal commands were repeated for a total of five times, allowing the observation of multiple PAR events.

Again, data was acquired using the Eyetribe sensor, located at an approximate distance of 40 centimeters from the patient's face, set to a sampling frequency of 30 Hz. The recordings and software were executed on an Asus P2530U Notebook with an Intel Core i7-6500 (4 CPUs) processor, 8GB of RAM and a 64-bit Windows 10. The resulting data was processed via a MATLAB algorithm: PAR amplitude was evaluated as the pupillary diameter variation between the pupillary baseline value, calculated as the mean pupillary value of the last 3 to 1 seconds before each PAR event, and the minimum pupillary diameter value observed in the following 5 seconds after the beginning of each PAR event.

### **Other indices: ALSFRS-R, Stress and Tiredness**

In this database, another important index is reported, which it does not concern the pupillary activity, but it is a measure of the level of disability induced by the disease: this is the Amyotrophic Lateral Sclerosis Functional Rating Scale-Revised (ALSFRS-R). It's a clinical assessment scale that has been shown to accurately monitor the progression of disability in ALS patients[38] and to have good psychometric characteristics[39][40]. The ALSFR-R consists of 12 total items that investigate a precise function, which frequently in the SLA is compromised: language, salivation, swallowing, hand movements, cutting food and using tools, dressing and hygiene, turning over on the bed and adjusting blankets, walking, climbing stairs and 3 items for respiratory function. For each item a score from 0 (severe disability) to 4 (no disability) is proposed. The score can vary from a minimum of 0 to a maximum of 48 and a score  $\leq 29$  indicates rapid progression of the disease.

Every ALSFRS-R score is completely personal and unique: even if two people have the exact same score, they could still be experiencing drastically different symptoms. This is because symptoms affect different regions of the body and can vary from person to person (Figure 3.12).

During each visit, the patients of the Longitudinal Group filled out the questionnaire, so that they would be given a score. Sometimes, the score in some visits was missing, therefore a value equal to the average of the scores of the same subjects' other visits has been assigned.

In addition, patients were also asked to assess their state of stress and tiredness with a score in a scale from 0 to 5.

In Table 3.2, the indices extracted from pupillographic recording are shown in a summarized way.

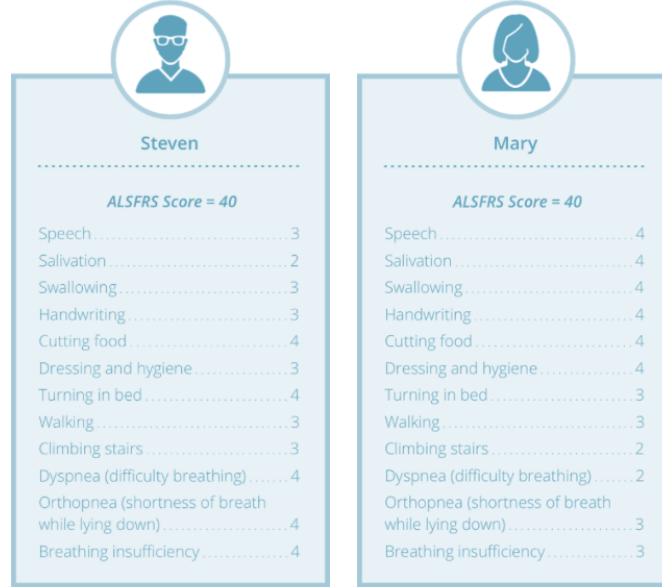


**Figure 3.12:** Example of questionnaires filled by two hypothetical ALS patients. Each questionnaire is composed by 12 items about subject's physical functions, ranging from 4 (normal) to 0 (no ability). Even if the ALSFRS-R score is the same, each patient experiences drastically different symptoms. For instance, both Steven and Mary have the same ALSFRS-R score; however, while Steven experiences symptoms in his head, throat, and upper body, Mary experiences symptoms in her legs and respiratory system.

Indices			
Hippus		PLR	Other indices
Time domain	Frequency domain	Time domain	
mean diameter	$P_{LF}/P_{HF}$	$\tau_{dis}$	ALSFRS-R
variance	$P_{LF}$	$\tau_{asc}$	Stress
skewness	$P_{HF}$	r.t - constriction	Tiredness
kurtosis	MNF	r.t - dilatation	PAR mean amplitude
		PLR range	

**Table 3.2:** Summary table of the indices extracted from the pupillographic recordings.

### 3.4 Data analysis

Starting from the study of the pupillographic signals recordings, it was possible to obtain a set of information about the behaviour of the pupil in the rest and light stimulation conditions. The idea was to check if there is a correlation between the stage of the disease and the extracted indices: for example, it can be evaluated if there is a time-dependent trend of the features or whether they vary according to the ALSFRS-R score. Moreover, choosing a suitable combination of the indices related to the pupil behaviour, different classifiers have been tested in order to predict the severity of patients' disability.

#### 3.4.1 Trend over time of power percentages in the LF and HF bands

Considering the Longitudinal Group of the data set, of which the pupillographic signals were taken during several visits, the evolution over time of the PSD percentages, included in the LF and HF bands, has been assessed.

To do so, the PSD functions, derived from the recordings of the pupillary hippus, have been integrated, by summing the power values in the respective frequency bands; then, the two resulting power values were divided by the sum of the whole function values and multiplied by 100, to obtain the percentage quantities. The LF and HF frequency bands have been selected using the adaptive method described in Section 3.3.1.

Subsequently, these values were interpolated through the linear function

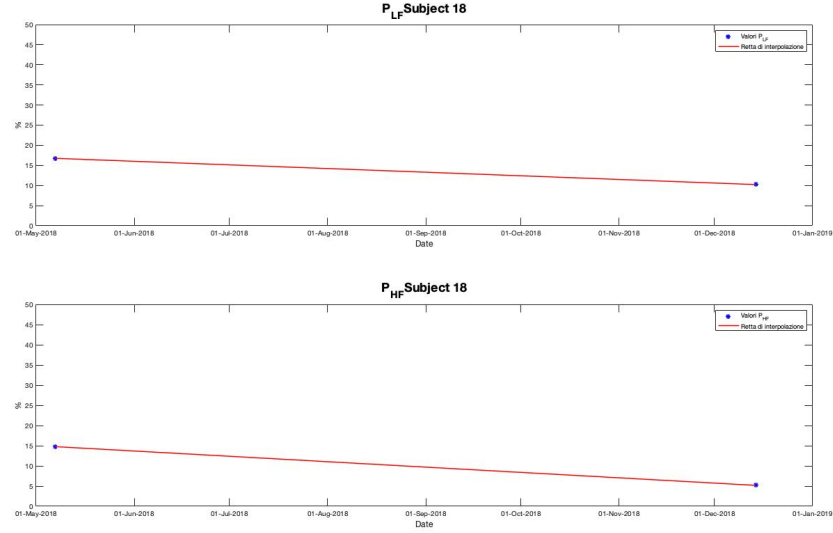
$$p(x) = mx + q \quad (3.6)$$

via the MATLAB® routines *polyfit* (which returns the one-degree polynomial coefficients that best fit data in a least-squares sense) and *polyval*. An example of this operation is shown in Figure 3.13. In this way, for each patient, two fitting lines have been obtained, related to LF and HF frequency bands respectively.

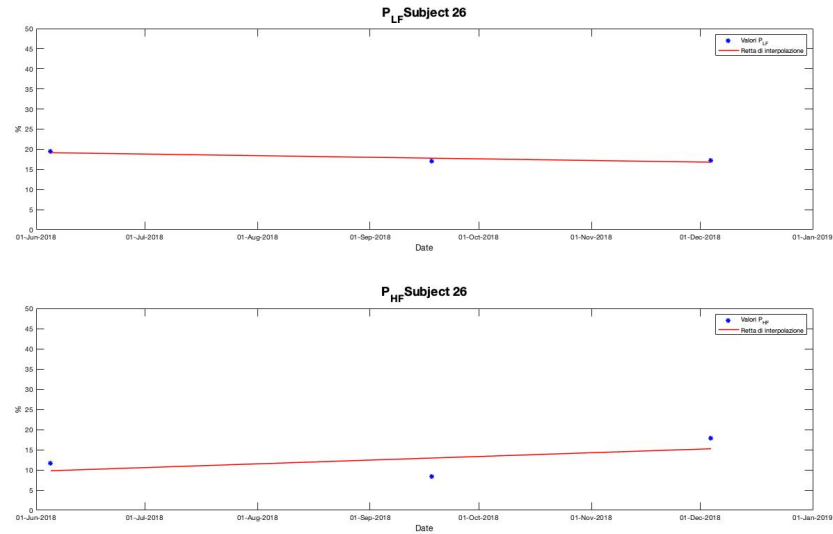
Starting from the interpolating straight lines, obtained in the previous step, the relative angular coefficients  $m$  (from Equation 3.6) have been considered, in order to assess if  $P_{LF}$  and  $P_{HF}$  increase or decrease significantly over time, between one visit and the next one. Therefore, the angular coefficients of the linear functions have been considered and their summary statistics were represented through two box plots (Figure 3.14).

It can be observed that in most cases the slope  $m$  takes on a value close to zero: the median is 0.0025 %/month for the  $P_{LF}$  group and 0.0006 %/month for the  $P_{HF}$  one and also the 25<sup>th</sup> and the 75<sup>th</sup> percentiles are concentrated around zero. This implies that the power percentage in the frequency bands LF and HF do not

vary significantly over time, remaining about constant between one visit and the other one.



(a) Subject 18 - Longitudinal group



(b) Subject 26 - Longitudinal group

**Figure 3.13:** Representation of the trend over time of power percentages in the LF and HF bands ( $P_{LF}$  and  $P_{HF}$ ), related to subjects 18 (Figure 3.13a) and 26 (Figure 3.13b) of Longitudinal Group.

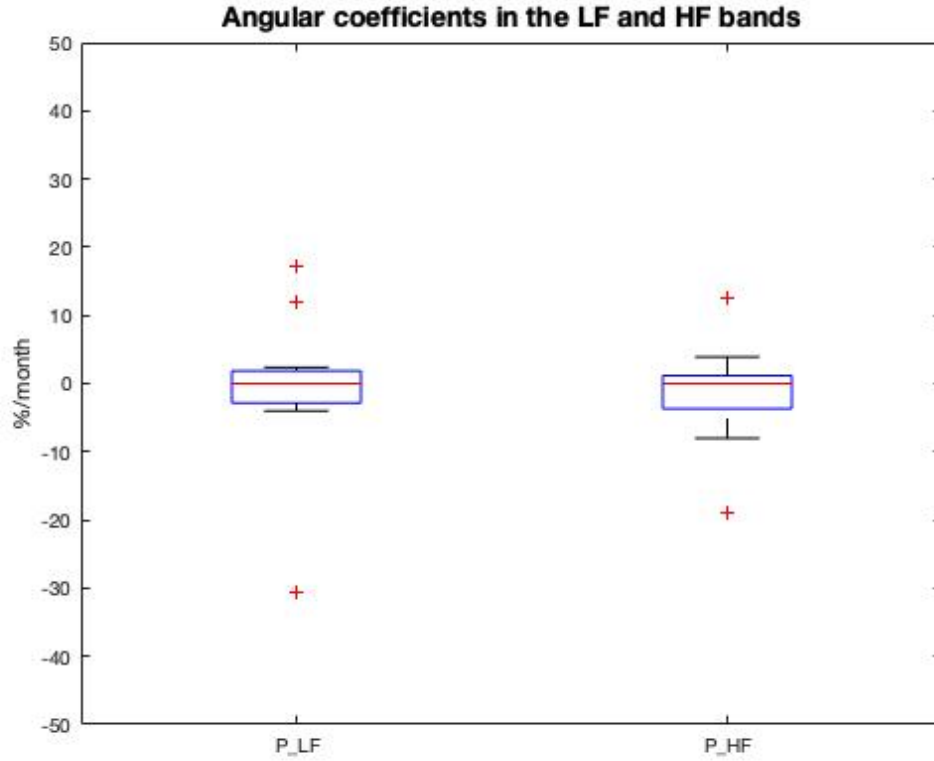


**Figure 3.14:** Box plots related to angular coefficients  $m$  of the fitting straight lines in the LF and HF frequency bands.

### 3.4.2 Pupillary indices as a function of the ALSFRS score

In Figure 3.15, 3.16 and 3.17 the indices extracted from the pupillary recordings of ALS patients are reported, as a function of the ALSFRS-R score, by means of a scatter plot.

For the creation of the data set to be studied, the following strategies have been introduced:

1. LIS patients, of which an ALSFRS-R score is obviously not available, have been assigned a fixed score of 5 by default. In this way, LIS patients' indices are distinguishable from those of Longitudinal Group.
2. the visits of each Longitudinal Group subject were considered as separate observations: each score corresponds to a subject of the data set.

The indices have been grouped in:

- Pupillary Hippius - Time domain (mean, variance, skewness and kurtosis of the average pupil diameter in Figure 3.15);
- Pupillary Hippius - Frequency domain ( $P_{LF}/P_{HF}$ ,  $P_{LF}$ ,  $P_{HF}$  and MNF in Figure 3.16)
- PLR - Time domain ( $\tau_{dis}$ ,  $\tau_{asc}$ ,  $response\_time_{dis}$ ,  $response\_time_{asc}$  PLR average diameter range in Figure 3.17)

In the charts, the distinction between LIS and Longitudinal subjects is also shown. The purpose of such representation is to verify if a recognizable trend in the data exists, in function of the ALSFRS-R score (and therefore of the time).

However, by observing the scatter plots, a precise trend of the indices as the score varies is not evident. For this reason, no marked difference is observed between subjects with moderate symptoms and more severe patients.

In the next phase of the study, a verification about the existence of a real difference between healthy people and ALS patients will be carried out, in order to assess whether or not the progression of the disease compromises the activity of the Autonomic Nervous System.

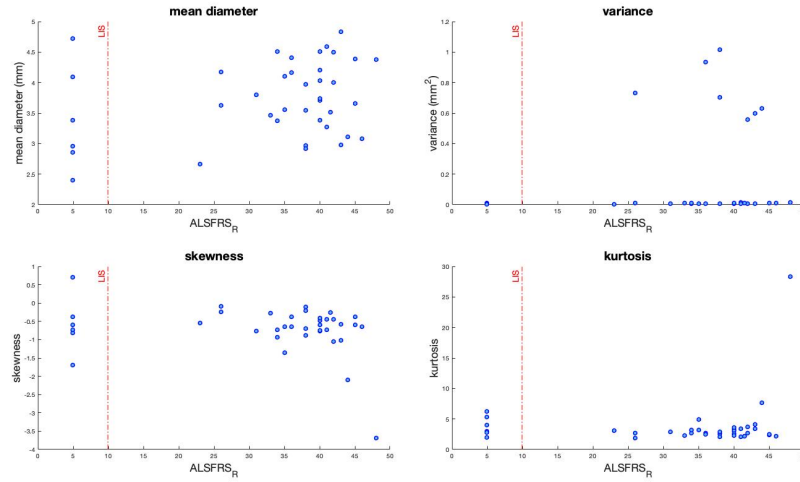


**Figure 3.15:** Pupillary Hippius - Time domain indices as function of ALSFRS-R score



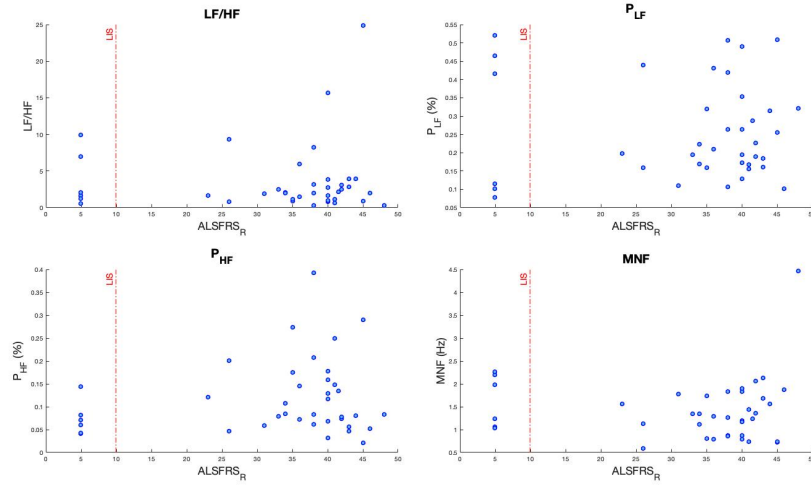


**Figure 3.16:** Pupillary Hippus - Frequency domain indices as function of ALSFRS-R score

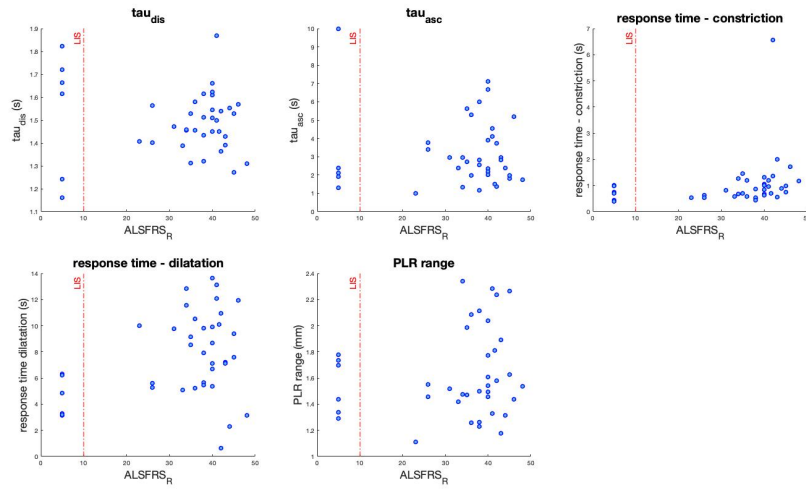


**Figure 3.17:** PLR - Time domain indices as function of ALSFRS-R score

### 3.4.3 Stage of the disease classification

Another type of analysis was conducted on the indices extracted from the pupillographic signals, in order to predict the severity of the disease starting from the value assumed by the features. It could be useful, for example, for clinicians who can estimate the impairment level of the patient by considering the features value.

The idea is to divide the patients of the data set into three classes, according to the level of motor impairment due to the disease. For this purpose, the ALSFRS-R score assigned to each patients during the visits has been considered.

The division into classes was arbitrary and followed the criteria below:

1. **Class 0** :  $0 \leq \text{score} \leq 29$ ;
2. **Class 1**:  $30 \leq \text{score} \leq 39$ ;
3. **Class 2**:  $40 \leq \text{score} \leq 48$ .

In other words, Class 0 is composed by LIS patients and very impaired ALS subjects (17 elements), Class 1 represents ALS patients with a moderate disability (12 elements) level and Class 2 contains patients at a beginning stage of the disease, whose motor skills are still almost intact (9 elements).

#### Training set and Test set

Given the limited number of subjects belonging to the data set (38 subjects), a "Leave-one-out Cross Validation" (LOOCV) approach has been adopted. This method consists in building the Training set with all the elements of the data set, leaving out one of them, that represents the Test set. Proceeding in this way, the model is constructed using only data from the Training set and it is then applied to predict the response value of the one observation left out (Figure 3.18). The process is repeated  $n$  times (where  $n$  is the total number of observations in the data set), leaving out a different observation from the Training set each time.

LOOCV results in a reliable and unbiased estimate of model performance and it is suitable when the data set is composed by limited data. However, it is a computationally very expensive technique, so that it is used to estimate the performance of a machine learning algorithm especially when an accurate model more important than the computational cost.

#### Binary decision tree and classification loss

Then, to evaluate the model's performance on the data set, a measure about how well its predictions match the observed data was carried out. The most common way to measure the classification loss ( $L$ ) is trough the MATLAB® algorithm *kfoldLoss*[41]. This function measures the predictive inaccuracy of classification

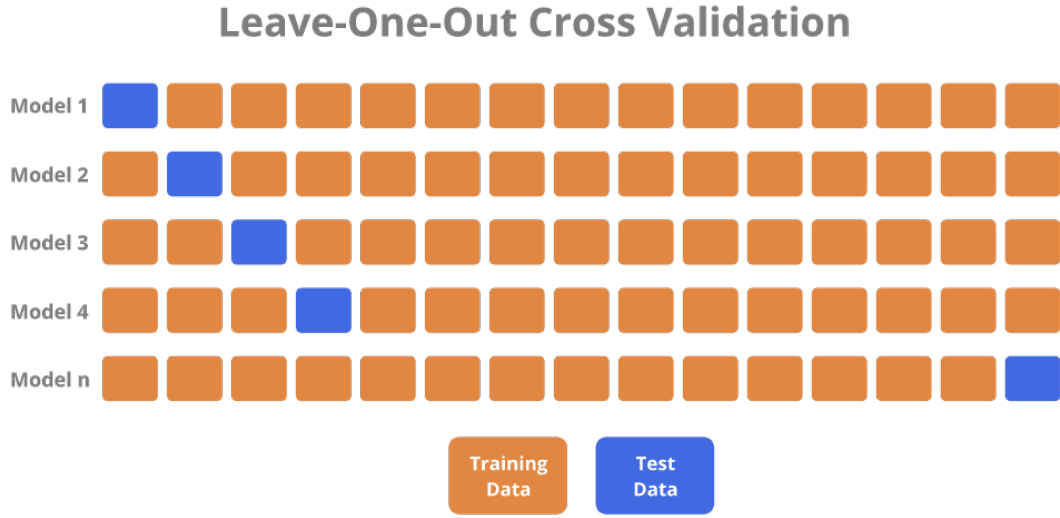


**Figure 3.18:** Data set partition through LOOCV.

models, allowing to choose the better predictive one with a lower loss.

In this context, a **binary decision tree** for multiclass classification has been chosen, which showed good performance among tested models in terms of accuracy. For a generic classifier with a number of classes  $K = 3$ , the classification loss is calculated as follows:

- $L$  is the weighted average classification loss;
- $n$  is the number of elements in the data set;
- For a multiclass classification :
  - $y_j^*$  is a vector of  $K - 1$  zeros, with 1 in the position corresponding to the true, observed class  $y_j$ . For example, if the true class of the second observation is the third class and  $K = 3$ , then  $y_2^* = [0 \ 0 \ 1]^T$ .
  - $f(X_j)$  is the length  $K$  vector of class scores for observation  $j$  of the predictor data  $X$ .
  - $m_j = y_j^{*T} f(X_j)$ . Therefore,  $m_j$  is the scalar classification score that the model predicts for the true, observed class.
- The weight for observation  $j$  is  $w_j$ . The observation weights are normalized,

so that:

$$\sum_{j=1}^n w_j = 1. \quad (3.7)$$

For a tree classifier, the *kfoldLoss* routine exploits the "minimal expected misclassification cost" as a criterion to compute the classification loss.

The software computes the weighted minimal expected classification cost using this procedure for observations  $j = 1, \dots, n$ :

1. Estimate the expected misclassification cost of classifying the observation  $X_j$  into the class  $k$ :

$$\gamma_{jk} = (f(X_j)^T C)_k \quad (3.8)$$

where  $X_j$  is the column vector of class posterior probabilities for the observation  $X_j$  and  $C$  is the cost matrix of the model.

2. For observation  $j$ , predict the class label corresponding to the minimal expected misclassification cost:

$$\hat{y}_j = \arg \min_{k=1, \dots, K} \gamma_{jk} \quad (3.9)$$

3. Using  $C$ , identify the cost incurred ( $c_j$ ) for making the prediction.

The weighted average of the minimal expected misclassification cost loss is:

$$L = \sum_{j=1}^n w_j c_j \quad (3.10)$$

## Feature Selection

Feature selection is the process of detecting relevant features and removing irrelevant, redundant, or noisy data. This process speeds up data mining algorithms, improves predictive accuracy and increases comprehensibility. Irrelevant features are those that provide no useful information, and redundant features provide no more information than the currently selected features[42].

Therefore, among the 13 features obtained from each acquisition, not all are useful for the classification, but only a combination of them is the best one, in terms of classification loss.

In order to find it, the binary tree classifier has been trained by testing all the possible combinations of the indices: at each step, the number of indices to be combined increased by one and all possible combinations of the 13 features have been selected from the data set. As a result, for each set of features, a LOOCV

process was applied (Figure 3.19). The number of combinations of  $n$  items taken  $k$  at a time is

$$\binom{n}{k} = \frac{n!}{k!(n-k)!} \quad (3.11)$$

where, in this case,  $n = 13$  and  $k = 1, \dots, 13$ .

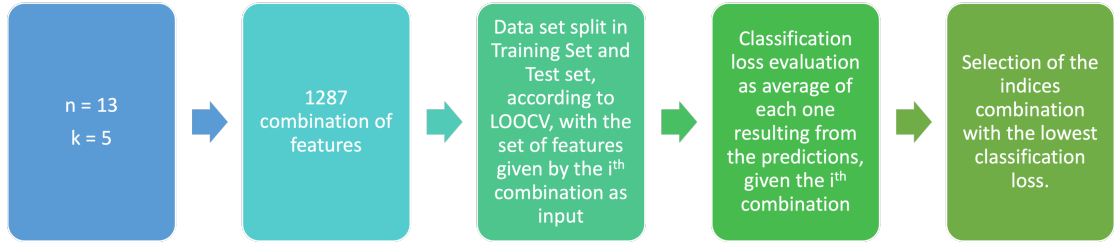


**Figure 3.19:** Training of the classifier through all possible combinations of the 13 indices. As an example, the case  $k = 5$  items is represented.

Following the LOOCV method, at  $j^{th}$  iteration, the  $j^{th}$  element is taken as Test set and a classification loss is evaluated. An average value of the classification loss has been associated to each indices combination, therefore **the best set of features is given by that with the lowest prediction error.**

### 3.4.4 Classification results

From the analysis of the classification errors, resulting from the tested models, it could be deduced that the combination of features that provides the greatest accuracy (and thus the lowest classification loss) in the prediction of the Test set classes consisted of:

1. average amplitude of pupil diameter (before high-pass filtering)
2. kurtosis of the probability distribution of pupil size

with a classification loss  $L = 0.4417$ . This set of features was obtained by comparing the classification errors of each tested model and for each possible combination of

indices. The rules of the decision tree are shown in Figure 3.20 and the classification results in Figure 3.21.

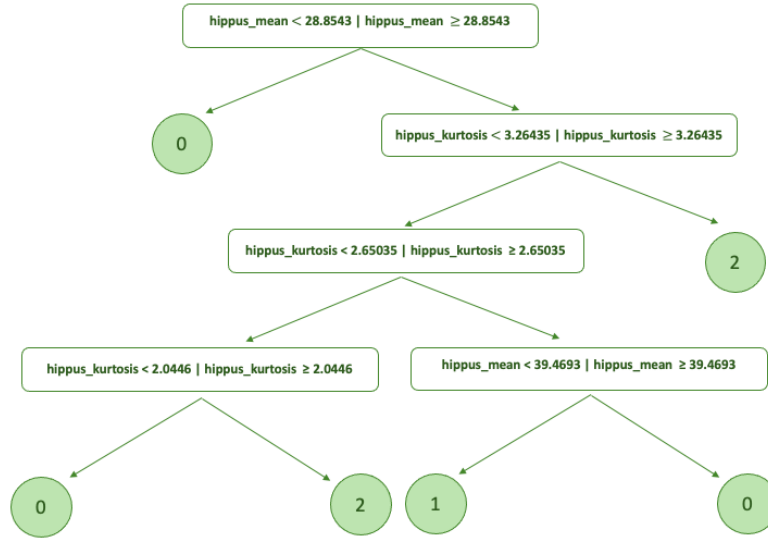


**Figure 3.20:** Binary decision tree rules of classification, exploiting the amplitude of pupil diameter and the kurtosis as input for the classification.

The binary tree is characterized by 5 *branch nodes*. The *depth* of a node  $n$  is the length of the path from the root to that node; the maximum depth of a knot inside a tree is called the *height* of the tree and in this case it is equal to 4. The accuracy of classification, that is:

$$accuracy(\%) = \frac{\sum \text{correctly classified}}{\sum \text{all elements of data set}} \cdot 100 \quad (3.12)$$

assumed a value of 60,53%. By analyzing the confusion matrix in Figure 3.21, it can also be gathered that the binary tree recognizes very well the elements at the beginning stage of the disease, belonging to Class 2 (82.35% correctly predicted), whereas the percentage of correctly classified of Class 0 and Class 1, related to LIS subjects and moderately impaired patients, is quite low (44.44% and 41.67%, respectively). These results suggest that **the classifier is not able to reliably distinguish severe patients from those with moderate symptoms**, since the percentage of correct prediction in each case is less than 50%: this means that the quantity of mis-classifications exceeds that of the correct predictions. This effect could be due to the fact that these two categories of subjects have a very similar

pupillary activity, so that they cannot be clearly distinguished. The classification results are summarized in Table 3.3.

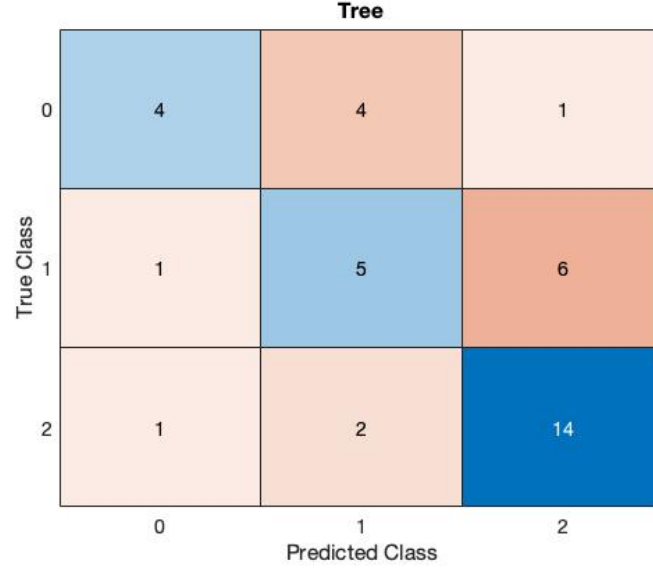


**Figure 3.21:** Confusion matrix related to the binary decision tree predictions. For each class, the number of correct classifications is reported on the diagonal of the matrix (blue boxes), whereas wrong classifications are inserted in the orange boxes.

Classification results	
Accuracy	60.53%
Correctly classified Class 0	44.44%
Correctly classified Class 1	41.67%
Correctly classified Class 2	82.35%
Misclassification Cost Loss	44.17%

**Table 3.3:** Classification performance results.

In the next stage of the study, the data set has been completed with the addition of healthy subjects' recordings and the same operations have been carried out to assess whether there is a difference between healthy and pathological people, in terms of pupillary activity.

## Chapter 4

# Pupillary acquisitions on healthy subjects

In order to significantly assess whether the progression of the disease affects the proper functioning of the ANS, and therefore the respective control of pupillary reflexes, a new data set of healthy subjects has been created, from which the same pupillary indices have been extracted and compared with those of ALS patients.

### 4.1 Pupillometry system

The new subjects' pupillographic signals have been recorded through the Pupil Core® eye tracking system[43], which is a platform that is comprised of an open source software suite and a wearable eye tracking headset (Figure 4.1).

The system consists of two inward-facing eye infrared cameras (maximum sampling frequency of 200 Hz) and one forward-facing world camera mounted on a wearable eyeglasses-like frame. The device provides information about gaze and pupil diameter, detected through a 2D and a 3D models. The former provides a pupil diameter relative size in eye camera pixels, while the absolute size in mm is obtained through the 3D eye model.

The Pupil Core® has a USB-C connector clip that allows to connect the headset to a computer via USB-C to USB-A cable. Once the device is connected to the computer, data reading and recording occur through two Pupil Core® software: Pupil Capture and Pupil Player.

#### 4.1.1 Pupil Capture

Pupil Capture is the software used with the Pupil Core Headset. The software reads the video streams coming in from the world camera and the eye cameras.





**Figure 4.1:** Pupil Core® headset.

Pupil Capture uses the video streams to detect pupil, track gaze, detect and track markers in the environment, record video and events, and stream data in real-time. The World window is the main control center for Pupil Capture. The World window (Figure 4.2) displays a live world camera video feed from the devices.



**Figure 4.2:** Pupil Capture World window.

There are four buttons groups:

1. **Graphs:** This area contains performance graphs. By default, the graphs CPU, FPS, and pupil algorithm detection confidence is displayed.
2. **Hot keys:** This area contains clickable buttons for plugins.

3. **Menu:** This area contains settings and contextual information for each plugin.
4. **Sidebar:** This area contains clickable buttons for each plugin. System plugins are loaded in the top and user added plugins are added below a horizontal separator.

The recording focuses on the pupillary diameter, so the calibration of the gaze was skipped. In order to view images recorded by eye cameras and to check their correct positioning, select *General Settings* from the Sidebar and enable the features *Detect eye 0* and *Detect eye 1* (Figure 4.3).

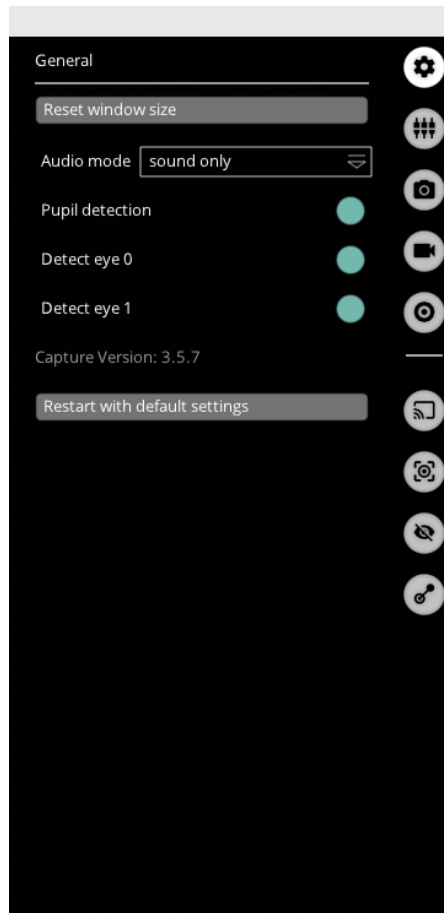


**Figure 4.3:** Eye cameras enabling from *General Settings* menu.

In this way, two windows open on the computer screen that show the eyes captured by the two cameras and the pupils detection (red lines). An example is reported in Figure 4.4.

Once the correct positioning of the eye cameras is verified, the recording starts by

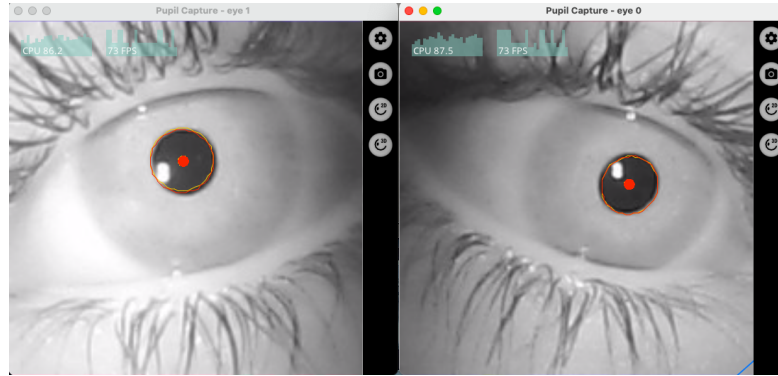


**Figure 4.4:** Pupil Capture windows that shows eye recordings and pupil detection.

clicking the *R* button on the *Hot keys* area (Figure 4.2). Finally, select *Recording* from the *Slidebar* and insert it in *Path to recordings* to choose the path to save the records.

### 4.1.2 Pupil Player

Pupil Player is the second tool to use after Pupil Capture. It is a media and data visualizer which allows to look at Pupil Capture recordings, visualize data and export it. Firstly, the folder containing pupil recordings is dropped by dragging it to the home screen (Figure 4.6).

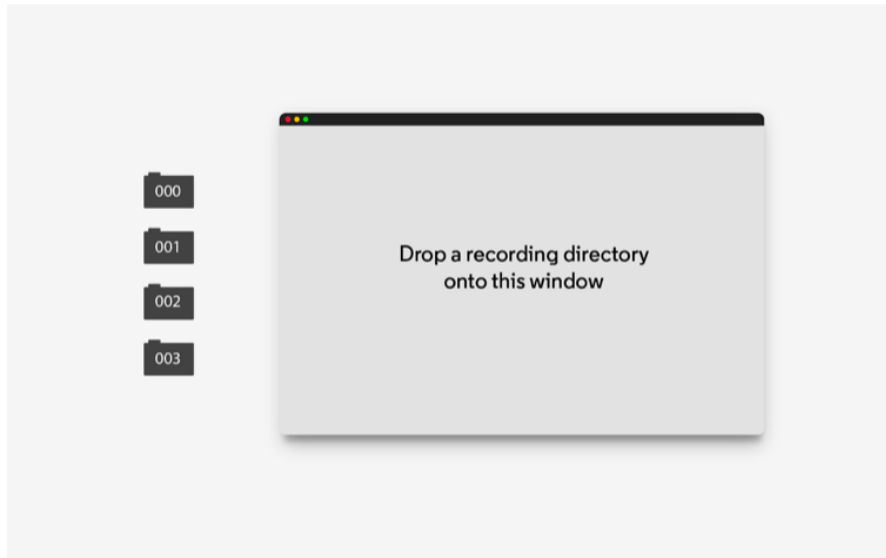


**Figure 4.5:** Pupil Player home screen.

After that, the Player window appears, which is the main control center.



**Figure 4.6:** Player window.

There are six button groups:

1. **Graphs:** This area contains performance graphs. It display CPU, FPS and pupil algorithm detection confidence.
2. **Hot keys:** This area contains clickable buttons for plugins.
3. **Timeline Events:** Plugins that can add temporal events to this expandable panel.
4. **Timeline:** Control the playback of the video with the play/pause button (or spacebar on the keyboard). The playhead (vertical line) can be dragget to the desired point in time.
5. **Menu:** This area contains settings and contextual information for each plugin.
6. **Sidebar:** This area contains clickable buttons for each plugin.

Pupil Player allows to reproduce the World Video recording and to export pupil data. To do this, click on the *Raw data exporter* button in the *Hot keys* area: the data is saved into a sub-folder named "export", in which the pupillary signal is

stored in *.csv* format. In particular, a table with 34 columns is generated: each column represents a certain measurement obtained from the pupil record. This table can be read in MATLAB®, via the *readtable* command and the time axis and the right and left pupillary diameter measure can be extracted from it. The right and left pupillary diameters are then separated by considering the value in the column *eye\_id*: 0 for the right eye and 1 for the left one.

## 4.2 Data set

In order to complete the data set with indices extracted from the pupillogram of healthy people, 10 students of the Polytechnic of Turin (7 men and 3 women) were recruited. The median age of subjects is 24.7 years with a standard deviation of 1.77. The new recordings were made at the Laboratory of Integrative Physiology (Department of Neuroscience) of University of Turin, between the 3<sup>rd</sup> and the 12<sup>th</sup> June 2022.

The new data set, which includes both ALS patients and healthy people recordings, consists of **48 subjects** in total.

## 4.3 Experimental setup

The aim of the experiment is to evaluate the pupil oscillations in a completely dark environment and the response to light stimuli. In order to simulate these conditions, a canopy made from thick black cloth (the same involved for ALS patients in the previous recording session) has been set up, inside which the subject has been located. Each subject wore the Pupil Core headset, adjusting it properly so that the eye cameras could get a good view of the pupils, and got inside the canopy. Here, a computer was placed on a little table to manage the stimulation.

The stimulation consisted in black and white screens alternation, as follows: 120 seconds of dark screen, in order to give the pupil the necessary time to adapt to the dark and to record the Hippus oscillation (in the last 60 seconds); then, four cycles of light stimulation, with a white screen lasting 2 seconds, followed by a black screen 30 seconds long. A small gray square (20 by 20 pixels) was also displayed at the center of the screen to allow subjects to focus on a single point. To do this, the Psychtoolbox-3[44] was exploited, a package of functions implemented in MATLAB®, allowing the control of the display frame buffer.

The recordings and the stimuli were managed by a MacBook Air with an Intel Core i5 dual-core processor, 8 GB of RAM and a 64-bit MacOS Big Sur 11.6. Moreover, an external operator could control the MATLAB® script execution and the pupillary signals registration by duplicating the screen on an external monitor, via HDMI connection.

## 4.4 Signal processing

As for the pupil recording belonging to ALS patients, the pupillographic signals taken from healthy subjects have undergone a signal processing phase for the removal of eye blinks and other artifacts. Again, the hippus and the PLR records have been analyzed separately.

### 4.4.1 First part: Pupillary Hippus

The data has been imported into MATLAB® from the file named "pupil\_position.csv". A  $n \times m$  table is generated in the workspace, where:

- $n$  is the number of recording samples, it depends on its duration;
- $m$  is the number of features extracted from the pupillogram, that is 34.

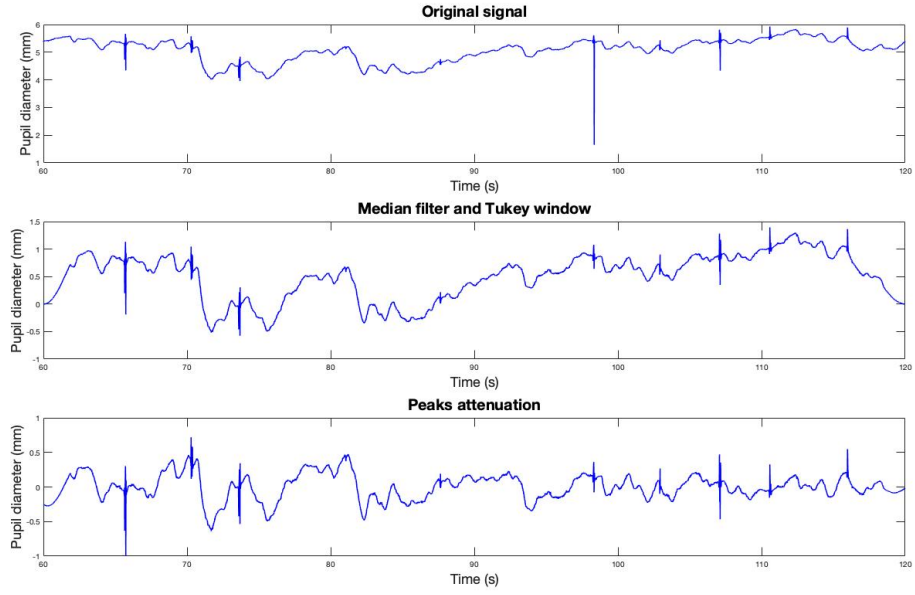
Among these features, only a few of them are useful for the purpose of the study. For this reason, the following columns have been selected:

- *pupil\_timestamp*, that is the time axis;
- *method*, that allows to distinguish the data acquired in 2D from those in 3D;
- *eye\_id*, that allows to distinguish the right eye (*eye\_id* = 0) from the left eye (*eye\_id* = 1);
- *diameter\_3d*, which contains the samples of the signal acquired through the 3D method, of both eyes.

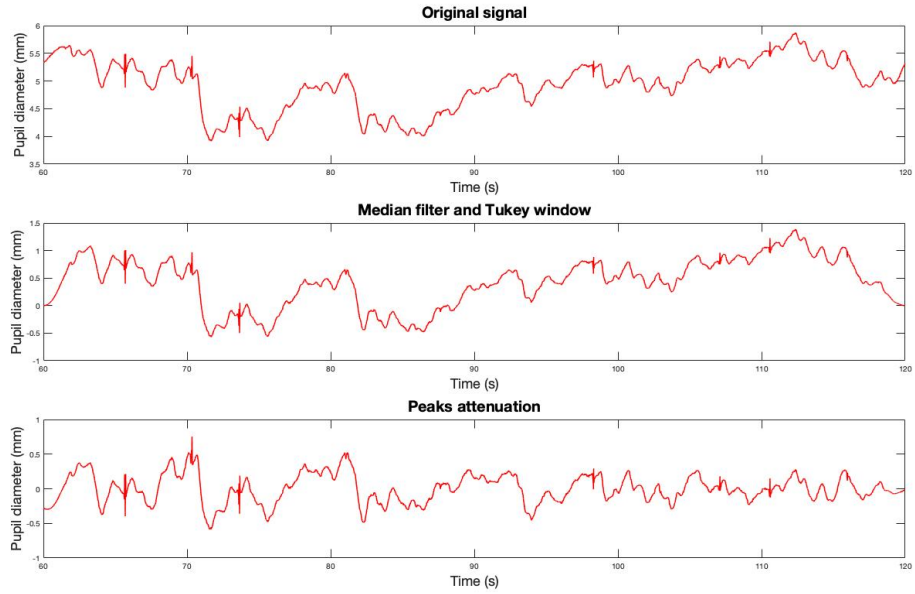
Firstly, the time axis was shifted to 0 seconds by subtracting the value of the first sample from the whole vector.

Then, the samples acquired in 2D and 3D have been separated into two matrices, according to the string in the *method* column: "2d c++" refers to 2D data and "pye3d 0.3.0 real-time" refers to 3D recordings.

The 3D data matrix was considered, since this method offers more precise acquisitions and the pupillary diameter absolute value in mm. This matrix was further divided into two matrices, one for each eye (according to the value reported in the *eye\_id* column). Therefore, for each subject, two matrices have been studied, one for each eye, containing the pupillographic signal samples, obtained by the 3D method. Finally, the columns to be isolated for the study of the hippus were *pupil\_timestamp* and *diameter\_3d*.



(a) Right eye



(b) Left eye

**Figure 4.7:** Representation of the pupillary diameter as a function of time, in the second minute of the recording. In each plot the original signal, the results of the median filter and Tukey's window application, and the signal obtained after high-pass filtering are reported. This signal has been taken from Subject 006 of Healthy Subjects Group.

Initially, the recordings of the left and right eye signals were processed separately. A linear interpolation was applied on the two signals, since the sample frequency was not constant. From the original time axis, the shortest time interval between one sample and the other one has been calculated (0.0081 s) and it has been taken as reference for the creation of a new time axis with a constant sampling rate of 123.46 Hz (whereas the Eye Tribe provided a sampling frequency of about 55 Hz).

For the hippus analysis, a time window between 60 s and 120 s has been selected: in this way, the first minute of recording, useful to the pupil to get used to the dark environment, has been discarded and the pupillary diameter under steady-state conditions was considered. Then, the following procedures have been applied:

1. application of a 21<sup>st</sup> order median filter, aiming to remove the abnormal peaks due to eye blinks;
2. removal of the pupil diameter mean value;
3. application of a Tukey's window with a cosine fraction of 0.1, in order to cut off the first and the last three seconds of the recording, that could be distorted by the application of the high-pass filter;
4. third-order highpass Chebyshev II filtering, with a stopband edge frequency of 0.05 Hz and a stop band ripple attenuation of 20 decibels: this allows to attenuate any low frequency trends.

The results are shown in Figure 4.7a and Figure 4.7b.

The two resulting signals have been averaged. Then, the right and left pupillary diameters and the average diameter have been represented together on a single graph (Figure 4.8), which showed that they have a comparable low-frequency trend over time. This allowed to conceive the study on the average diameter pupillogram, from which the same indices of ALS patients have been extracted:

- Time domain indices
  - average amplitude of pupil diameter (before high-pass filtering);
  - variance of the probability distribution of pupil size;
  - skewness of the probability distribution of pupil size;
  - kurtosis of the probability distribution of pupil size.
- Frequency domain indices
  - $P_{LF}/P_{HF}$ 
    - \* 1<sup>st</sup> method: Literature intervals;



- \* 2<sup>nd</sup> method: Extended literature intervals;
- \* 3<sup>rd</sup> method: Adaptive intervals;
- % of PSD included in the LF band ( $P_{LF}$ ), compared to the total power;
- % of PSD included in the HF band ( $P_{HF}$ ), compared to the total power;
- PSD mean frequency (MNF).

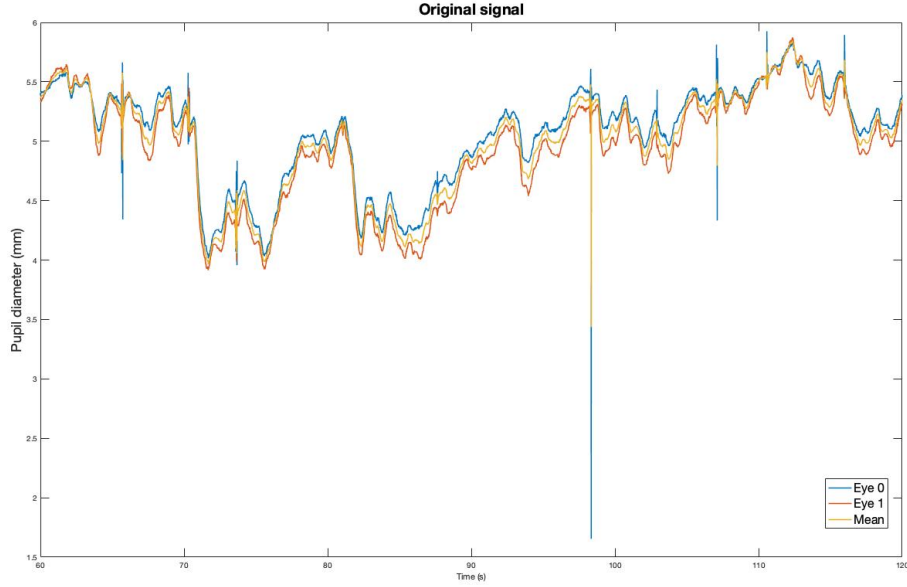


**Figure 4.8:** Pupillograms comparison, referring to right pupil (in blue), left pupil (in red) and to the average signal (in yellow) over time.

#### 4.4.2 Second part: Pupillary Light Reflex

In order to study pupillary response to light stimuli (PLR), the second part of the time series has been selected, by discarding the first two minutes of the recording. The aim is to study the speed of pupillary constriction and dilation when a light pulse is provided.

As in the case of the hippus, the signals related to the pupillary diameter of both eyes were extracted from the file "pupi\_position.csv" and they have undergone a pre-processing step, consisting of the following operations:

1. 21<sup>st</sup> order median filter application, for eye blinks attenuation;
2. pupil diameter mean value removal;

3. average pupillary diameter calculation, starting from the right and left pupils traces.

The resulting signal has been displayed on the screen, allowing the user to select the intervals related to the descending and the ascending tracts, for each PLR (Figure 4.9).

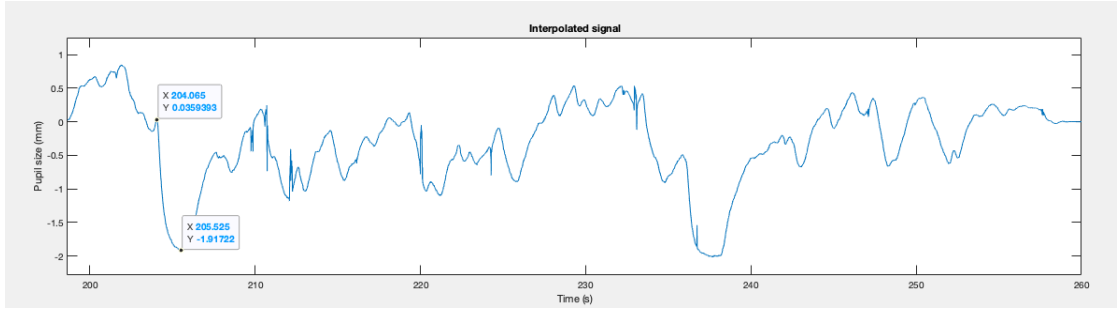


**Figure 4.9:** Constriction and dilatation intervals selection for PLRs' indices evaluation. The signal has been taken from Subject 006 of Healthy Subjects Group.

This operation is carried out twice:

- i. firstly, the intervals selection was required in order to perform the exponential interpolation of the signal;
- ii. then, the intervals were selected by choosing the maximum and the minimum value of the pupil size. In this way, the response time and the range of variation of the diameter could be assessed.

From the selected ranges, the following indices have been extrapolated:

- time constant  $\tau_{dis}$  related to the interpolating exponential of the PLR descender (average value on three PLRs);
- time constant  $\tau_{asc}$  related to the interpolating exponential of the PLR riser (average value on three PLRs);
- response time of pupil constriction after the light pulse, that is the time interval required to reach the 66% of the minimum diameter amplitude, taking as reference the average diameter evaluated in the 0.5 s before the stimulus (average value on three PLRs);
- response time of pupil dilatation to reach the rest size, that represents the time interval needed for the pupil to reach the 66% of amplitude between the maximum construction value and the average diameter calculated in the 0.5 s before the stimulus (average value on three PLRs).

Healthy subjects and the indices extracted from their pupillogram have been analyzed and provided to the classifier to assess whether there is an effective change in autonomic functionalities due to the progress of ALS.

## 4.5 Data analysis

Firstly, the data set has been split into classes, according to the ALSFRS-R score associated to each patient. Two types of subdivisions have been carried out: division into **two classes** and division into **three classes**. The aim is to understand what is the division into groups that evokes a relevant difference among them and which provides the highest percentages of correct classifications. To achieve this purpose, statistical tests on the data distribution were introduced and the features set providing the highest classification accuracy was extracted.

### 4.5.1 Two classes partition

The first considered data set division was between **healthy** and **pathological** subjects. By referring to the ALSFRS-R score, subjects were divided as follows:

- **Class 0:**  $0 \leq \text{ALSFRS-R} \leq 44$ ;
- **Class 1:**  $45 \leq \text{ALSFRS-R} \leq 48$ .

As a result, Class 0 is composed by 34 observations and it refers to the group of pathological subjects, while the remaining 14 ones constitute Class 1, which instead represents healthy people.

For each feature, the distribution of values has been represented by two box-plots, one for each class (Figure 4.10, Figure 4.11 and Figure 4.12), in order to assess qualitatively whether the two categories of subjects actually belong to two different populations, by considering the position of the respective medians and the dispersion of the values around them.

For convenience, the graphs have been divided into three groups, according to the type of the indices, whose observations are described below:

- **Pupillary hippus - time domain indices distribution** (Figure 4.10): healthy and pathological subjects show a very different distribution of values in terms of *skewness* and *kurtosis*. In the case of third and fourth order moments, distributions have values of the median line qualitatively distinguishable for the two classes and the data are much more scattered around the median in the case of Class 1.

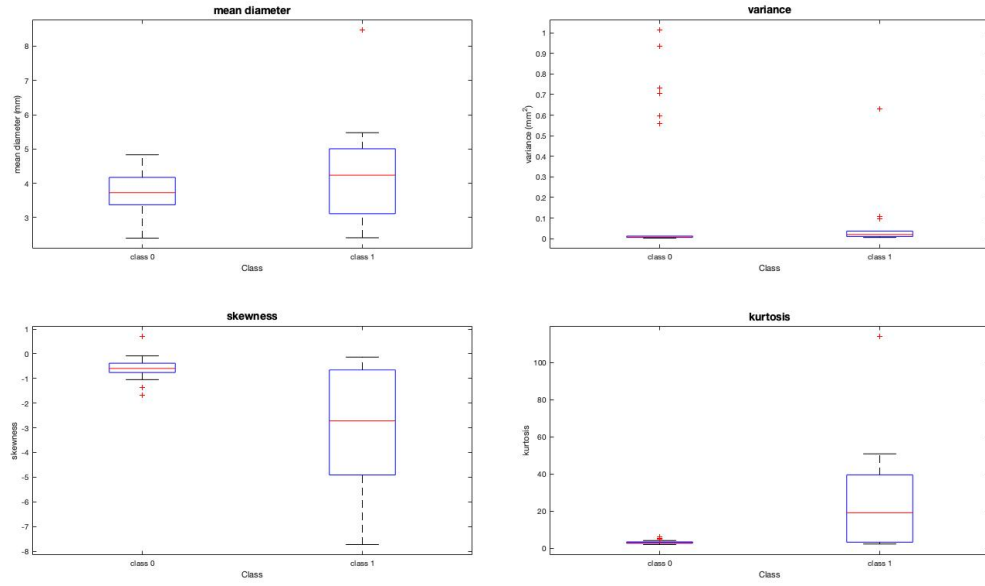


**Figure 4.10:** Pupillary hippus - time domain indices distribution, represented by box-plots.

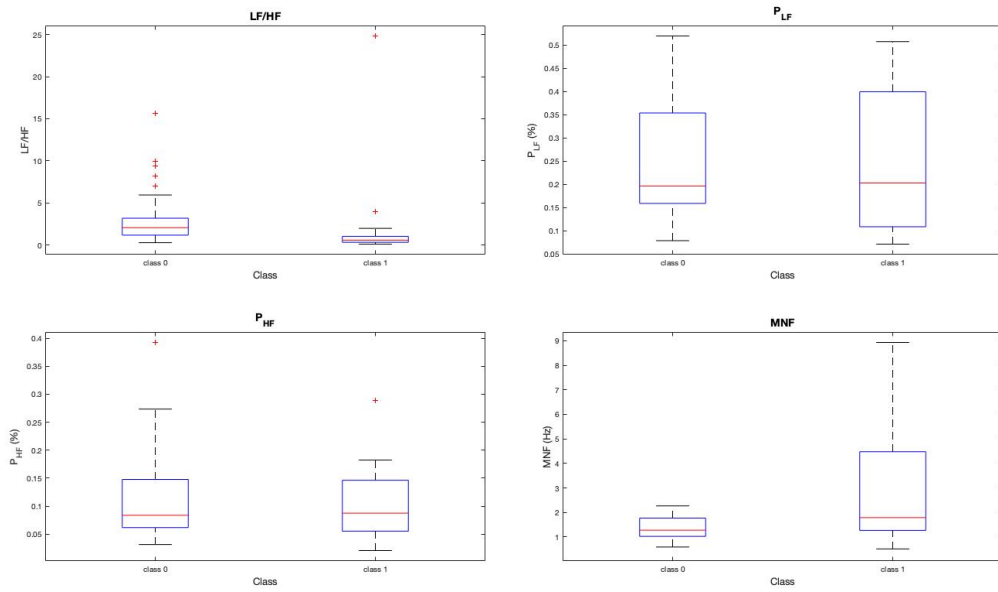


**Figure 4.11:** Pupillary hippus - frequency domain indices distribution, represented by box-plots.

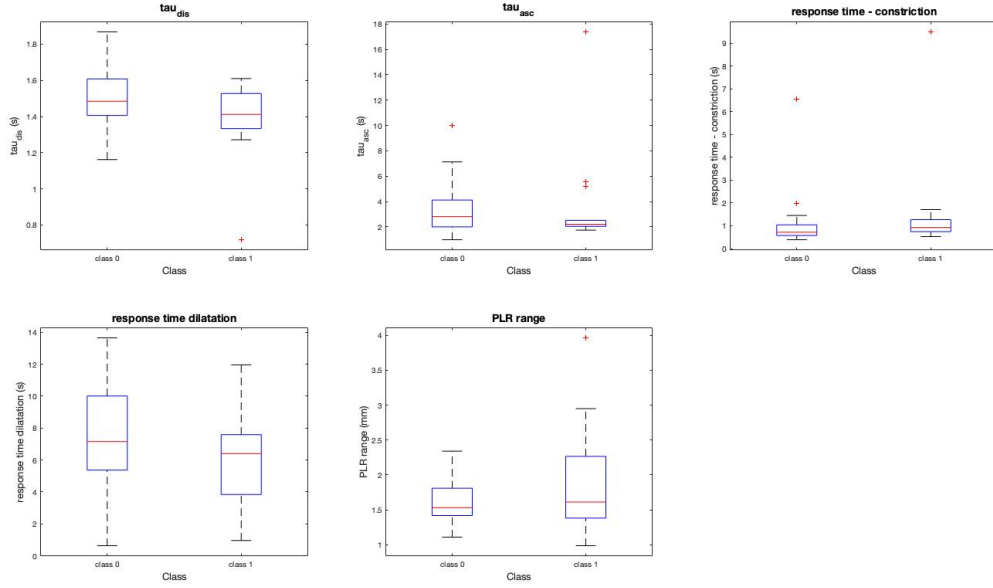


**Figure 4.12:** PLR - time domain indices distribution, represented by box-plots.

- **Pupillary hippus - frequency domain indices distribution** (Figure 4.11): the « $LF/HF$ », « $P_{LF}$ » and « $P_{HF}$ » indices show no substantial differences between the two classes in terms of data distribution. In the case of Class 1, the « $MNF$ » distribution has more scattered values compared to the median line.
- **PLR - time domain indices distribution** (Figure 4.12): for this set of indices, there are no clear differences between the two classes.

### Wilcoxon test

A more concrete measure to determine whether two classes differ significantly, was provided by the **Wilcoxon test**.

The Wilcoxon test is a non-parametric test, since it is based on ranks. It is chosen whenever the purpose is to compare two populations taking as reference an index different from the mean value and where the form of the distribution of the sampled population is not known. Indeed, in this case, the test was conducted on the median value.

The test returns the p-value of a two-sided Wilcoxon rank sum test, which allows to accept or reject the null hypothesis ( $H_0$ ) whereby data in Class 0 and Class 1 are samples from continuous distributions with equal medians.

The **p-value** is the probability, for a supposedly true hypothesis, of obtaining results that are equally or less compatible, than those observed during the test, with the aforementioned hypothesis. In other words, the p-value helps to understand if the difference between the observed and the assumed result is due to the randomness introduced by the sampling, or if this difference is statistically significant, that is difficult to explain by the randomness due to sampling.

The p-values have been obtained through the MATLAB® routine *ranksum*, which took as input the two distributions for each index. For the two classes subdivision, the function provided the p-values reported in Table 4.1.

p-values	
mean diameter	0.2520
variance	0.0201
skewness	0.0023
kurtosis	0.0011
$P_{LF}/P_{HF}$	0.0018
$P_{LF}$	0.5180
$P_{HF}$	0.8471
MNF	0.0613
$\tau_{dis}$	0.1001
$\tau_{asc}$	0.3238
response time - constriction	0.0768
response time - dilatation	0.2164
PLR range	0.4207

**Table 4.1:** p-values resulting from the Wilcoxon rank sum test.

The p-value is compared with an index, known as **significance level  $\alpha$** , through which it is assessed whether the null hypothesis can be accepted or rejected, according to the following rules:

- p-value  $\leq \alpha \longrightarrow$  the null hypothesis is true;
- p-value  $> \alpha \longrightarrow$  the null hypothesis is rejected.

Typically, a value of  $\alpha = 0.05$  is considered.

The values collected in Table 4.1 show that **variance**, **skewness**, **kurtosis** and  **$P_{LF}/P_{HF}$**  have a p-value lower than  $\alpha$  (Figure 4.13), therefore these indices are associated to frequency distributions which are significantly different between healthy and pathological subjects. Such indices could be taken as a reference to assess whether there is a real difference between Class 0 and Class 1.

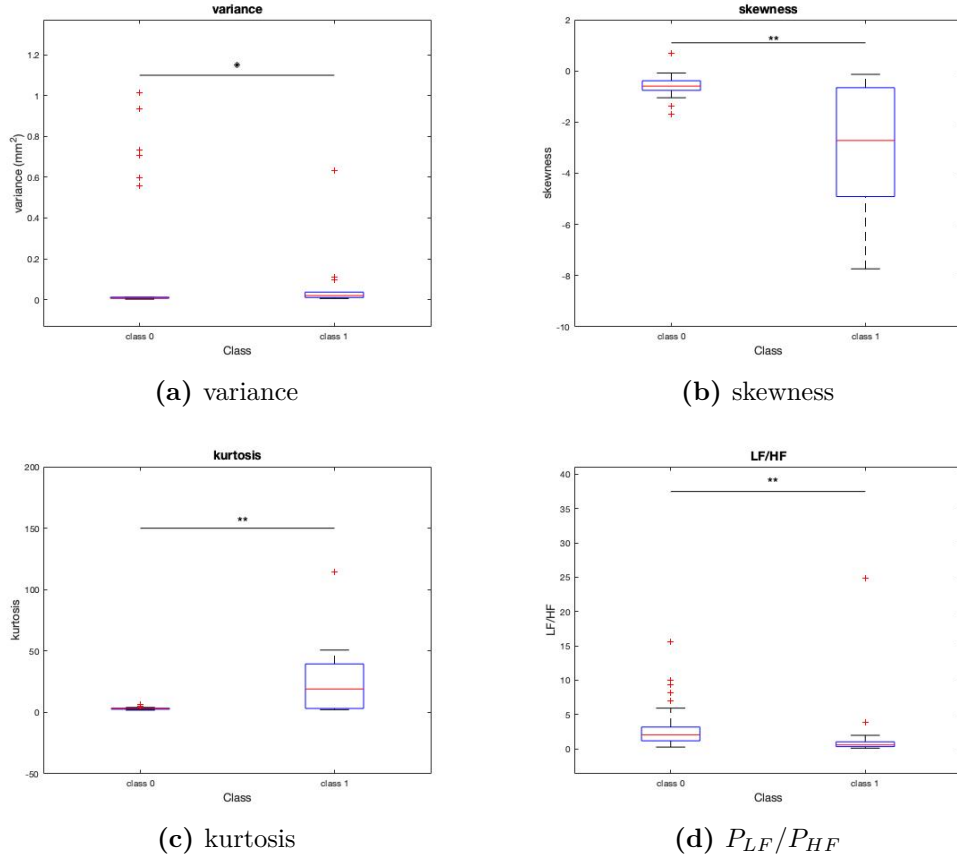


**Figure 4.13:** Boxplots showing the significantly different frequency distributions of variance, skewness, kurtosis and  $P_{LF}/P_{HF}$  related to Class 0 and Class 1. The levels of significance are also reported: \* $p < 0.05$  and \*\* $p < 0.01$ .

### Binary tree classification

As described in Section 3.4.3, a binary decision tree which was able to make a distinction between healthy and pathological subjects has been trained, by providing each time all possible combinations of the 13 features. Even in this case, the Training Set and the Test Set have been determined using the LOOCV approach to avoid over-fitting effects.

The rules of classification followed by the binary decision tree are represented in Figure 4.14. The tree is characterized by 2 branches nodes and a height of 2.

The most performing classifier has been chosen by evaluating the classification accuracy that is the percentage of correctly classified for each class:

$$accuracy(\%) = \frac{\sum \text{correctly classified}}{\sum \text{all elements of data set}} \cdot 100 \quad (4.1)$$

$$\% \text{ correctly classified} = \frac{\sum \text{correctly classified Class } X}{\sum \text{True Class } X} \cdot 100 \quad (4.2)$$

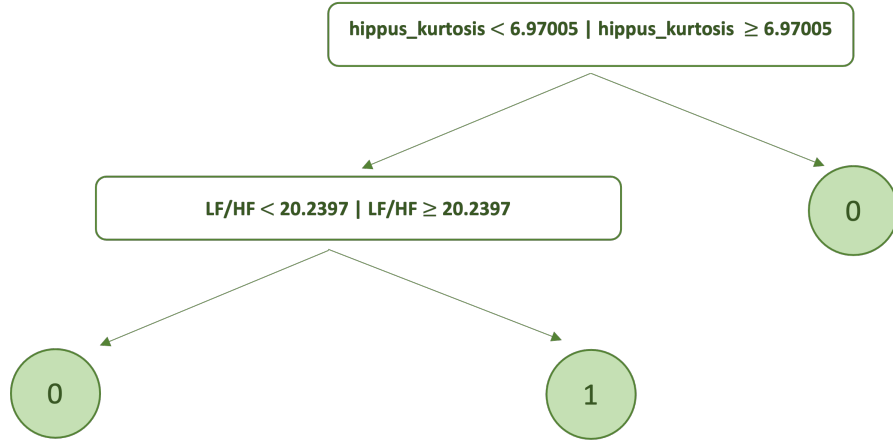


**Figure 4.14:** Decision tree rules for Class 0 and Class 1 prediction.

In this case, the combination of indices which provided the higher accuracy was: **variance - kurtosis -  $P_{LF}/P_{HF}$  -  $\tau_{dis}$  - PLR range**. The results of the classification are shown in Figure 4.15.

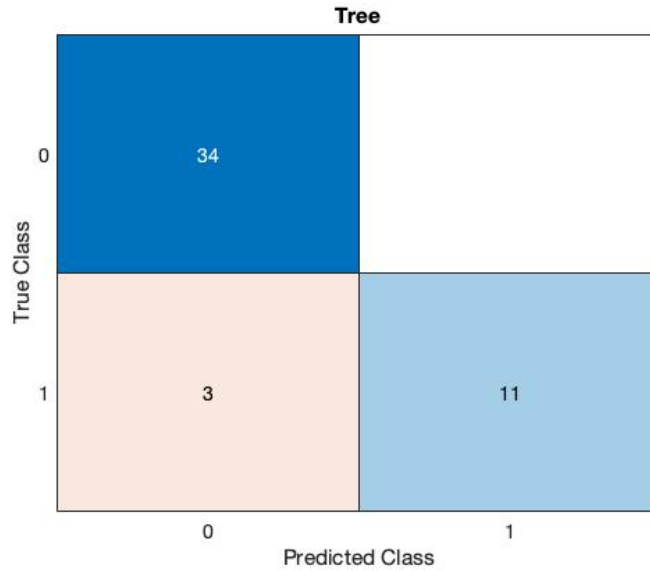


**Figure 4.15:** Confusion matrix showing the results of the binary tree classification for Class 0 and Class 1 with *variance*, *kurtosis*,  $P_{LF}/P_{HF}$  -  $\tau_{dis}$  and *PLR range* as input variables.



From the confusion matrix, the accuracy (4.1), the percentage of correctly classified for each class (4.2) and the misclassification cost loss (3.10) have been evaluated:

Classification results	
Accuracy	93.75%
Correctly classified Class 0	100%
Correctly classified Class 1	78.57%
Misclassification Cost Loss	6.91%

**Table 4.2:** Classification performance results - 2 classes

### 4.5.2 Three classes partition

The data set has been now divided into three groups, according to the motor impairment level of the subject, represented by the ALSFRS-R score. The aim is to try to distinguish severe patients from those at a moderate stage of the disease. The data set subdivision was carried out as follows:

- **Class 0:**  $0 \leq \text{ALSFRS-R} \leq 29$ ;
- **Class 1:**  $30 \leq \text{ALSFRS-R} \leq 44$ ;
- **Class 2:**  $43 \leq \text{ALSFRS-R} \leq 48$ .

Consequently, Class 0 is composed by 9 subjects comprising LIS and very impaired ALS patients; Class 1 represents ALS patients moderately compromised and it includes 24 subjects; Class 2 comprises 15 subjects, including healthy people and those with mild symptoms.

For each feature and for each class, the frequency distribution has been represented through box-plots in order to compare them among classes. This kind of representation allow to appreciate any differences among the values distribution and how they are scattered around the median line. Even in this case, the graphs have been divided into three groups according to the type of represented variable (Figure 4.16, Figure 4.17 and Figure 4.18). Some observations about data are reported below:

- **Pupillary hippus - time domain indices distribution** (Figure 4.16): the indices extracted from the pupillary diameter at rest, are distributed in ranges of values that superimpose in the three classes. Among them, the high variability of skewness and kurtosis in the case of healthy subjects can be observed, compared to Classes 1 and 0, whose values are more concentrated around the median.

- **Pupillary hippus - frequency domain indices distribution** (Figure 4.17): the indices extracted from the pupillogram PSD have a very similar behavior in the 3 classes: the ranges of values overlap and there are no obvious differences between the categories.
- **PLR - time domain indices distribution** (Figure 4.18): again, the distributions are placed in overlapped ranges, except in the case of the **response time - dilatation**, in which Class 1 seems to stand out from the other two. The high variability of the data does not allow a clear distinction between the three classes.

### Kruskal-Wallis and Wilcoxon tests

When the classes to be compared are more than two, like in this case, the Wilcoxon rank sum test cannot be directly exploit, but it is necessary to introduce another type of statistical test before, so as to understand which variables have significantly different distributions of values among the three classes. The Wilcoxon test has been subsequently exploited in order to compare the classes, in pairs. The Kruskal-Wallis test has been chosen for this purpose.

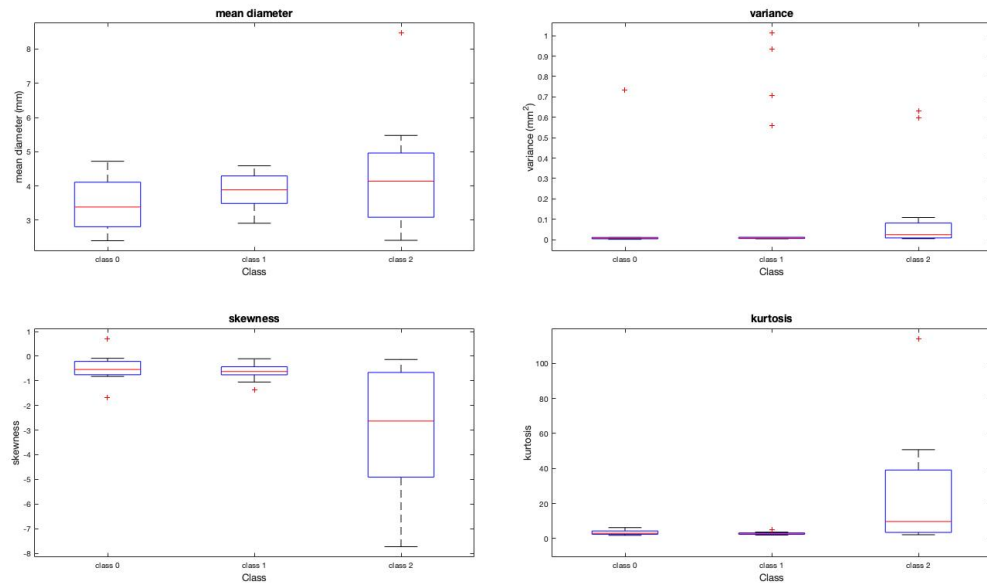


**Figure 4.16:** Pupillary hippus - Time domain indices distribution, represented by box-plots.

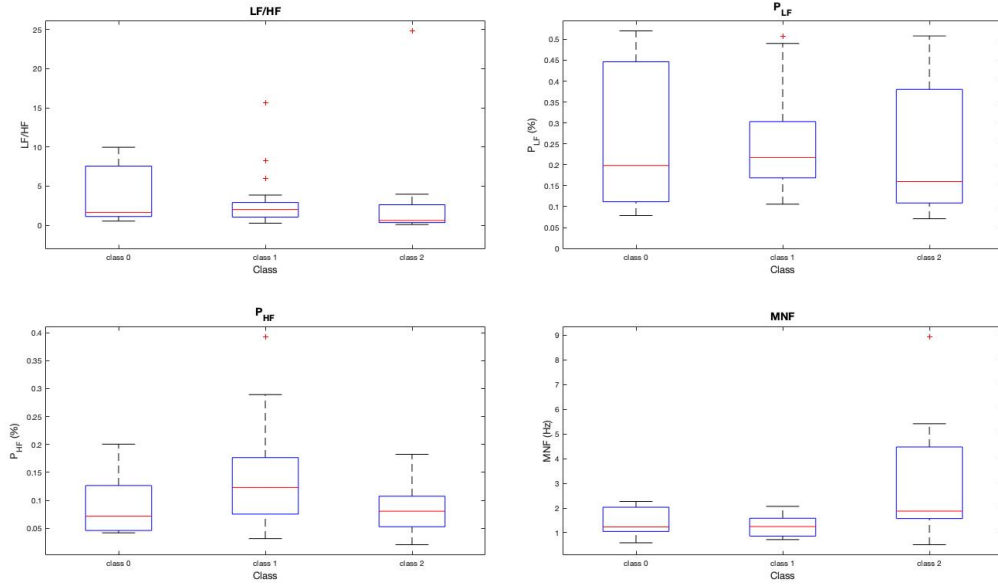


**Figure 4.17:** Pupillary hippus - frequency domain indices distribution, represented by box-plots.

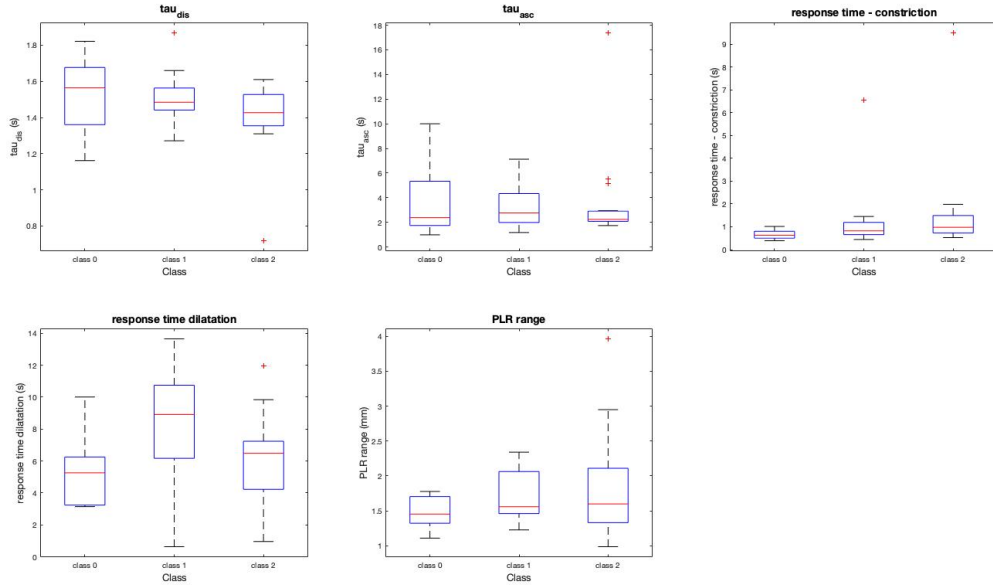


**Figure 4.18:** PLR - time domain indices distribution, represented by box-plots.

The Kruskal-Wallis test is a non-parametric version of classical one-way ANOVA, and an extension of the Wilcoxon rank sum test to more than two groups. It compares the medians of the groups of data to determine if the samples come from the same population. The test returns the p-value for the null hypothesis ( $H_0$ ) that the data in each groups comes from the same distribution, against the alternative hypothesis ( $H_1$ ) according to which not all samples come from the same distribution. The resulting p-values, for each index, are shown in Table 4.3.

p-values	
mean diameter	0.2148
variance	0.0355
skewness	0.0045
kurtosis	0.0004
$P_{LF}/P_{HF}$	0.0810
$P_{LF}$	0.6096
$P_{HF}$	0.0560
MNF	0.0163
$\tau_{dis}$	0.2669
$\tau_{asc}$	0.8822
response time - constriction	0.0274
response time - dilatation	0.0068
PLR range	0.4253

**Table 4.3:** p-values resulting from the Kruskal-Wallis test.

By comparing the p-values with the significance level  $\alpha = 0.05$ , it is deduced that the null hypothesis can be rejected in the case of **variance**, **skewness**, **kurtosis**, **MNF**, **response time - constriction** and **response time - dilatation**. Therefore, for these features, the probability that the three groups belongs to the same population is very low.

A more detailed study has been carried out on the above mentioned variables, in order to understand which classes are significantly different. To do so, for each possible pair of classes, a Wilcoxon test has been carried out, from which new p-values were obtained (Table 4.4).

Even in this case, the p-values have been compared with the significance level  $\alpha$  and the couples of classes that are significantly different have been obtained and represented in Figure (4.19).

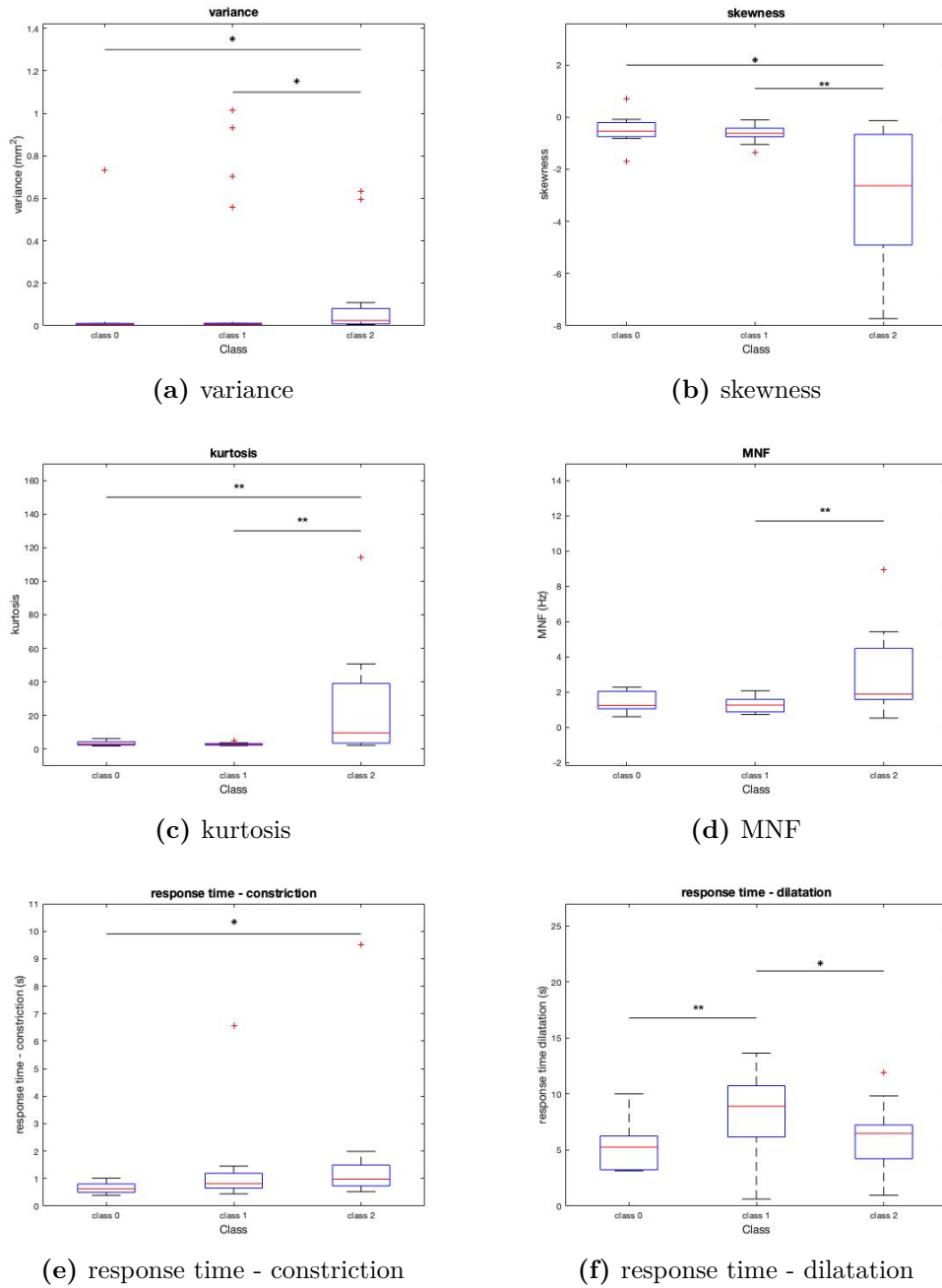


**Figure 4.19:** Boxplots showing the significantly different frequency distributions of variance, skewness, kurtosis, MNF, response time - constriction and response time - dilatation, related to Class 0, Class 1 and Class 2. The levels of significance are also reported: \*p<0.05 and \*\*p<0.01.

classes	p-values					
	variance	skewness	kurtosis	MNF	r.t. - con.	r.t. - dil.
0 - 1	0.2176	0.4072	0.4305	0.4793	0.0574	0.0064
1 - 2	0.0480	0.0037	0.0002	0.0053	0.1989	0.0272
0 - 2	0.0318	0.01035	0.0073	0.0950	0.0123	0.2330

**Table 4.4:** p-values resulting from Wilcoxon test for each pair of classes.

### Binary tree classification

Once the frequency distributions of the various indices have been analysed, a binary decision tree has been trained and tested, exploiting the LOOCV strategy, aiming to distinguish the three classes of subjects.

Even in this case, all the possible combinations of variables have been tested and the best one, i.e. the combination which provided the higher classification accuracy, has been selected and provided as input of the binary tree.

The set of features which provided the higher accuracy was: **variance - kurtosis**. The rules followed by the binary decision tree are shown in Figure 4.20. This tree is characterized by 6 branches nodes and a height of 6.

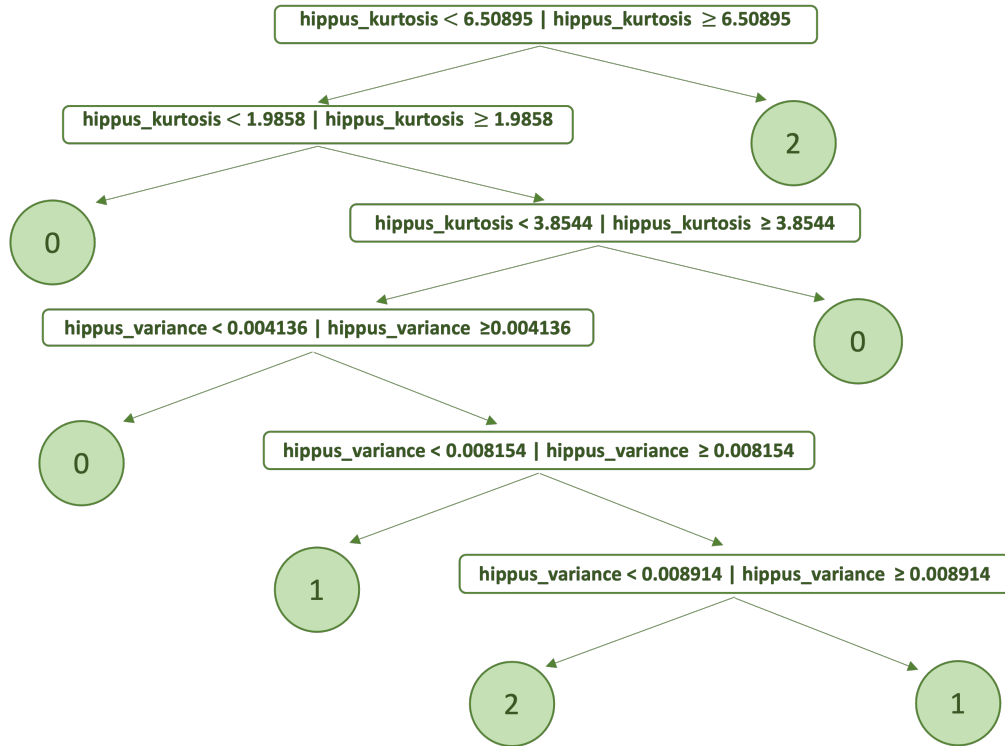


**Figure 4.20:** Decision tree rules for Class 0, Class 1 and Class 2 prediction.

The results of the classification are represented through a confusion matrix (Figure 4.21). In order to evaluate the performance of this classifier, the accuracy of classification (4.1), the percentage of correctly classified for each class (4.2) and the misclassification cost loss (3.10) have been calculated and reported in Table 4.5.

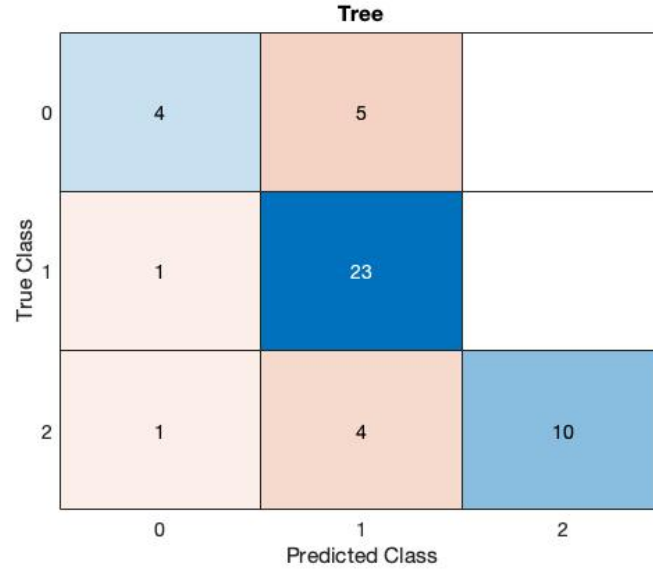


**Figure 4.21:** Confusion matrix showing the results of the binary tree classification for Class 0, Class 1 and Class 2.

Classification results	
Accuracy	77.08%
Correctly classified Class 0	44.44%
Correctly classified Class 1	95.83%
Correctly classified Class 2	66.67%
Misclassification Cost Loss	28.55%

**Table 4.5:** Classification performance results - 3 classes

## Chapter 5

# Discussion of results and conclusions

The features extracted from the pupillographic signals of the subjects recruited for this study enabled to carry out a series of tests on pupil's response over time and some comparisons among the different groups.

By considering the set of indices extracted from the hippus time series, the one that is taken very often as a reference, in the literature, is the ratio between powers in the LF and HF bands ( $P_{LF}/P_{HF}$ ). As already mentioned, the power percentages concentrated in these two frequency bands reflect the activity of the SNS and the PNS, respectively. In this context, an analysis of  $P_{LF}$  and  $P_{HF}$  variations over time has been conducted and, as shown in Figure 3.14, it can be observed that the angular coefficients of the linear functions interpolating the indices are very low. The median values of the angular coefficients frequency distributions are:

- $P_{LF} \longrightarrow 0.00250 \text{ \%}/month$
- $P_{HF} \longrightarrow 0.00063 \text{ \%}/month$

with very low values variability. This suggests that the power values calculated on the hippus PSD do not vary significantly over time, remaining almost constant between one visit and the next one, as well as the  $P_{LF}/P_{HF}$  index. It could be an evidence of pupillary activity invariability, despite the ALS disease, in accordance with the literature.

Moreover, from the representation of the features as a function of the ALSFRS-R score, in both cases of data set with ALS patients only (Figures 3.15, 3.16 and 3.17) and that consisting of both healthy and pathological subjects (Figures 5.1, 5.2 and 5.3), there are no evident increasing or decreasing trends, whereas a high data variability, like in the  $P_{LF}$  and the response time dilatation cases, can be observed.



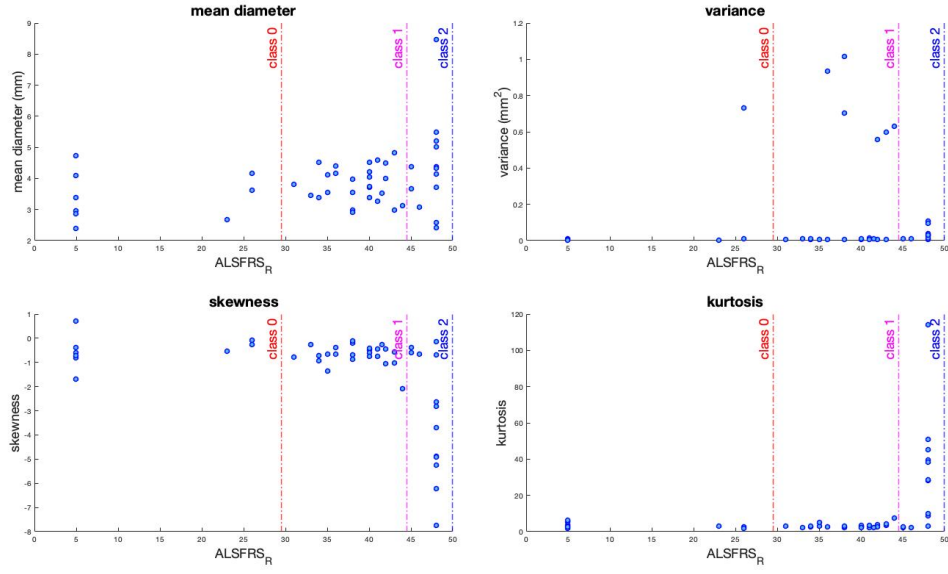


**Figure 5.1:** Pupillary Hippus - time domain indices as a function of the ALSFRS-R score.

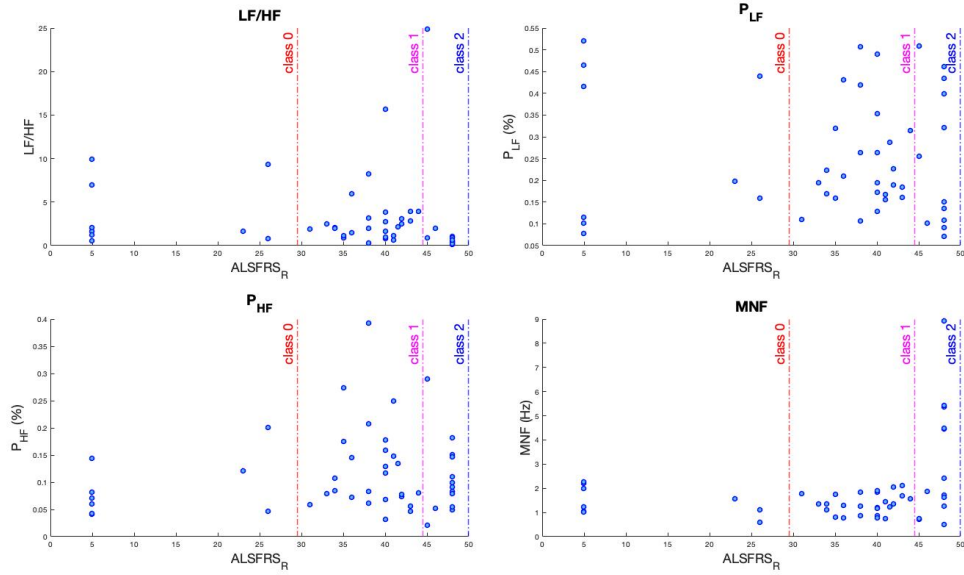


**Figure 5.2:** Pupillary Hippus - frequency domain indices as a function of the ALSFRS-R score.

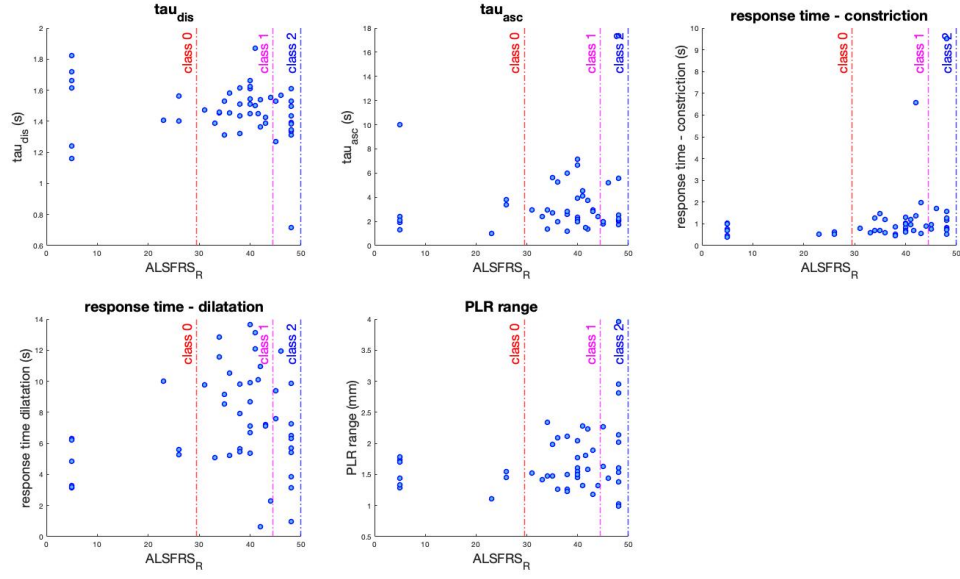


**Figure 5.3:** PLR - time domain indices as a function of the ALSFRS-R score.

By focusing on the binary tree classifier results, its performance varies significantly depending on the data set that is provided. In Table 5.2 the results of classification for each input are summarized.

Classification performance results			
	First data set	Second data set	
	3 classes	2 classes	3 classes
Accuracy (%)	60.53	93.75	77.08
Misclassification cost loss (%)	44.17	6.91	28.55

**Table 5.1:** Summary table of classification performance results of the three tests.

A comparison of the accuracy percentages shows that the best prediction performance is given by the second data set divided into 2 classes, with a classification accuracy of the 93.75%. Also the high percentages of correctly classified for each group (100% for Class 0 and 78.57% for Class 1) and the low misclassification cost loss obtained by cross-validation support the hypothesis that this is the most stable classifier.

In all cases, the binary tree classifier better recognizes the difference between healthy and pathological subjects, than that between ALS patients with severe disease and those with moderate symptoms. In fact, if the classification is performed on the first data set (with ALS patients only) the classification accuracy is about 60% and

the mis-classification error is quite high. The number of correctly classifications for Classes 0 and 1 is also less than half, so that the probability that the classifier is wrong in the prediction is higher than that of correct classification. For these reasons, the subdivision of the pathological group seems to not be optimal and therefore a pupillary activity variations do not emerge as the ALS progresses.

The Kruskal-Wallis and Wilcoxon tests also showed that the most discriminating features were the statistical moments calculated on the hippus values distribution: **variance**, **skewness** and **kurtosis** occur in both the cases of 2 classes and 3 classes data set subdivision (Figures 4.13 and 4.19). Moreover, among the best combinations of features for the binary tree classification, at least one statistical moment is always involved, as shown in Table 5.2.

Features sets		
First data set	Second data set	
<i>3 classes</i>	<i>2 classes</i>	<i>3 classes</i>
average diameter amplitude kurtosis	kurtosis $P_{LF}/P_{HF}$	variance kurtosis

**Table 5.2:** Summary table of the best features combinations provided to the binary tree classifier.

A further classification test was carried out with the K-Nearest Neighbors (KNN) method, with good performance results. In this case, the combinations of variables that provided the higher accuracy were:

- 2 classes: variance, kurtosis and MNF (accuracy = 91,66%);
- 3 classes: average diameter amplitude, skewness and  $\tau_{asc}$  (accuracy = 68,75%).

Again, the data set division into two classes is reconfirmed as the best one in terms of classification stability. In addition, the resulting features combinations confirm the hypothesis that the most discriminating features are those extracted from the hippus' recordings.

As for the pupillary response to light stimuli, no interesting differences between healthy and pathological subjects have arisen, neither from statistical tests between groups nor from the search for the best combinations of features. The greatest differences were mainly found on the indices related to the hippus, suggesting that the PLR (and, consequently, the ANS activity) remains intact as the ALSFRS-R score decreases.

Since the pupillary constriction and dilatation are preserved from the progression of ALS, there are good conditions for the creation of a BCI or other technologies that exploit the pupil's responses as a mean of communication with the outside.

Given the good performance of the 2 classes - predictor, it could be concluded that there is a clear distinction between healthy and pathological subjects in terms of pupillary oscillation in the hippus band; however, the high data variability and the limited size of the data set do not allow to reject the hypothesis that the pupillary activity is not affected by the pathology.

One of the critical aspects of this study was actually the limited number of subjects on which the acquisitions were conducted. It was very difficult to find patients willing to participate in this study, especially in an advanced stage of the disease. Moreover, some of the few available signals have been discarded from the analysis because of the too many artifacts and the poor information content, further reducing the size of the data set. This perspective justifies the choice of a "Leave-one-out" approach in the definition of Training and Test sets. While this method allows to train the classifier with the widest possible Training set and to reduce overfitting, on the other hand, it is very expensive procedure by a computational point of view, in particular in this study where all possible combinations of variables were tested to find the best one.

As future improvement, the data set could be expanded with new pupillary records of healthy and ALS subjects, in order to obtain more meaningful statistical results. Given the interesting results obtained from the analysis of the pupillary hippus, new statistical tests could be conducted and new indices could be extracted from the signals and processed. Furthermore, the expansion of the data set may be beneficial for the classifier: because of and the high data variability, a larger Training set is desirable, in order to reduce the risk of model overfitting and to give up the LOOCV approach which results very expensive from a computational point of view. Moreover, a more balanced classes subdivision could be obtained, by increasing the number of acquisitions on healthy subjects and LIS patients.

In conclusion, given the results of this analysis, the hypothesis of non-variability of the pupillary reflexes and of the Autonomic Nervous System activity is still valid, coherently with the scientific literature. Therefore, it is reasonable to base a communication system on pupil responses, but these assumptions should be confirmed by further analysis on a new data set, consisting of a greater number of subjects.

# Bibliography

- [1] Marchetti M. and K. Priftis. «Brain-computer interfaces in amyotrophic lateral sclerosis: A metanalysis.» In: *Clinical neurophysiology: official journal of the International Federation of Clinical Neurophysiology* 126(6) (2015) (cit. on p. 1).
- [2] Wijesekera Lokesh C. and P. Nigel Leigh. «Amyotrophic lateral sclerosis». In: *Orphanet Journal of Rare Diseases* 4.1 (2009). DOI: 10.1186/1750-1172-4-3 (cit. on p. 3).
- [3] Grad L.I., Rouleau G.A., Ravits J., and Cashman N.R. «Clinical Spectrum of Amyotrophic Lateral Sclerosis (ALS)». In: *Cold Spring Harbor perspectives in medicine* 7.8 (Aug. 2017). DOI: 10.1101/cshperspect.a024117 (cit. on p. 3).
- [4] Hulisz D. «Amyotrophic lateral sclerosis: disease state overview.» In: *Am J Manag Care*. 24(15 Suppl) (Nov. 2018), S320–S326 (cit. on pp. 3, 4).
- [5] Oskarsson B., Gendron T.F., and Staff N.P. «Amyotrophic Lateral Sclerosis: An Update for 2018.» In: *Mayo Clin Proc*. 93(11) (Nov. 2018), pp. 1617–1628 (cit. on pp. 3, 7).
- [6] Elman LB. Ferguson TA. «Clinical presentation and diagnosis of amyotrophic lateral sclerosis.» In: *NeuroRehabilitation*. 22(6) (2007), pp. 409–416 (cit. on p. 4).
- [7] *La sclerosi laterale amiotrofica: scheda scientifica*. AriSLA - Fondazione italiana di ricerca per la sclerosi laterale amiotrofica. URL: <https://www.arisla.org/wp-content/uploads/2014/11/Scheda-scientifica-SLA-approfondita-.pdf> (cit. on p. 5).
- [8] Piccione E.A., Sletten D.M., Staff N.P., and Low P.A. «Autonomic system and amyotrophic lateral sclerosis.» In: *Muscle Nerve* 51(5) (2015), pp. 676–679 (cit. on p. 5).
- [9] Nijssen J., Comley L.H., and Hedlund E. «Motor neuron vulnerability and resistance in amyotrophic lateral sclerosis». In: *Acta Neuropathol* 133(6) (2017), pp. 863–885 (cit. on p. 5).

- [10] Colette Donaghy and Matthew J Thurtell. «Eye movements in amyotrophic lateral sclerosis and its mimics: a review with illustrative cases». In: *J Neurol Neurosurg Psychiatry* 82 (2011), pp. 110–116 (cit. on p. 5).
- [11] Mizutani T., Aki M., Shiozawa R., et al. «Development of ophthalmoplegia in amyotrophic lateral sclerosis during long-term use of respirators». In: *JNeurol Sci* (1990) (cit. on p. 5).
- [12] Hayashi H. and Kato S. «Total manifestations of amyotrophic lateral sclerosis: ALS in totally locked-in state». In: *J Neurol Sci* 93 (1989), pp. 19–35 (cit. on p. 5).
- [13] Ingre C., Roos P.M., Piehl F., Kamel F., and Fang F. «Risk factors for amyotrophic lateral sclerosis». In: *Clin Epidemiol* 7 (2015), pp. 181–193 (cit. on p. 5).
- [14] *La SLA in Italia*. AISLA Onlus - Associazione Italiana Sclerosi Laterale Amiotrofica. URL: <https://www.aisla.it/> (cit. on pp. 5, 6).
- [15] *Stages of ALS*. ALS Association. URL: <https://www.als.org/> (cit. on p. 6).
- [16] Saitoh Y. and Takahashi Y. «Riluzole for the treatment of amyotrophic lateral sclerosis». In: *Neurodegenerative disease management* 10(6) (Aug. 2020) (cit. on p. 7).
- [17] Bedlack R.S., Joyce N., Carter G.T., Paganoni S., and Karam C. «Complementary and Alternative Therapies in Amyotrophic Lateral Sclerosis.» In: *Neurol Clin.* 33(4) (2015), pp. 909–936 (cit. on p. 7).
- [18] Writing Group; Edaravone (MCI-186) ALS 19 Study Group. «Safety and efficacy of edaravone in well defined patients with amyotrophic lateral sclerosis: a randomised, double- blind, placebo-controlled trial». In: *Lancet Neurol.* 16(7) (2017), pp. 505–512 (cit. on p. 7).
- [19] Staff N.P., Madigan N.N., Morris J., et al. «Safety of intrathecal autologous adipose-derived mesenchymal stromal cells in patients with ALS.» In: *Neurology.* 87(21) (2016), pp. 2230–2234 (cit. on p. 7).
- [20] Mazzini L. et al. «Human neural stem cell transplantation in ALS: initial results from a phase I trial.» In: *Journal of translational medicine.* 13(17) (2015) (cit. on p. 8).
- [21] Fried-Oken M., Mooney A., and Peters B. «Supporting communication for patients with neurodegenerative disease». In: *NeuroRehabilitation* 37(1) (2015), pp. 69–87 (cit. on p. 8).
- [22] Hanson E., Yorkston K., and Britton D. «Dysarthria in amyotrophic lateral sclerosis: a systematic review of characteristics, speech treatment, and AAC options». In: *Journal of Medical Speech Language Pathology* 19(3) (2011), pp. 12–30 (cit. on p. 8).

- [23] Beukelman D., Fager S., and Nordness A. «Communication Support for People with ALS». In: *Neurol Res Int* 2011 (2011) (cit. on p. 8).
- [24] Josef Stoll, Camille Chatelle, Olivia Carter, Christof Koch, Steven Laureys, and Wolfgang Einhäuser. «Pupil responses allow communication in locked-in syndrome patients». In: *Curr Biol* 23.15 (Aug. 2013), pp. 647–8 (cit. on p. 9).
- [25] Conti F. *Fisiologia medica. Vol. 1*. Milano, MI: Edi Ermes, 2005 (cit. on p. 10).
- [26] Stanfield C. L. *Principles of human physiology*. EdiSES, 2017 (cit. on p. 10).
- [27] Ferencová N., Višňovcová Z., Bona Olexová L., and Tonhajzerová I. «Eye pupil - a window into central autonomic regulation via emotional/cognitive processing». In: *Physiol Res* 70(4) (2021), pp. 669–682 (cit. on p. 15).
- [28] McDougal D.H. and Gamlin P. D. «Autonomic control of the eye». In: *Compr Physiol* 5(1) (2015), pp. 439–473 (cit. on pp. 16, 17).
- [29] Turnbull P.R.K., Irani N., Lim N., and Phillips J.R. «Origins of pupillary hippus in the autonomic nervous system.» In: *Invest Ophthalmol Vis Sci*. 58 (2017), pp. 197–203 (cit. on p. 18).
- [30] Centeno M., Feldmann M., Harrison N.A., Rugg-Gunn F.J., Chaudhary U., Lemieux L. Falcon C., Thom M., Smith S.J., and Sisodiya S.M. «Epilepsy causing pupillary hippus: an unusual semiology.» In: *Epilepsia*. 52(8) (2011) (cit. on p. 18).
- [31] Denny J.C., Arndt F.V., Dupont W.D., and Neilson E.G. «Increased hospital mortality in patients with bedside hippus.» In: *Am J Med*. 121 (2008), pp. 239–245 (cit. on p. 18).
- [32] Pomè A., Burr D.C., Capuozzo A., and Binda P. «Spontaneous pupillary oscillations increase during mindfulness meditation.» In: *Current Biology*. 30 (2020), pp. 1009–1035 (cit. on p. 18).
- [33] Binda P. and Lunghi C. «Short-Term Monocular Deprivation Enhances Physiological Pupillary Oscillations.» In: *Neural Plast*. 2017 (2017) (cit. on p. 19).
- [34] Barral J. and Croibier A. *Manual Therapy for the Cranial Nerves*. Elsevier, 2009 (cit. on p. 20).
- [35] URL: <https://imotions.com/hardware/the-eye-tribe-tracker/> (cit. on p. 23).
- [36] Doret M., Spilka J., Chudáček V., Gonçalves P., and Abry P. «Fractal Analysis and Hurst Parameter for Intrapartum Fetal Heart Rate Variability Analysis: A Versatile Alternative to Frequency Bands and LF/HF Ratio». In: *PLoS One*. 10(8) (Aug. 2015) (cit. on p. 27).

- [37] Franco A., Marques Neves C., Quintão C., Vigário R., and Vieira P. «Singular Spectrum Analysis of Pupillometry Data. Identification of the Sympathetic and Parasympathetic Activity». In: *Procedia Technology* 17 (2014), pp. 273–280 (cit. on p. 28).
- [38] ALS CNTF Treatment Study Phase I–II Group et al. «The ALS functional rating scale: assessment of activities of daily living in patients with amyotrophic lateral sclerosis.» In: *Arch Neurol.* 53 (1996), pp. 141–7 (cit. on p. 39).
- [39] Brooks BR. «Amyotrophic lateral sclerosis clinimetric scales — guidelines for administration and scoring.» In: *Handbook of clinical neurologic scales* (1997), pp. 27–80 (cit. on p. 39).
- [40] Moore DH. Gordon PH Miller RG. «ALSFRS-R. Amyotroph Lateral Scler Other Motor Neuron Disord.» In: *Handbook of clinical neurologic scales* 5 (2004), pp. 90–3 (cit. on p. 39).
- [41] *Classification loss for cross-validated classification model.* URL: <https://it.mathworks.com/help/stats/classreg.learning.partition.classificationpartitionedmodel.kfoldloss.html> (cit. on p. 46).
- [42] Vipin Kumar and Sonajharia Minz. «Feature selection: a literature review». In: *SmartCR* 4.3 (2014), pp. 211–229 (cit. on p. 48).
- [43] URL: <https://pupil-labs.com/products/core/> (cit. on p. 52).
- [44] URL: <http://psychtoolbox.org/> (cit. on p. 57).